Numerical modelling of the preloaded bolted connections

Kalauz, Matija

Master's thesis / Diplomski rad

2020

UNIVERSITY OF ZAGREB

FACULTY OF MECHANICAL ENGINEERING AND NAVAL ARCHITECTURE

MASTER'S THESIS

Matija Kalauz

Zagreb, 2020.

UNIVERSITY OF ZAGREB
FACULTY OF MECHANICAL ENGINEERING AND NAVAL
ARCHITECTURE

MASTER'S THESIS
NUMERICAL MODELLING OF THE PRELOADED BOLTED CONNECTIONS

Mentor: Student:

Full Prof. Zdenko Tonković, PhD   Matija Kalauz

Zagreb, 2020.

Izjavljujem da sam ovaj rad izradio samostalno koristeći znanja stečena tijekom studija i navedenu literaturu.

I hereby declare that this thesis is entirely the result of my own work, using the knowledge, which I gained during my studies and the cited literature.

Generalno, jedno veliko hvala svima koji su me podupirali tokom cijelog života i poticali me da završim fakultet.

Najprije bih želio izraziti zahvalnost mom mentoru, profesoru Zdenku Tonkoviću. Hvala mu na odluci da mi bude mentor tokom ovog rada, iako u trenutku kada sam ja počeo raditi na ovoj temi nije bio dogovor da mi bude mentor. Hvala mu na pomoći da osmisli kako da se ova tema ipak provede u slučaju da rezultati eksperimenta nisu dostupni. I naravno, hvala mu na podršci, izdvojenom vremenu i savjetima tokom izrade ovog rada, ali i općenito za vrijeme studija.

Također, veliko hvala gospodinu Nikoli Naranči, što mi je omogućio da napravim ovaj rad u sklopu tvrtki *AVL-AST d.o.o.* i *AVL List GmbH.*

Moram veliku zahvalnost iskazati gospodinu Kazimierz Czubernat, koji je bio moj neslužbeni mentor u kompaniji, te koji mi je svojim diskusijama i savjetima također pomogao riješiti probleme koji su se nalazi ispred mene.

Želim izraziti zahvalnost svim kolega iz AVL i iz Graza i iz Zagreba. Posebno bih istaknuo kolege iz Zagreba Romana Baranju i Anu Vrgoč, koji su mi i za vrijeme boravaka u Grazu i pri povratku u Zagrebu bile od izuzetne pomoći. Stručne i moralne.

Nadalje, moje velike zahvalnosti idu mom studentskom kolegi i prijatelju Antunu Mariću, s kojim sam se međusobno poticao i s kojim sam prolazio sve lijepe i loše trenutku na fakultetu.

Moje najveće zahvalnosti odlaze mojim roditeljima, jer ipak bez njih ne bih bio tu gdje sam sad. Neizmjerno i vječno vam hvala na tome što ste me uvijek gurali naprijed i na tome što ste uvijek vjerovali u mene. Ovaj rad je vaš koliko i moj.
Volio bih se također sjetiti svih svojih prijatelja, od vrtića pa do studentskih dana, koji isto tako imaju veliku ulogu u ovom radu.

Na kraju želim izraziti zahvalnost svojoj djevojci Sari. Hvala joj na svim riječima podrške, na nesebičnom pomaganju da mi olakša boravak u Grazu i na kraju hvala joj što je uvijek svoja i pomaže i meni da budem bolja osoba.
Ovaj rad posvećujem svom djedu Josi.

<div align="right">Matija Kalauz</div>

In general, I want to say one huge thank you to everyone who were supporting me through my whole life and encouraging me to finish my faculty.

Before everything, I want to express my gratitude to my mentor, full professor Zdenko Tonković. Thank you for being my mentor during this work, even though at the moment when I started to work on this thesis, there wasn't an arrangement that you will be my mentor. Thank you for your help to develop a task in case that experimental results are not available. And of course, thank you for your support, your time and advice during this work, but also during the whole studies.

Also, big thanks go to Mr. Nikola Naranča, for giving me the opportunity to make this work in collaboration with the companies *AVL-AST d.o.o.* and *AVL List GmbH.*

I have to express enormous gratitude to Mr. Kazimierz Czubernat, who was my unofficial mentor at the company, and who helped me with his discussions and advice to solve all the problems, which were in front of me.

I want to say thank you to all colleagues at AVL in Graz and Zagreb. Especially to Roman Baranja and Ana Vrgoč, who were of enormous help. Professionally and morally.

Further, my huge gratefulness goes to my student colleague and friend Antun Marić, with who I shared mutual encouragement and passing through the nice and bad moments at the faculty.

My biggest gratitude goes to my parents, because without them I wouldn't be where I am now. Immensely and eternally thank you for pushing me forward and for always believing in me. This work is yours as much as mine.
 I would like to remember all my friend, from kindergarten to faculty, who also have a big role in this work.

Last, but not least I want to express my gratitude to my girlfriend Sara. Thank you for all your supporting words, for your unselfish helping to make my stay in Graz as easier as it can be, and thank you for always being yourself, and making me a better person.
This work I dedicate to my grandfather Joso.

<div align="right">Matija Kalauz</div>

Sveučilište u Zagrebu	
Fakultet strojarstva i brodogradnje	
Datum:	Prilog:
Klasa: 602 - 04 / 20 - 6 / 3	
Ur. broj: 15 - 1703 - 20 -	

DIPLOMSKI ZADATAK

Student: **Matija Kalauz** Mat. br.: **0035195555**

Naslov rada na
hrvatskom jeziku: **Numeričko modeliranje prednapregnutih vijčanih spojeva**

Naslov rada na
engleskom jeziku: **Numerical modelling of the preloaded bolted connections**

Opis zadatka:

Bolted connections are a very convenient joining method in automobile manufacturing industry due to simple assembly and disassembly together with a high load-carrying capacity. Appropriate preloading methods can further improve their performance. However, the creep and stress relaxation effects in the preloaded bolt assemblies will lead to certain loss of clamping force and may cause the failure of the connection. Finite element (FE) models are a very convenient way to predict the behaviour of bolted connections during the whole service life of the structure.

Now days, with the strong growing development of the hybrid and electric powertrains, small bolts like M6 and M8 are present in battery packs very often and can be used to hold all kind components together. Those bolts are used in all vehicle battery systems to some extent. The exact effects of thermal and mechanical cycling on battery operation and performance are not fully defined/known, and because of that it is necessary to perform some tests on that. This master thesis will focus on the bolted connection evaluation methods and criteria's in vehicle powertrain applications.

Based on everything said above in this study it is necessary to:
1. Study available literature of the preloaded bolted joints.
2. Investigate available procedures for the strain rate dependent material definition.
3. Develop FE model and apply it to a simple problem as well as compare the obtained results with the available theoretical ones.
4. Validate FE simulations against experimental measurements if they are available.

During thesis preparation one must comply with the standard rules for preparation of master thesis. It is necessary to list all literature used and received assistance.

Zadatak zadan: Datum predaje rada: Predviđeni datum obrane:
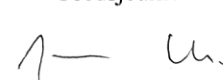
5. ožujka 2020.   7. svibnja 2020.   11. – 15.5.2020.

Zadatak zadao: Predsjednica Povjerenstva:

Prof. dr. sc. Zdenko Tonković   Prof. dr. sc. Tanja Jurčević Lulić

CONTENTS

LIST OF FIGURES

LIST OF TABLES

LIST OF SYMBOLS AND UNITS

Symbol	Units	Description
T	Nmm	Torque
F_0	N	Preload of the Bolted Joints
P	mm	Pitch
d_2	mm	Thread Diameter
μ_t		Friction Coefficient of Thread Surface
μ_b		Friction Coefficient in the Nut Bearing Area
d_m	mm	Average Diameter
K		Torque Factor
F_c	N	Clamping Force
F_t	N	Tension Force
F_s	N	Shear Force
e_v	mm	Bolt Extension
e_p	mm	Surface Extension
ϕ	°	Thread Angle
T_h	Nmm	Resisting Torque
T_t	Nmm	Total Torque
t	s	Time
δ_0	mm	Displacement Amplitude
$T_{twisting}$	Nmm	Twisting Torque
$F_{P,C}$	N	Pretension Force
ΔF_P	N	Difference in Pretension
F_{P0}	N	Pretension Before Relaxation
F_P	N	Pretension After Relaxation
a	m/s^2	Acceleration
f	Hz	Frequency
F_{shear}	N	Magnitude Shear Force
$F_{magnitude}$	N	Total Forces
T_{RT}	Nmm	Retightening Torque
σ	MPa	Stress
ε		Strain

ε_e		Elastic Strain
ε_v		Viscoleastic Strain
D_{ijkl}		Elastictiy Tensor of the Foruth Order
E	N/mm^2	Young's Modulus
G	N/mm^2	Shear Modulus
δ_{ij}		Kronecker Symbol
λ		Lame Parameters
μ		Lame Paramters
η	Ns/mm^2	Coefficient of Viscous Damper
τ	s	Time of Creep or Relaxation
σ_0	MPa	Initial Stress
σ	MPa	Relaxed Stress
$\mathbf{V}$		Global Nodal Displacement Vector
$\mathbf{R}$		Global Nodal Force Vector
$\mathbf{K}$		Global Stiffness Matrix
$\overline{\mathbf{V}}$		Initial Dispalcement Vector
$\mathbf{\Delta V}$		Increment Displacement Vector
$\mathbf{R}_{ext}$		External Force Vector
$\mathbf{R}_{int}$		Internal Force Vector
$\mathbf{K}_t$		Tangent Stiffness Vector
$\mathbf{D}^{ep}$		Elasto-Plastic Stiffness Tensor
$\mathbf{k}_e$		Elastic Stiffness Matrix
$\mathbf{k}_{uL}$		Linear Initial Displacement Vector
$\mathbf{k}_{uN}$		Nonlinear Initial Displacement Vector
$\mathbf{k}_{\sigma L}$		Linear Initial Stress
$\mathbf{k}_{\sigma N}$		Nonlinear Initial Stress
$\mathbf{D}$		Elasticity Matrix
$\mathbf{B}_L$		Linear Strain-Displacement Matrix
$\mathbf{B}_N$		Nonlinear Strain-Displacement Matrix
$\mathbf{D}_{KL}$		Linear Kinematic Differential Operator
$\mathbf{D}_{KN}$		Nonlinear Kinematic Differntial Operator
$\mathbf{q}$		Volume Load Vector
$\mathbf{q}_b$		Surface Load Displacement

N$_s$		Edge Shape Function Matrix
v		Nodal Displacement Vector
u		Displacement Components
N		Shape Function Matrix
C3D10		Quadratic Tetrahedron Element
C3D8		Linear Brick Element
σ_{UTS}	MPa	Ultimate Stress
σ_Y	MPa	Yield Stress
ν		Poisson Coefficient
δ	t/mm^3	Density

LIST OF ABBREVIATION

Abbreviation	Description
ICE	Internal Combustion Engine
HEV	Hybrid Electric Vehicles
PHEV	Plug-in Electric Vehicles
EV	Electric Vehicles
BEV	Battery Electric Vehicles
FT	Fully Threaded
PT	Partially Threaded
cpm	Cycles per minute
DUT	Device Under Test
PDF	Probability Density Function
PSD	Power Spectral Density
FFT	Fast Fourier Transform
RMS	Root Mean Square
ASD	Acceleration Spectral Density
FEM	Finite Element Method
DOF	Degrees of Freedom

SAŽETAK (Abstract in Croatian)

Vijci i vijčani spojevi su najzastupljeniji spojevi koji se koriste u gotovo svim industrijama, a pogotvo u automobilskoj. Zbog velike zastupljenosti predstavljaju izazov kako bi se zaustavilo njihovo popuštanje, te kako bi se detektiralo koliko je njihovo popuštanje uslijed različitih utjecaja. U novije vrijeme sve više se auto industrija okreće proizvodnji hibridnih i električnih automobila. Kako se okreće tom segmentu proizvodnje razvijaju se različite baterije koje trebaju zadovoljiti testiranja prije upotrebe u stvarnom svijetu. Mnogo dijelova u samim baterijama upravo je spojeno vijcima, te zbog toga je potrebno ispitati koliko će uistinu ti vijci moći zadržati 100% svog prednapregnutog stanja, pod različitim utjecajem. Isto tako, uvelike je poznato u svijetu vijaka i vijčanih spojeva da čim se pojedini vijčani spoj pritegne, njegova sila prednaprezanja počinje gubiti svoju vrijednost. Zbog viskoelastičnog ponašanja podložnog materijala taj efekt gubitka sila prednaprezanja postoji. S toga u ovom radu će pomoću teorijske pozadine i pomoću metode konačnih elemenata biti ispitano koliki je gubitak sile prednaprezanja uslijed viskoelastičnog ponašanja materijala s kojima su vijak i matica spojeni. Iz tog razloga, potrebno je razviti metodu pomoću koje će se moći ispitiati kako relaksiranje vijčanog spoja utječe na gubitak prednaprezanja i koja će biti upotrebljiva onog trenutka kada stvarna testiranja budu gotova.

Ključne riječi: vijak, relaksacija, metoda konačnih elemenata, prednaprezanje

ABSTRACT

Bolts and bolted connections are the most common compounds that are used in almost all industries, especially in the car industry. Because they are so commonly used, they represent a certain challenge to find a way to stop their loosening and to detect what is their pretension loss due to various influences. In recent times, the car industry is turning to manufacture hybrid and electrical vehicles more and more. Since they are turning to that segment of production, various batteries, which first have to be tested before "the real time use" are developing. Bolts connect many parts in all batteries, and because of that, it is necessary to investigate how much those bolts are able to keep 100% of their initial pretension force, under various conditions. Also, in the world of the bolts and the bolted connections it is very familiar when certain pretension force is applied, it starts to drop immediately. Because of the viscoelastic behavior of the underlaying material, that effect of pretension loss exists. Considering all of that, in this thesis using the theoretical background and finite element method it is going to be investigated what is the pretension loss due to the viscoelastic behavior of the material with which the bolt and the nut are connected. Because of that, it is necessary to develop a method, which will be able to examine how relaxing of the bolted connection is influencing the pretension and which will be usable when real tests are done.

Key words: bolt, relaxation, finite element method, pretension

Prošireni sažetak

Ovaj rad napravljen je u sklopu austrijske tvrtke *AVL-List GmbH* i hrvatske tvrtke *AVL-AST d.o.o.* To su kompanije koje se bave razvojem pogonskih sklopova u motorima s unutarnjim izgaranjem i električnih pogonskih sklopova.

Vijci i vijčani spojevi su najzastupljeniji spojevi koji se koriste u gotovo svim industrijama, a pogotovo u automobilskoj. Također, vijci kada su u određenom trenutku prednapregnuti, odmah počinju gubiti inicijalnu silu prednaprezanja. Osim što je logično da će pod različitim utjecajima poput šokova i vibracija doći do gubitka sile prednaprezanja, veliki je fenomen kako vijci čim se prvi put pritegnu, odmah im počinje opadati sila prednaprezanja. Uzrok popuštanju sile prednaprezanja je zbog viskoelastičnog ponašanja podložnog materijala s kojim je vijak spojen. Iz tog razloga potrebno je razviti metodu koja će numerički prikazati kako viskoelastično ponašanje materijala utječe na gubitak sile s kojom je vijčani spoj prednapregnut. Stoga se ovaj diplomski rad može podijeliti na četiri dijela:

- Potrebno je bilo proučiti detaljno teorijsku pozadini sile prednaprezanja u vijcima i vijčanim spojevima, te kako dolazi do gubitka iste.

- Konektori koji su predstavljali tijelo vijka bili su podvrgnuti određenom opterećenju, te sile koje su dobile kao rezultati bile su uspoređivane s ostatkom momenta koji se dobio iz stvarnih testiranja.

- Treći dio je opisivao viskoelastično ponašanje materijala, modele i procedure koje opisuju viskoelastično ponašanje materijala, te koji model najbolje može opisati relaksaciju, jer se to odvija u vijčanim spojevima. Također bilo je potrebno provesti verifikaciju jednostavnog modela za materijal koji bi se koristio u vijčanim spojevima.

- Na kraju se napravila numerička analiza koja je pokazala kako utjecaj viskoelastičnog ponašanja materijala utječe na gubitak prednaprezanja u vijčanim spojevima.

Nakon što su navedena četiri područja s kojima se ovaj diplomski rad bavio, kratak opis svakog poglavlja će također biti iznesen.

U prvom poglavlju dan je kratak opis hibridnih i električnih automobila, kao i baterija koje se koriste u hibridnim i električnim automobila. Također su opisani vijci i vijčani spojevi, te njihova primjena.

Drugo poglavlje se bavi eksperimentima i testovima koji su provedeni na vijcima i vijčanim spojevima. Opisani su destruktivni testovi, te kako se vijci opterećuju do loma. Nadalje je opisano prednaprezanje u vijku i važnost prednaprezanja. Na posljetku su opisani eksperimenti koji su rađeni na vijcima koji su bili prednapredgnuti i kako su ti isti testovi utjecali na gubitak prednaprezanja u vijčanima spojevima.

U trećem poglavlju korišten je model u kojem su konektori predstavljali tijelo vijka, te su bili opterećeni na nasumičnu vibracijsku uzbudu. Potrebno je bilo odrediti sile koje su nastale u konektorima nakon opterećenja, te su sile bile uspoređene s ostatkom momenta u vijcima koji su dobiveni iz realnog eksperimenta.

Četvrto poglavlje opisuje viskoelastično ponašanje materijala. Opisuje procedure i modele koji mogu takvu vrstu ponašanja materijala prikazati. Također u tom poglavlju su opisani konačni elementi koji će se koristiti u numeričkoj analizi kao i verifikacija jednostavnog modela koja pokazuje koliko je točno numerički moguće opisati relaksaciju.

U petom poglavlju materijal koji je korišten za verifikaciju u prethodnom poglavlju, uzet je kako bi opisao utjecaj viskoelastičnog ponašanja materijala da bi se vidjelo koliko to utječe na gubitak prednaprezanja u vijčanom spoju.

Na kraju u zadnjem poglavlju napisan je zaključak i sugestije za daljnji rad.

1. INTRODUCTION

1.1.   Motivation

Bolts and bolted connections are very common connections that are used in the car industries. Since bolts are loosening their pretension immediately when that pretension was applied, it is very important and challenging to detect and to find a way to stop that loosening. That phenomenon when pretension immediately starts to drop is called relaxation of the bolted connections. Relaxation is caused by the viscoelastic behavior of the underlaying material. In recent times, numerical simulations have had a major impact to improve any type of assembly. Because of that, as it is said, it is very important to check if that pretension is dropping. It is necessary to find a method, which will tell us how the viscoelastic behavior of the material is affecting that pretension, which was applied on the bolt, and that is the real motivation behind this thesis.

1.2.   Thesis overview

In the first chapter is given a description of the batteries, which are used in electrical and hybrid vehicles, and a little bit about the bolts and bolted connection.

The second chapter deals with the bolt and experiments, which were performed on the bolts and the bolted connections. Also, in that chapter is studied the theoretical background of the bolted connections, pretension, and how pretension is loosening due to various effects.

Chapter 3 describes connectors, and the retightening method. In that section are presented a comparison of the results, that are obtained from numerical simulation and from real tests. The aim was to define if a correlation between forces in connectors and torque loss exists.

Chapter 4 shows the verification of the viscoelastic problem for the material, which is going to be used in the following chapter.

Chapter 5 is giving a description how the viscoelastic behavior of the material, which was verified in the previous chapter is affecting pretension loss of the bolted connection.

In the last chapter is possible to find what is the conclusion of the whole thesis, and what are the recommendations for further works.

1.3.   Conventional and hybrid vehicles

There are three basic vehicle configurations used on the road presently: conventional vehicles, electric vehicles, and hybrid vehicles. Conventional vehicles utilize an Internal Combustion Engine (ICE) which performs a conversion between chemical and mechanical forms of energy to propel the vehicle in the form of combustion. These cars feature a driving range of around 500 – 600 km on a regular tank and can be filled in only a few minutes at a convenient re-fueling station. The combustion process uses a source of ignition, air, and fuel which often produces harmful emissions into the environment. These emissions are in the form of Nitrogen Oxides (NOx), Carbon Dioxide (CO2), Hydrocarbons (HC), Sulphur Oxides (SOx), Particulate Matter (PM10), or Ozone (O3).

Hybrid vehicles attempt to combine the advantages of both the combustion and electric vehicles into one package. They traditionally feature a downsized combustion engine to burn less fuel to meet the consumer's desired vehicle range, in conjunction with one or more electric motors. There are two main variants of hybrids: Hybrid Electric Vehicles (HEVs), and Plug-In Hybrid Electric Vehicles (PHEVs). HEVs are designed with smaller battery packs, benefitting from the use of regenerative braking in city driving to charge the onboard battery. For a PHEV, the battery is often much larger and is a dominant source of propulsion power [1, 2]. Simple scheme of hybrid vehicles is depicted in Figure 1.
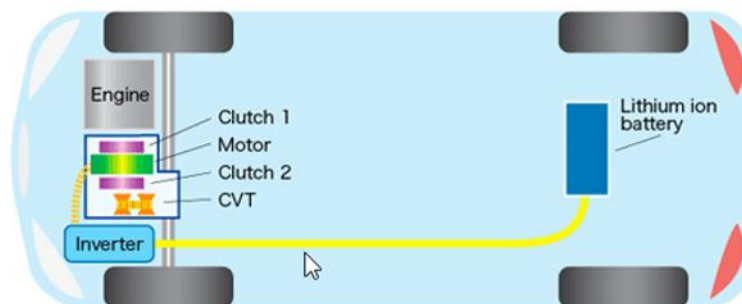
Figure 1. Configuration of Hybrid Vehicles [2]

Electric vehicles (EVs) replace the combustion engine in the conventional vehicle with a battery pack and an electric motor. The battery pack provides an onboard storage area for electrical energy which can be used later by the motor. The biggest advantages of the use of an electric motor are the offsetting of vehicle tailpipe emissions and the ability to employ regenerative braking. Through the use of the motor, the vehicle will not create any emissions and leave all sources to upstream generation. This use of upstream energy is beneficial to the environment as 70,1 % of the energy mix is made up of nuclear, hydro, wind, and solar energy; all forms of generation which do not pollute the air. The biggest disadvantage to the use of electric vehicles is the limited range, lack of re-fueling infrastructure, and increased cost of the powertrain. The increased cost is mainly due to the incorporation of large Lithium-ion battery packs to store onboard energy. Additionally, it can take up to twenty hours to charge an onboard pack; an aspect of an electric vehicle's design which inhibits consumer acceptance. [1, 2, 3] Simple scheme of electric vehicles is depicted in Figure 2
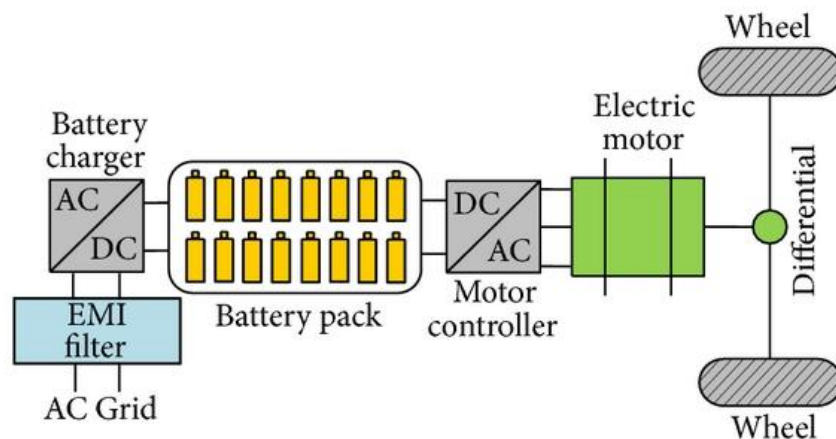
Figure 2. Configuration of a Conventional Electric Vehicles [3]

1.4. Battery fundamentals and definitions

It is in interest on a global scale to replace fossil fuels vehicles with EVs for protecting the environment and achieving energy sustainable. Because of that EVs have gained wide attention from the past years as one of the effective solutions for environment deterioration and energy shortages. The main barrier issue for gaining acceptance for EVs is the high cost and cycle life of batteries. An electric-vehicle battery (EVB) used for industrial vehicles, are batteries which main purpose is to power the propulsion system of battery electric vehicles (BEVs). These batteries are usually rechargeable batteries and are typically lithium-ion batteries. A battery is

fundamentally defined as 'a container consisting of one or more cells, in which chemical energy is converted into electricity and used as a source of power'. Batteries are used in many applications, to power systems which are disconnected from the utility grid during use. As technology progresses, battery technology has changed in order to maximize power and energy density. Currently, Lithium-ion (Li-Ion) technology is at the forefront and is utilized in applications ranging from computers to EVs [1, 2, 3]. Battery for electrical vehicles is shown in Figure 3.

Figure 3. Example of Battery of Electrical Vehicle [3]

1.5.   Bolts and bolted connections

Bolted connection is more frequently used than other connection methods. They are very easy to operate, and no special equipment is required. This is in particular due to the development of higher strength bolts, the easy to use and strong structural steel connections become possible. In the bolt design, two kinds of forces including tension and shear forces should be considered. Bolted connection can be divided into ordinary bolted connection or high-strength bolted connection. Both of them are easy in installation, particularly suitable for connection in the construction site. Ordinary bolts are easy to disassemble and are generally used in temporary connections or those need to be disassembled. High-strength bolts are easy to disassemble, and they have higher strength and stiffness. However, the bolted connections also have some disadvantages because it is necessary to drill holes and adjust the holes during

the installation. The cutting of the holes may weaken the steel members and increase the use steel materials due to the member overlapping, and also this will increase the workload in the construction. There are many reasons that may result in the failure of the bolted connections, such as overloading, over torqueing, or damage due to corrosion [4]. Simple bolted connection is shown in Figure 4.
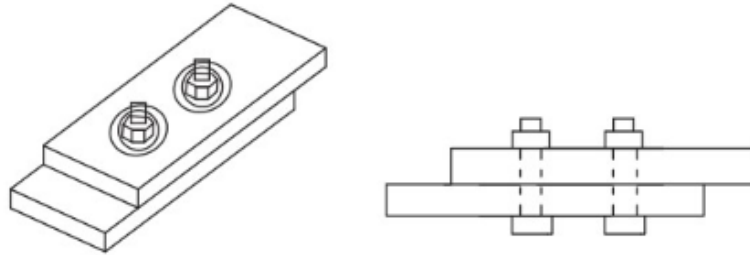
Figure 4. Bolted Connection [4]

Bolt joints of beams and columns, high pressure vessels and other structures are critical components often determining reliability of the whole structure. To increase reliability of this type of joints it is necessary to apply design and calculation methods, based on consistent tests. Bolt is one of the most common connecting devices. Used in a wide range of applications, one would expect that the knowledge of how a bolt performs under certain loading conditions would be well known. While the behavior of bolts under static tensile and shear forces is fairly well understood, their behavior under dynamic loads, such as vibration, is not. Many theories have been developed in an attempt to describe the way that a bolt and nut interact under vibratory loads. While these theories have proven helpful in understanding the bolt/nut interaction, none have proven adequate in predicting bolt loosening. In order to predict bolt loosening, it is important to first identify the parameters that contribute to bolt loosening so they can be quantified [5, 6]. Simple bolt and nut are shown in Figure 5.
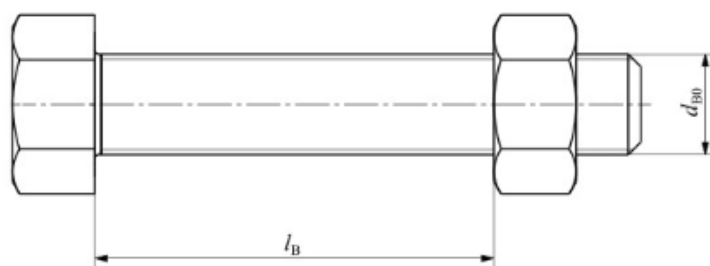
Figure 5. Bolt and Nut [7]

2. EXPERIMENTS WITH BOLTS AND BOLTED CONNECTIONS

Since bolts and bolted connections are often used fastener connections many tests were performed on them. While the literature data was being studied, pretension loss of bolts due to vibration and embedding was something that has been addressed the most. Also, during the research of the literature there were multiple tests used for defining the behavior of bolts under certain load.

Those tests that are important for this work are:

- Destructive bolt and nut assemblies testing
- Durability of bolts under vibrations
- Loss of preload due to relaxation

2.1.   Destructive bolt and nut assemblies testing

There are three common failure modes of bolt and nut assemblies under tension: bolt fracture, bolt thread failure, and nut thread failure. This paper demonstrates that using partially rather than fully threaded bolts in connections may increase the chance of thread failure. This failure mode is less ductile than bolt fracture and is therefore generally not desired. The failure mode of bolt and nut assemblies subjected to tensile loading is determined by several factors, such as geometry and dimensions (e.g., the cross-sectional area of the bolt, thread dimensions, and thread engagement length), mechanical properties of the bolt and nut material. [8]. The current paper presents results from a series of direct tension tests on partially (PT) and fully (FT) threaded bolt and nut assemblies, where the grip length Lg, and thus the threaded length Lt, was varied. Definitions of dimension used for tests are shown in Figure 6.
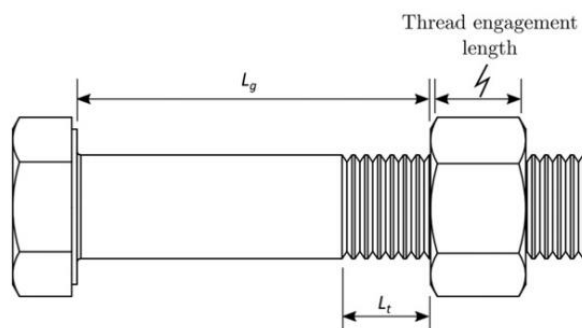
Figure 6. Definition of grip Length L_g, threaded length L_t, and thread engagement length [8]

2.1.1.   *Experiments and results of destructive bolt and nut assemblies*

The tested bolts were partially threaded (PT) or fully threaded (FT) M16 × 160 mm bolts of grade 8.8 manufactured according to the standards ISO 4014. The property class of the nuts was 8, and they were manufactured according to ISO 4032. Five replicate material tests were performed on each of the two bolt types, PT and FT, giving the results shown in Figure 7 [8].
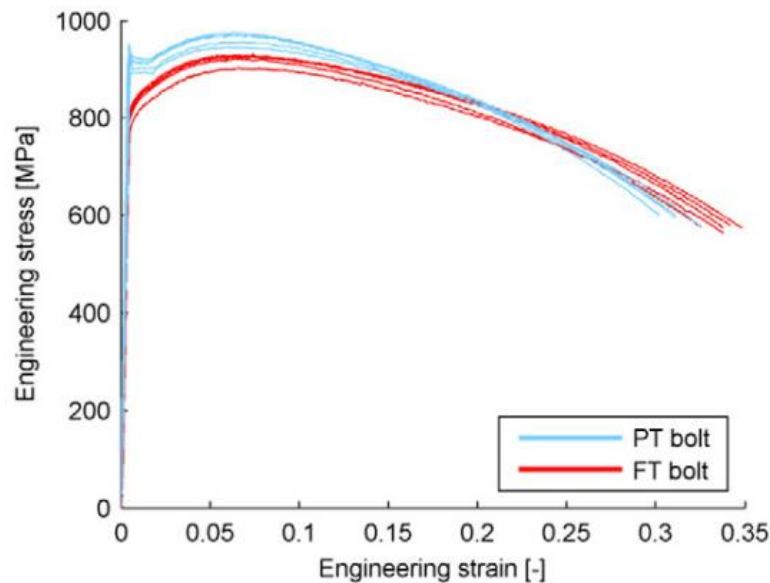
Figure 7. Engineering Stress-Strain Curves Obtained from the Uniaxial Tension Tests [8]

In Figure 7 it is possible to see that PT bolts material is clearly stronger than FT bolts. It is noticeable that PT bolts are stronger in both terms, yield and ultimate strength.

Average ultimate strengths of 963,5 and 922,1 MPa were found for the PT and FT bolt materials. The average stress value of the yield plateau for the PT bolts was 908.7 MPa, whereas the average stress value at the first indication of yield for the FT bolts was 796.5 MPa [8].

Also, the test was repeated for each specimen 5 times. For partially threaded bolts grip length and threaded length were changeable. After the tests it is noticeable that all fully threaded bolts experienced bolt fracture and for partially threaded bolts results vary. or different threaded length L_t results are shown in Figure 8.
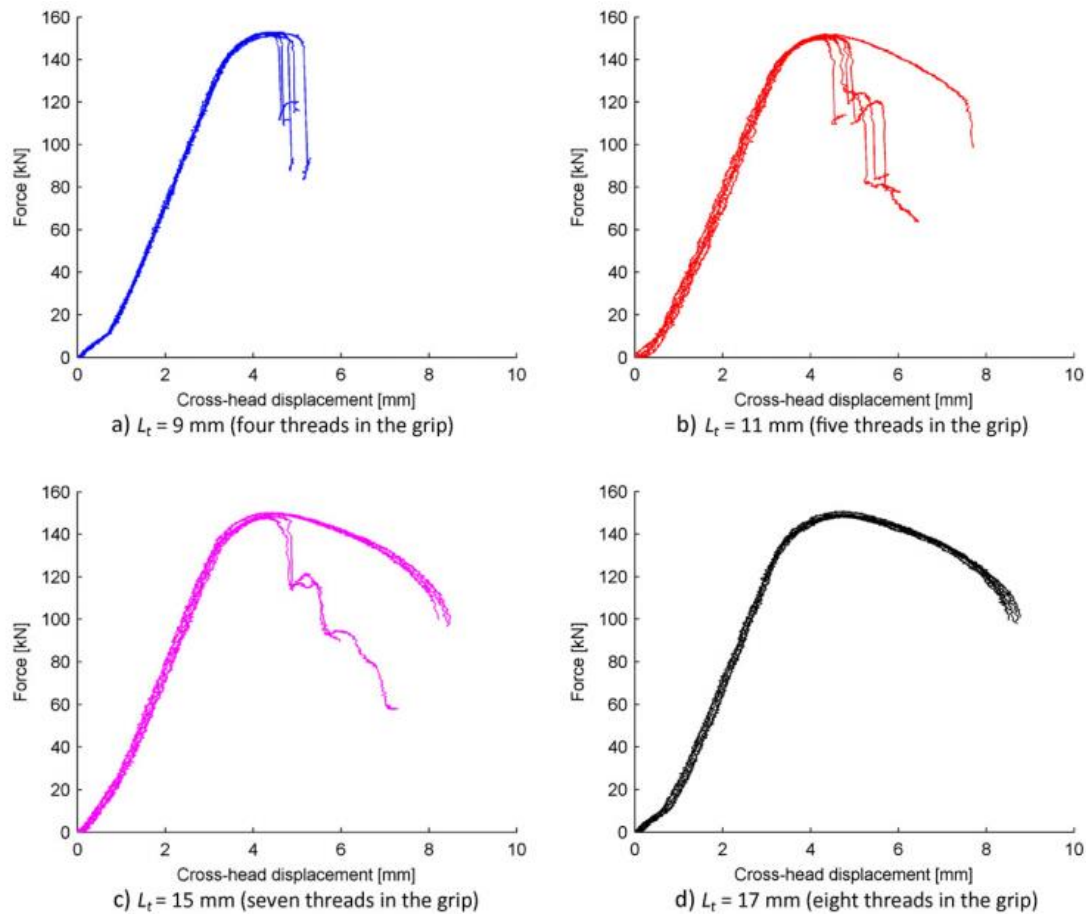
Figure 8. Force-Displacement Curves Obtained from Partially Threaded Bolts with Different Threaded Lengths [8]

From these figures it is possible to notice that thread failure occurred when threaded length was short (L_t = 9 mm), but when threaded lengths were extended and when threaded lengths was big enough (L_t = 17 mm) bolt fracture occurred.

Thread failure can be reduced by the introductions of washers and shims because these increase the threaded length L_t, also the probability of thread failure can be reduced by increasing the length L_t or by increasing the nut height, i.e., the thread engagement length. Fracture surface examination and metallographic analysis are used to determine the cause of failure [8, 9].

In many cases bolted joints are the weakest elements in structures or mechanisms, so that understanding their mechanical behavior turns out to be the key when they are subjected to an increasing monotonic load until fracture (for instance due to a bad design) or in presence of cyclic loads (fatigue). Fatigue in bolts is usually characterized by Wöhler curves, where the

increase of the *R*-ratio decreases fatigue life. Calculation of the fatigue strength is usually a factor conditioned by time.

The specimens were commercial M10x200 bolts with 8.8 grade (DIN 931), made of blued steel. The mechanical behavior of steel in bolts has been characterized by simple tension tests. Tests with axial monotonic stress controlling the displacement (crosshead speed of 2 mm/min) were carried out on the specimens with the bolted joint until fracture. For the fatigue characterization, load control tests were performed (constant stress range $\Delta\sigma$), with the form of a sinusoidal wave, frequency of 10 Hz and different values for the *R*-ratio (0, 0.25 and 0.50). These tests were carried out until fracture or until they reached 106 cycles. Some specimens were subjected to a tensile preload of 80% of the theoretical yield strength of the bolt material, in order to study how it affected the fatigue life.

Wöhler curves were obtained (σ_{max}-N_f and $\Delta\sigma$-N_f) for specimens with bolted joints subjected to a cyclic load, for constant $\Delta\sigma$ and several values of the *R*-ratio (0, 0.25 and 0.50) [10]. Which is shown in Figure 9.
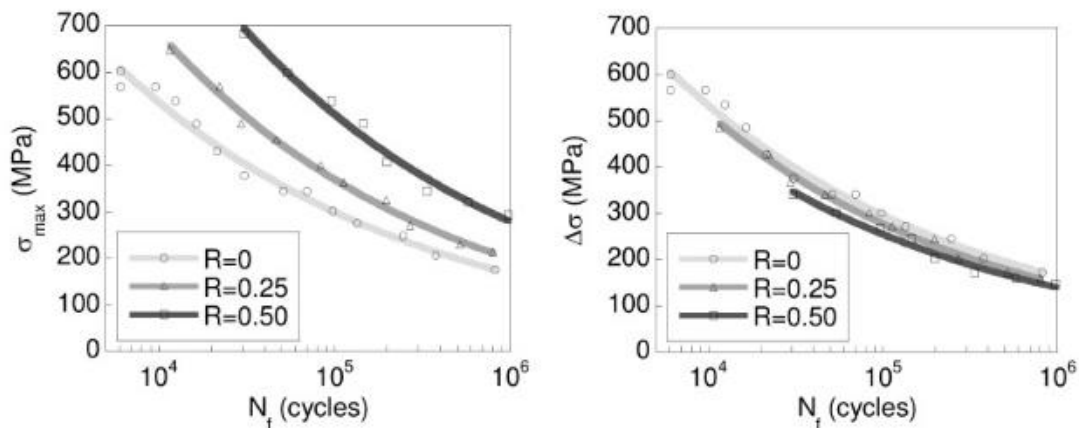
Figure 9. Wöhler Curves: σmax-N$_f$ (left) and $\Delta\sigma$-N$_f$ (right) [11]

In fatigue, the σ_{max}-N_f curve for steel specimens with bolted joints moves to the right while the R-ratio increases; whereas the $\Delta\sigma$-N_f curve moves to the left. Fatigue is, therefore, a biparametric phenomenon, where the increase of the σ_{max} or the $\Delta\sigma$ diminishes fatigue life [10].

2.2. Durability of bolts under vibration

When vibrations are applied in some bolted assembly, the biggest question is if those vibrations will cause any loosening in one of the bolted connections. Therefore, some research has been done to see if vibrations are really affecting bolts in that way. In case that they are really affecting them, is it possible to stop self-loosening? This chapter will describe the importance of preload, theory of self-loosening and tests that have been done.

2.2.1. *Importance of preload*

The torque method is widely used in engineering assembly as a control method for bolt preload. Its working principle is that the preload force can be obtained by using a torque wrench applied to the nut, where torque wrench sets a tightening torque according to the design requirements. When a nut and bolt are used to join mechanical members together the nut is tightened by applying torque, thus causing the bolt to axially stretch. As the bolt head and nut clamp the joint members together, the bolt is left in tension and the mechanical members are compressed together. Bearing friction between nut and clamped part, and thread friction generated by the rotation of nut on bolt are two friction coefficient that are supposed to be overcome by the tightening torque. An accurate mathematical model for characterizing torque-preload relationship can be expressed with the following equation:

$$T = F_0(0,159P + 0,578\mu_t d_2 + \frac{\mu_b}{2}d_m), \qquad (2.1)$$

In this equation F_0 represents the assembly preload of bolted joints, P is the pitch, d_2 is the thread diameter, μ_t is the friction coefficient of thread surface, μ_b is the friction coefficient in the nut-bearing area, d_m is the average diameter for friction moment at the bolt head or nut-bearing surface.

When the bolted joint geometric parameters are known, the torque factor K and bolt nominal diameter d can be implemented in equation (2.1), and then the following equation is created:

$$T = KF_0 d. \qquad (2.2)$$

The most common reason why bolted joints fail is due to the bolt failing to provide sufficient preload to prevent the external applied forces overcoming the clamp force acting between the joint faces. A fully tightened bolt can survive in an application where an untightened or loose

bolt, would fail in a matter of seconds. Bolt-nut assemblies should be ideally tightened to produce an initial tensile force, which is also known as preload on bolt. Therefore, preload or the torque used to tighten the bolted joints is an important factor that affects the response of the structure subjected to static or dynamic load [11], [12], [13]. A bolt that is compared to a spring for a pretension is shown in Figure 10.
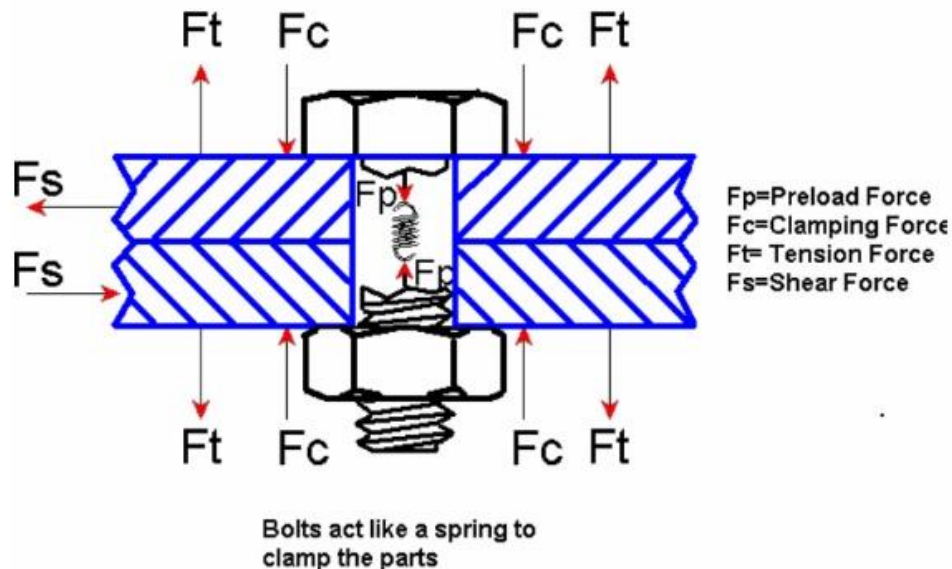
Figure 10. Bolt Compared to Spring for Preload Force [13]

The more the bolt is rotated, the more it stretches and generates a larger preload or tension. F_c, is the difference between the preload force and the tension force, F_t, on the joint. The clamping force is what holds the parts together, i.e., $F_c = F_p - F_t$.

The applied preload is one of the most significant factors which affect the fatigue behavior of bolted joints. On preloaded bolted joints, the load is mainly transferred by friction. The ultimate strength of the joint is limited by the strength of the bolt. Nevertheless, the higher the preload force the better the joint, because it will prevent the assembled parts from moving and the joint from loosening. A highly preloaded joint is also more resistant to static, cycling and shock loads. In general, the preload force determines the strength of the joint. Joints are stronger and more fatigue resistant with greater preload force. As the strength of the bolted joints is mainly dependent on the preload force, the preload has a significant effect on the response of the bolted joint to dynamic or shock loads. The best way to describe characteristics of bolt and surface is to use bolted joint diagram. Stiffness characteristics of bolt and surface are intersecting at the

same point, and that point represents preloaded force [12], [13][14], [15]. In Figure 11 the stiffness characteristic of a bolt, surface, and those characteristics joined together on same graph are shown.
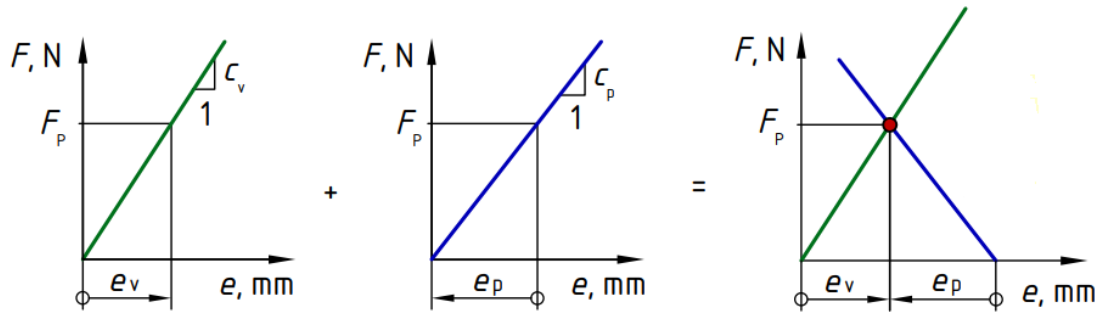
Figure 11. Bolted Joint Diagram [15]

In Figure 11 the graph on the far left shows the stiffness characteristic of the bolt, and e_v represents bolt extension. In the middle the stiffness characteristic of surface is shown, where e_p corresponds to surface extension. On the right the picture shows a bolted joint diagram where because of pretension force F_p, bolt was extended for e_v, and surface was shortened for e_p.

2.2.2. *Theory of self-loosening*

Self-loosening of the preloaded threaded fasteners is one of the main failure models for a threaded fastener. The self-loosening leads to the partial or complete loss of the clamp load. Clamp load loss may cause leakage at pressure boundaries and/or fatigue failure under cyclic service loads. The theory of the mechanism of self-loosening is based on the well-known law of physics that defines the effects of friction on two interacting solid bodies. As long as the friction force between two solid bodies is being overcome by an external force working in one direction, any additional movement in other directions can be caused by the introduction of forces that can be smaller than the friction force.

Due to the effect of the lead angle, an internal off-torque T_{off} is created under the application of the preload Q. This off-torque wants to rotate the bolt in the loosening direction and its value is equal to:

$$T_{off} = Q r_e tan\psi, \tag{2.3}$$

where r_e is the equivalent friction radius of the thread and ψ is the lead angle. Due to the friction on the threads, there exists a torque T_t resisting rotation of the bolt:

$$T_t = Q\mu_3 r_e / cos\phi, \tag{2.4}$$

where ϕ is the thread angle and μ_3 is the coefficient of friction at the threads. There also exists a resisting torque T_h on the bolt head:

$$T_h = Q\mu_2 r_{eh}. \tag{2.5}$$

where μ_2 is the coefficient of friction at the bolt head and r_{eh} is the equivalent friction radius of the bolt head.

In order for the bolt to rotate, it has to overcome the resistance of T_t and T_h. Generally, the value of T_{off} from equation (2.3) is smaller than either T_t (equation (2.4)) or Th (equation (2.5)), so that the bolt does not spontaneously loosen [16].

2.2.3. *Experiments and results of durability of bolts under vibration*

In a study by Zadoks [20], there was a plate mounted on a shaker table which was subjected to a harmonic transverse displacement. At first the shaker table was run at a fixed displacement amplitude while the harmonic excitation frequency was increased. As the frequency was increased the acceleration amplitude also increased, until the acceleration excitation was large enough to cause motion to occur between the mass and the plate. The experiment was stopped when Q_m (the measured preload) went to zero, signaling the total failure of the bolted connection, as it is shown in Figure 12.
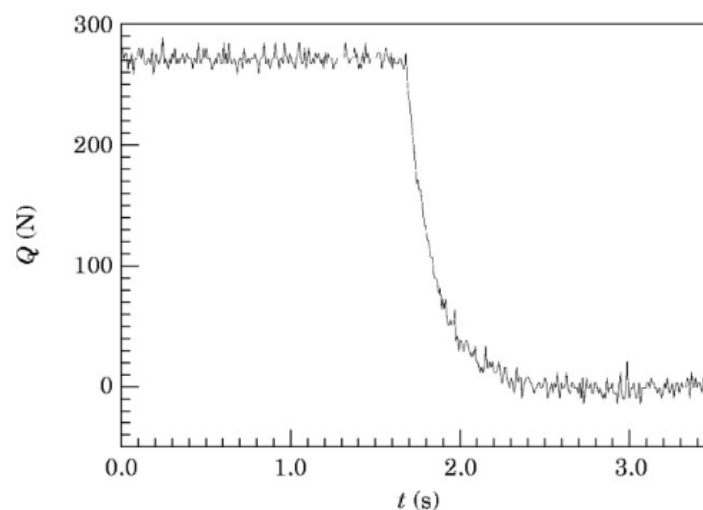
Figure 12. Time History of the Preload as the Excitation Frequency is Increased [20]

For the system described in this paper, the threshold frequency was found to be 10,3 Hz for an initial preload Q of 267 N. For comparison a second test was run with the same conditions as in the first test, but at a fixed frequency (9,85 Hz), which was selected to be just below the threshold frequency at which impacts occurred. This test lasted for 10 h (354 600 cycles of the excitation motion) and no dynamic loosening took place, [20] as it is shown in Figure 13.
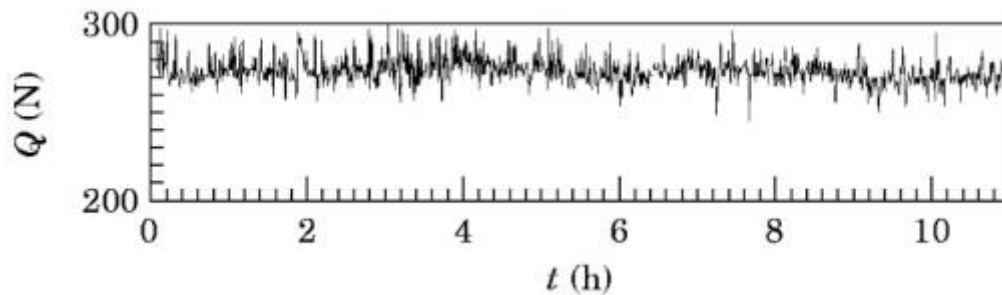
Figure 13. Time History of the Preload for a Fixed Excitation Frequency [20]

These results support the theory that impacts play a critical role in bolt self-loosening.

Second test was made by Junker. Since it has been researching a new way to investigate how bolts are acting when vibration occurred, a new machine was designed. How it works as well as the outcomes from its use will be described below.

This machine generates a transverse sliding motion between two clamped parts by means of an adjustable eccentric. The resulting transverse force is independent of frequency and starting speed of the machine. The clamping force is measured with a compression load cell through which a bushing with internal threads is placed for testing bolts. The relative movement between bed and top part is measured with special linear differential transformers. The tightening and loosening angles were measured with a linear potentiometer, which was attached to the test specimen by a flexible shaft. Exchangeable threaded bushings and inserts in the U-shaped top part make the mechanism usable for testing bolts from M6 to M16 thread sizes. The specimen used in this test was a M10 x 30 bolt. During all tests the specimen was originally preloaded to 2500 kgf. This relates to 75% of the proof load of screws with a strength level of ISO Class 8.8. All tests were run with a frequency of 3000 cpm [19]. During tests, the energy level was varying. Four tests were done and in those tests energy levels were 45, 80, 210, 450 mmKgf. After tests were done results of preload in dependence with number of cycles are shown in Figure 14.
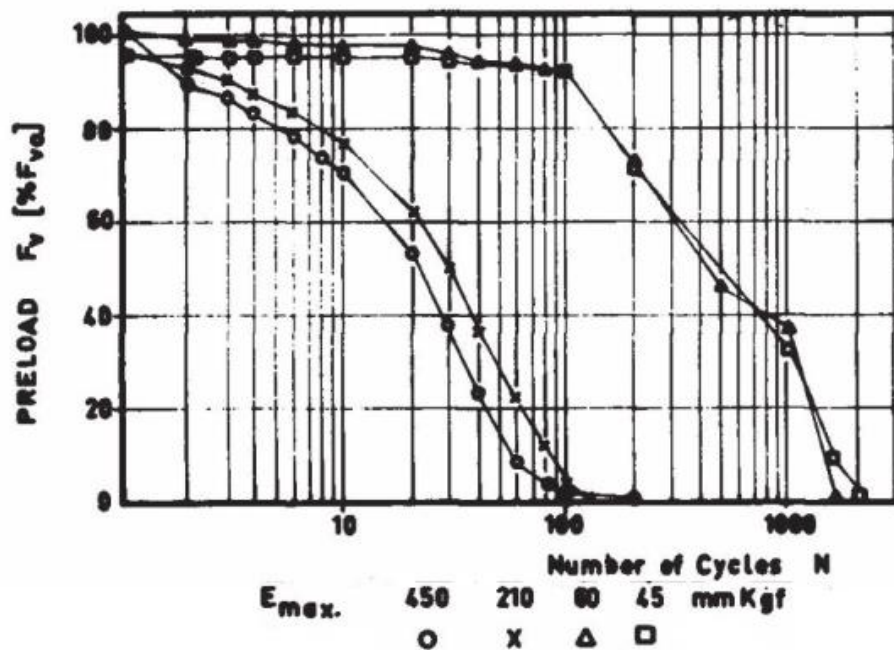
Figure 14. Preload versus Number of Cycles [19]

In Figure 14 it is noticeable that percentage of the preload (F_v) is dropping faster for higher energy level. Therefore, for energy levels of 210 and 450 mmKgf it is visible that preload started to drop very fast. Already after 100 cycles the preload dropped near to 0% of its initial value. But for energy levels of 45 and 80 mmKgf 100% of preload lasted longer. Even after 100 cycles the preload retained almost 100% of its initial preload. It was necessary to do over 1000 cycles so that preload drops to 0, while for energy levels of 210 and 450 mmKgf after 100 cycles dropped to 0.

The following test is related to the test described above. Since the same machine and same concept was used. Difference between these two tests is that in this test frequency was constant and it was 10 Hz. Instead the displacement amplitude was variable.

The experimental setup is used for monitoring the bolt twisting torque in a preloaded bolt, instrumented with a strain gauge that is subjected to cyclic transverse displacement excitation at 10 Hz. Two levels of the displacement amplitudes (δ_0) are used, namely, 0,3556 mm and 0,61 mm. Four levels of bolt preloads are used with each displacement amplitude. The change in the bolt twisting torque $T_{twisting}$ and pitch torque component T_p is monitored with time/cycles [17]. In Figure 15 the twisting torque variation with the number of cycles in a strain gauge instrumented bolt is depicted.
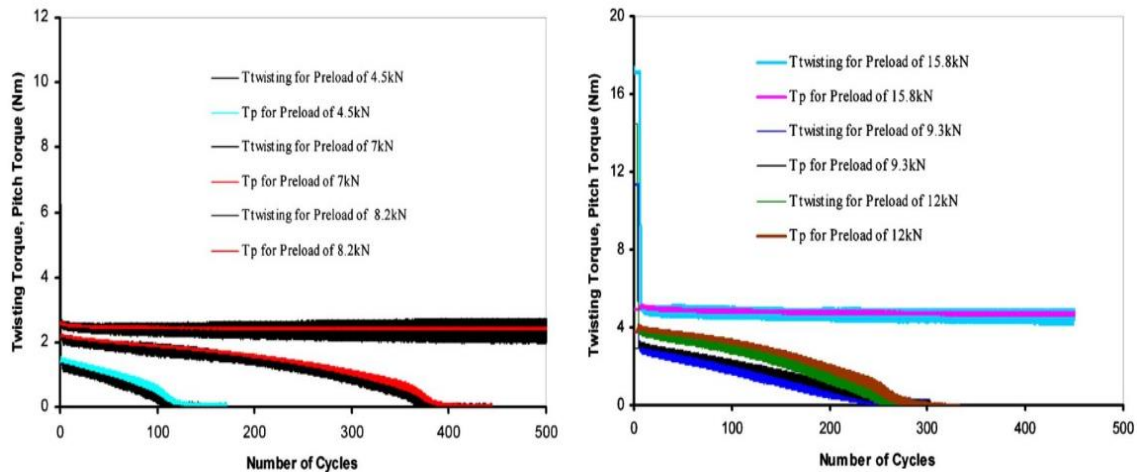
Figure 15. The Twisting Torque variation of the Strain Gauged Bolt under Displacement Amplitude 0,3556 mm (Left) and under Displacement Amplitude 0,61 mm (Right) [17]

In Figure 15 it is noticeable that the bolt twisting torque is reduced rapidly from its initial value, in fact it reaches the level of the pitch torque after the first full cycle and continues to insignificantly fluctuate around the pitch torque value during subsequent cycles [17].

Also, it is good to notice how bolt tension is acting in correlation with number of cycles. That kind of tests for different displacement amplitude is depicted in Figure 16.
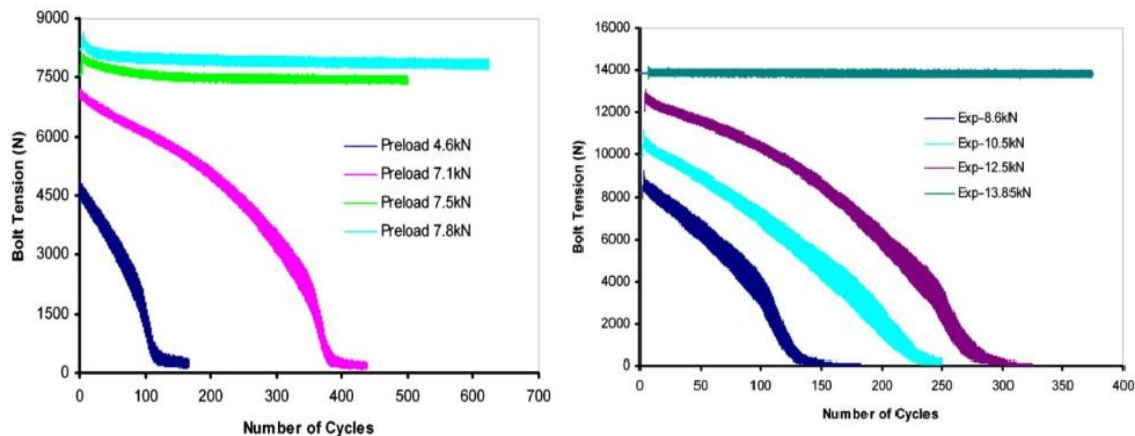
Figure 16. The Bolt Tension Variation with Number of Cycles at 10 Hz for Different Preload Levels under the Cyclic Transverse Displacement Amplitude of 0,3556 mm (left) and 0,61 mm (right) [17]

In Figure 16 is noticeable that for a given excitation, the self-loosening rate per cycle (dF_b/dN) of the clamp load is quite low for high bolt preloads and for a relatively lower preload level, the self-loosening rate per cycle (dF_b/dN) is higher. Obviously, the self-loosening will not occur if

the bolt preload is sufficiently high. From Figure 16, larger transverse displacement excitation amplitudes will require a higher preload level in order to prevent self-loosening, when all other variables remain unchanged. For the same level of bolt preload, larger transverse displacement amplitude δ_0 would increase the rate of self-loosening per cycle.

2.3.   Loss of preload due to relaxation

In the field of bolt pretensioning, a lot of research has been carried out on bolt relaxation. It is generally acknowledged that the pretension in the bolt is not constant, and because of that the preload level is a variable as function of time. The following equation, where $F_{p,C}$ represents pretension force, indicates that:

$$F_{p,C} = F_{p,C}(t). \qquad\qquad (2.6)$$

The reduction of this force in a connection is a well-known phenomenon, which occurs very often in mechanical engineering. That type of phenomenon can be divided into three sections: first, the initial loss of pretension, which mainly depends on the tightening process. Second, the short-term relaxation, which occurs within the first twelve hours after joint assembly. Thirdly, long term relaxation, which has been observed to continue asymptotically. The first drop in pretension force happens within the first ten seconds after the bolt is tightened. The bigger the maximum or initial pretension force is, the bigger the initial loss is. That loss would even increase if the bolt has been pulled beyond its yield limit. The short term relaxation occurs after the initial loss of pretension has happened. In consequence of leading past their yield point, the components in the joint may creep and thereby evoke a reduction of elongation in the bolt, which leads to a loss of clamping force. In case mistakes in installation and design of the bolts as well as a change in temperature can be excluded, the most common reason for short term relaxation is embedding [14][21]. In the following figure, it is possible to see how the bolted joint diagram looks after pretension force has dropped due to relaxation in the joint.
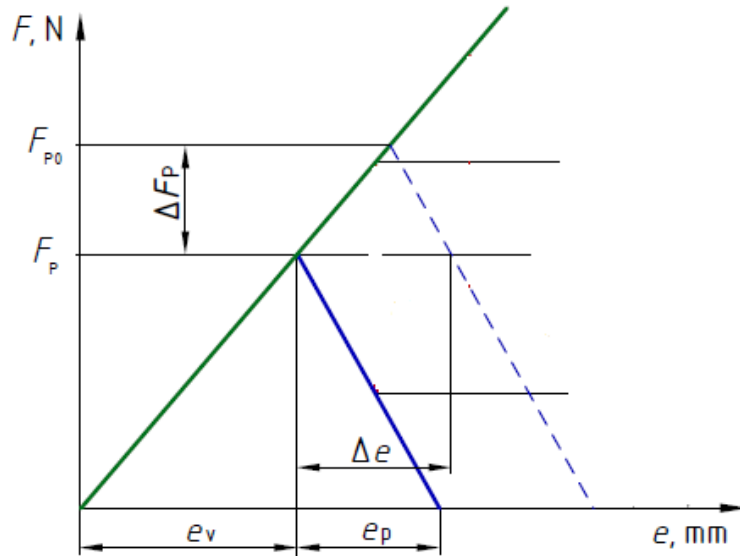
Figure 17. Bolted Joint Diagram of Reduction of Pretension Force [15]

In Figure 17, the diagram shows reduction in pretension force due to relaxation in bolted joints. In that case loss of pretension force can be expressed with the following equation:

$$\Delta F_{\mathrm{P}} = F_{\mathrm{P0}} - F_{\mathrm{P}}, \tag{2.7}$$

In this equation, F_{P0} is pretension force before relaxation, and F_{P} is pretension after relaxation. Also, the settlement of the joint, which is Δe can be expressed as:

$$\Delta e = \Delta(e_{\mathrm{v}} + e_{\mathrm{P}}). \tag{2.8}$$

Where e_{v} represents bolt extension, and e_{p} represents shortening of the surface.

The reason why relaxation loss is likely to appear is because of the difference in yield strength of one or more parts that are joined together with a bolt. This may occur when a combination of hard and soft material exists, for example copper and steel. Also, if the effective bolt thread diameter is smaller than the effective nut thread diameter, the effective contact area is comparably small, and that results in higher surface pressure. This has an increasing effect on relaxation [22].

2.3.1. *Embedding* [22][25]

As it was mentioned above embedding is the most common reason for a loss of preload due to relaxation. The phenomenon of embedding depends on a lot of factors, and some of them are: time, pressure, temperature, material, number of surfaces and surface roughness. The rougher the surface is, the less contact exists between two components. When surface imperfection exists embedding can occur. Mostly embedding happens wherever there is any discontinuity of the clamped package. Those discontinuities usually occur between the contact of bolt head and plate, in threads between nut and bolt, or contact between nut and plate.

When new fasteners are first tightened, where surface interaction exists, the material at these spots will be overloaded, and embedding relaxation starts immediately. Theoretically, embedding relaxation will last until perfect fit-up between contact surfaces is engaged together and the process is stabilized. In the following figures interaction surfaces of the fastener and microscopic view of surfaces, imperfections are shown.
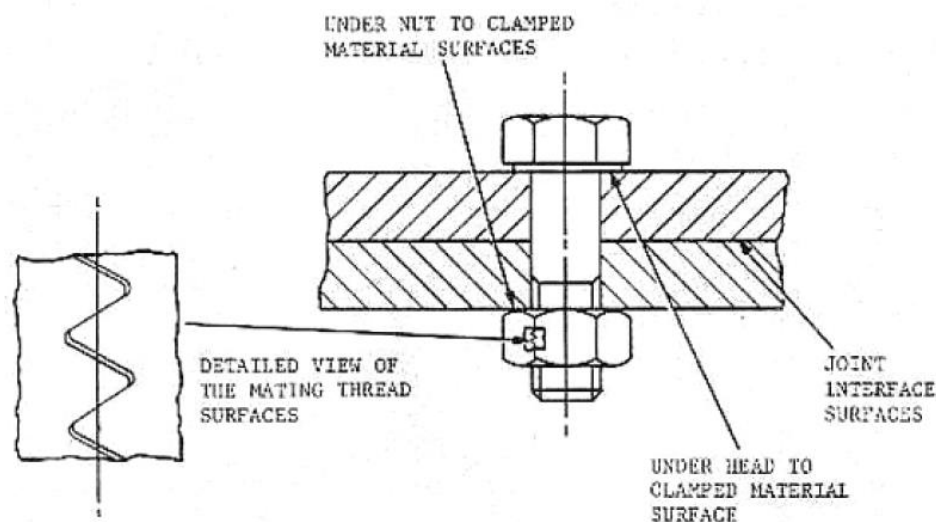
Figure 18. Surfaces Interaction of Fastener [24]
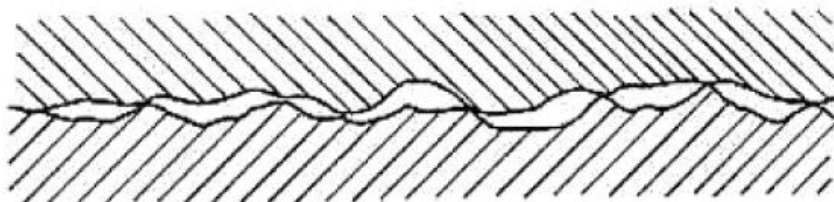
Figure 19. Microscopic View of Surfaces Between Bolt Head and Plate [24]

The rougher the surface, the less contact exists between two components. Also, that kind of situation could lead that relaxation process lasting longer, because normally, the process of relaxation starts over the first minutes after tightening.

2.3.2. *Experiments and results of loss of preload due to relaxation*

The tests that are performed to investigate relaxation are static tests, where bolts are preloaded and left for certain amount of time untouched to check if pretension is really decreasing under given conditions or considering underlying material.

In the test done by Yang [25], 3 steel plates were clamped together with M22, class 8.8 bolts, and the coating thickness used for steel plates was varied. Also, previous research based on Yang, indicated that thicker coating will lead to more relaxation, so because of that, that kind of test was performed. In the following figure, it is shown how test set up for relaxation looks like.
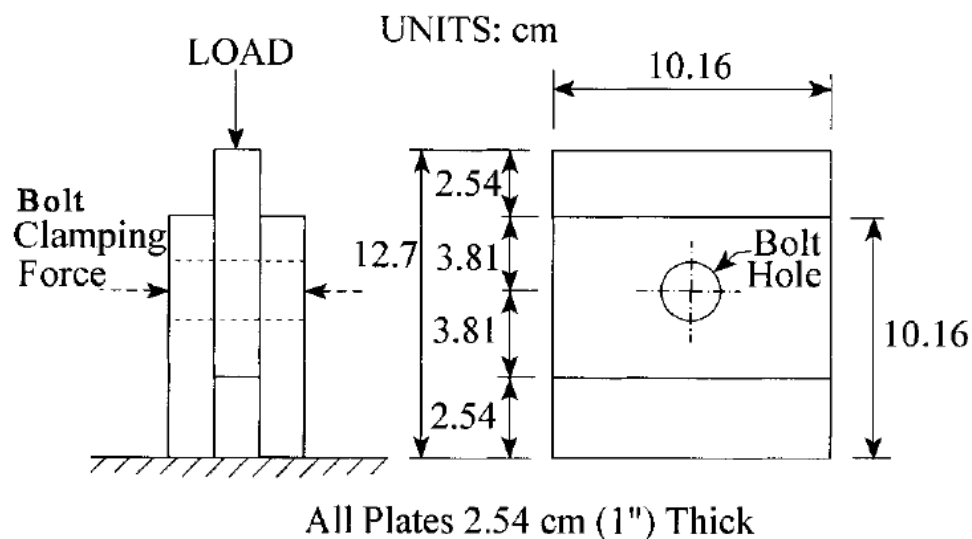
Figure 20. Relaxation test set up [25]

The coating thickness of plates was varying from 0 to 20 mils, where 1 mil is equal to 25,4 micrometers. As previously mentioned, it is expected that the thicker the coating, more loss will occur [25]. So, because of that typical stress relaxation curves for different coating thickness are shown in Figure 21.
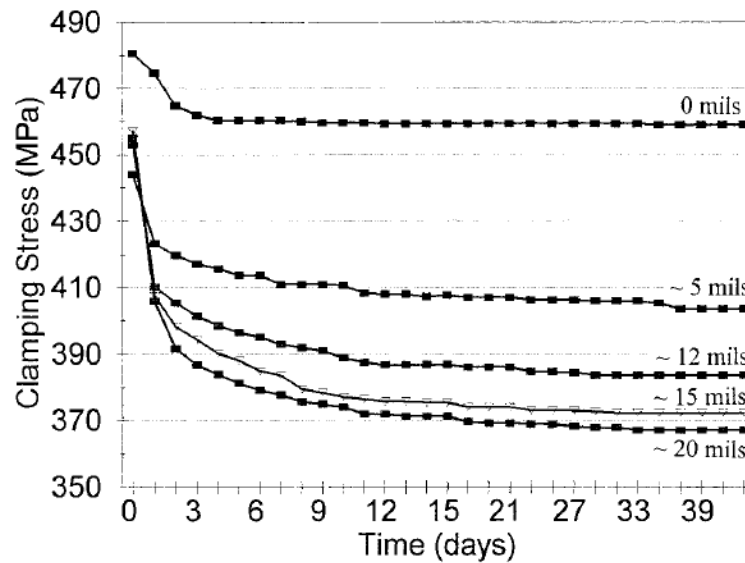
Figure 21. Typical stress relaxation curves with different coating thickness [25]

Since that relaxation test was performed, results are available and are shown in Figure 22, also in comparison with coating thickness.

Nominal galvanized coating thickness (mils) (1)	Loss of Clamping Force (%) after 42 Days			Average loss (%) (5)
	Specimen 1 (2)	Specimen 2 (3)	Specimen 3 (4)	
0	4.5	6.3	5.9	5.6
5	14.4	11.0	14.3	12.4
10	14.6	17.2	17.3	15.3
15	16.2	19.1	16.3	19.6
20	18.4	20.6	16.3	19.9

Figure 22. Relaxation of clamping force [25]

It is possible to notice that clamping force is reducing more as the coating thickness is increased. Also, considering the numbers that are shown in the figure above and comparing them to typical stress relaxation curves, it can be seen that they match almost exactly.

The second test done by [23], which can be found in the literature is very similar to the first one, but the difference is in the test set up, coating thickness and time for observing relaxation in a bolt.

For this test, an M20, class 10.9 bolt and two steel plates, with an overlapping section measuring 100x 100 mm, which thickness is 25 mm, were used. Five different coating thickness were used while the test was performed. System 0 was performed without coating thickness, system 1 with 80 micrometers, system 2 with 150 micrometers, system 3 with 160 micrometers, and system 4 with 230 micrometers thickness. In Figure 23, it is possible to see the relationship of the pretension loss versus time of each coating thickness.
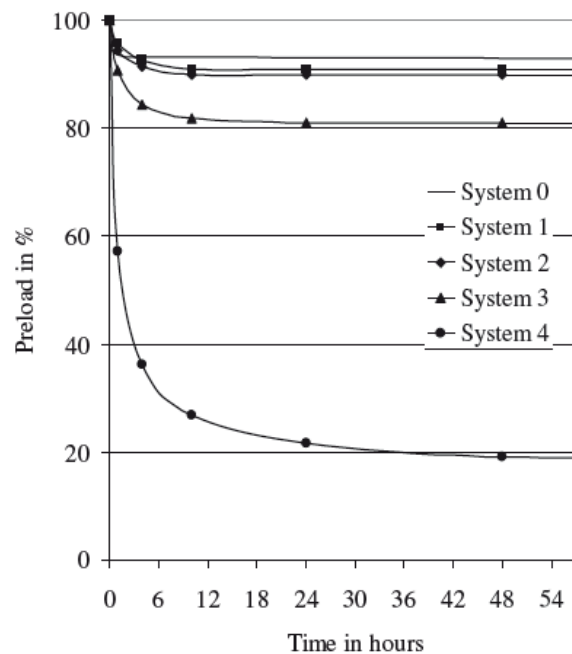
Figure 23. Pretension loss with different coating thickness [23]

What is possible to notice, is that coating definitely is affecting how pretension in bolts will behave. Even though that coating is increasing the possibility of pretension loss, it is also visible that even without any coating, pretension is losing in a few hours after pretension force is being applied. Also, comparing this test and the previous one, it can be seen that in the second test, pretension started to drop way faster, and stabilized earlier. But, when a typical stress relaxation curves diagram (Figure 21), and the curve, which describes clamping stress where no coating is present is observed, it is visible that clamping stress is stabilized after 3 to 4 days.

3. RANDOM VIBRATION ANALYSIS

3.1.   Introduction

Every structure can vibrate and has resonant frequencies in which it vibrates with the greatest amplitude. Therefore, sinusoidal vibration testing is important to help understand how any structure vibrates naturally. The good use of sine vibration is to assess the frequencies at which a particular device under test (DUT) resonates. But in the "real-world" vibrations are not found in the simple sinusoidal form, sine testing is therefore not the only method used in the vibration testing industry. Part of the usefulness of sine testing is its simplicity, so it's a good point of entry into the study of vibrations.

Vibrations found in everyday life scenarios are not repetitive or predictable like sinusoidal waveforms. So, there is an important need for tests that are not repetitive or predictable. Random vibration testing accomplishes this. A random vibration test, on the other hand, excites all the frequencies in a defined spectrum at any given time. One of the main goals or uses of random vibration testing in industry is to bring a DUT to failure. Testing the product to failure will teach us many important things about its product's weaknesses and ways to improve it. Random testing is the key testing method for this kind of application [26] [27].
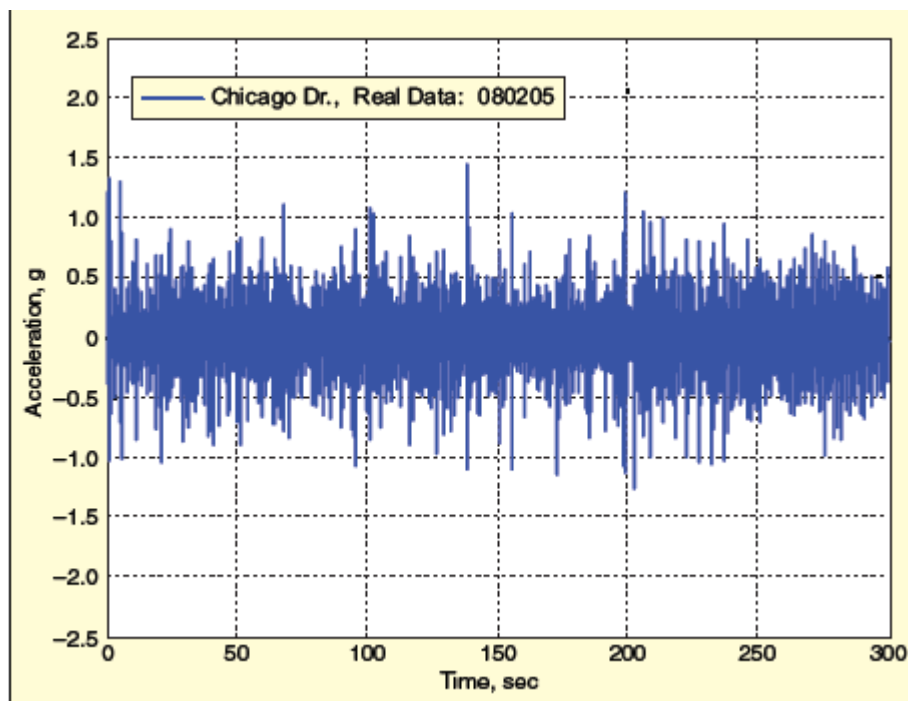
Figure 24. Random Acceleration Time History [26]

The complex nature of random vibrations is demonstrated with a Fourier analysis of the random time–history shown in Figure 25, it reveals that the random motion can be represented as a series of many overlapping sine waves, with each curve cycling at its own frequency and amplitude. Because of the mathematical complexity of working with these overlapping sine curves to find instantaneous amplitude as an exact function of time, a more efficient way of dealing with random vibrations is to use a statistical process to determine the probability of the occurrence of particular amplitudes [28].
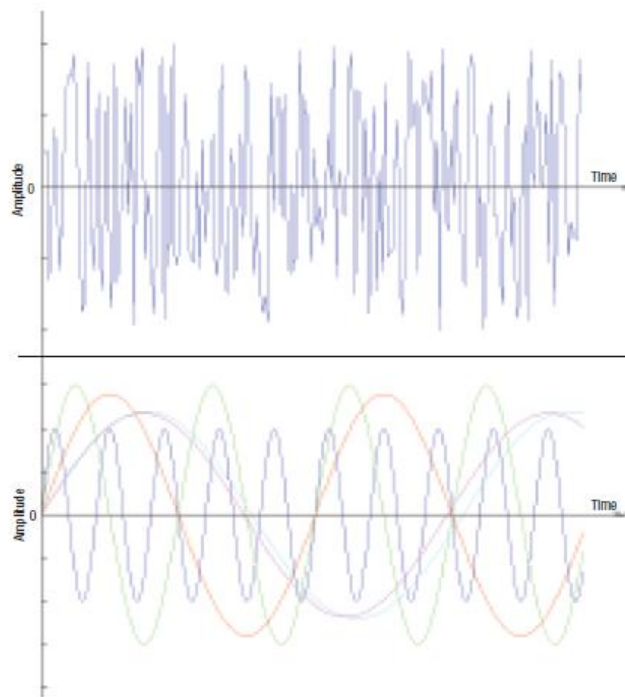
Figure 25. Random Motion Represented as a Series of Many Overlapping Sine waves [28]

The probability density of acceleration during traditional random vibration tests has a statistical representation. An important aspect of such a statistical representation is that most random processes follow a Gaussian probability distribution. This distribution can be seen in a frequency-of-occurrence histogram (sometimes referred to as probability density function (PDF). A PDF plots the number of times random acceleration peaks reached certain levels in small frequency segments called bins. The histogram shown in Figure 26 represents a random signal measured for 10000 seconds and indicates that this random signal follows a classic bell-shaped Gaussian probability distribution.

The most common tool used to analyze random vibration is Power Spectral Density (PSD). Resonances and harmonics, hidden in a time history graph, become clearly visible in a PSD graph. In practice, generating a PSD is usually the first step in examining and analyzing a random waveform [28][29].
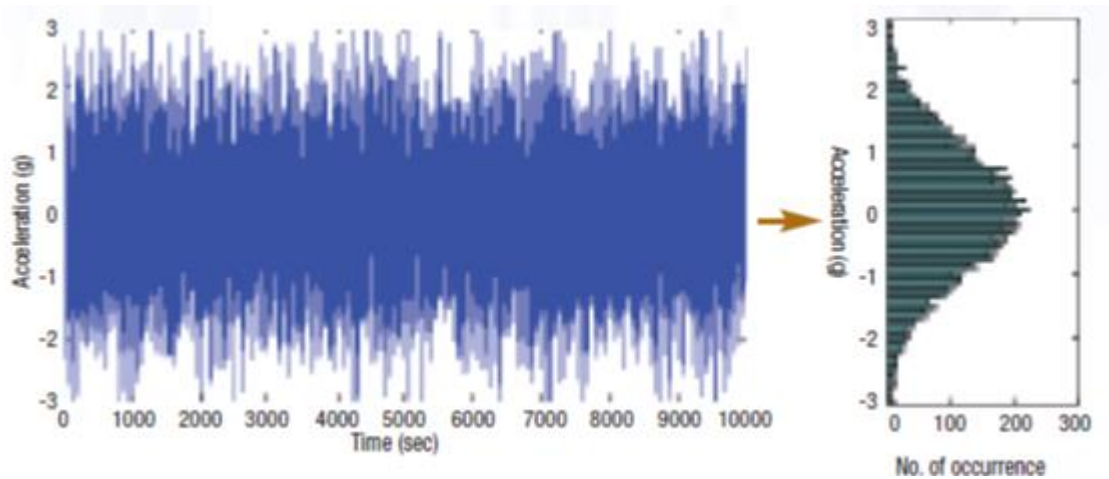
Figure 26. Gaussian Distribution of Random Signal [28]

3.2.   PSD random vibration

The following section will explain what a PSD is through the following topics:

- What is PSD and description of each word in abbreviation PSD
- Generating a PSD
- Calculation of the surface under the PSD curve (Root mean square)

3.2.1.   *What is PSD* [30]

PSD is a function that describes the energy content distribution of a quantity over a frequency range. The mean square value of the quantity of interest is found by integrating the PSD function with respect to the frequency.

Power refers to the fact that the magnitude of the PSD is the mean-square value of the signal being analyzed. It does not refer to the physical quantity power (as in watts or horsepower). But since power is proportional to the mean-square value of some quantity (such as the square of

current or voltage in an electrical circuit), the mean-square value of any quantity has become known as the power of that quantity.

Spectral refers to the fact that the PSD is a function of frequency. The PSD represents the distribution of a signal over a spectrum of frequencies just like a rainbow represents the distribution of light over a spectrum of wavelengths (or colors).

Density refers to the fact that the magnitude of the PSD is normalized to a single hertz bandwidth. For example, with a signal measuring acceleration in units of m/s^2, the PSD has units of $(m/s^2)^2/Hz$.

3.2.2. *Generating a PSD* [30][31]

When looking at random Acceleration vs Time History data as shown in Figure 27, it is hard to conclude or read anything meaningful from the signal except peak accelerations.
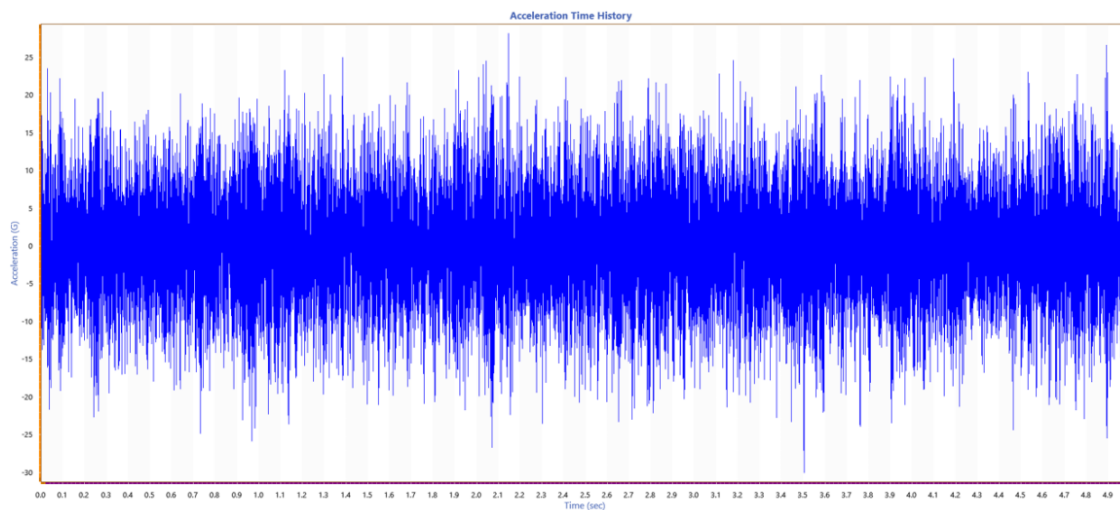
Figure 27. Acceleration vs Time History Data [30]

Since, it is hard to observe or make conclusions about the signal visually, the signal can alternatively be viewed in the frequency domain. The Fast Fourier Transform (FFT) algorithm can be used to convert a signal from the time domain to the frequency domain and vice versa. The PSD of a signal can also be calculated in order to get an idea of the strength of a signal normalized with respect to frequency.

An FFT graph is often used to monitor the frequency spectrum and focus in on changes in that frequency spectrum, while viewing live data or playing through a time history file. But, to check and analyze energy distribution across the frequency spectrum, the PSD must be calculated.

Process of FFT starts by dividing a time history file into frames of equal time length. Lines of Resolution and the Sample Rate are used to determine the width of each frame. Example of dividing history time that was shown in the figure above is shown in Figure 28.
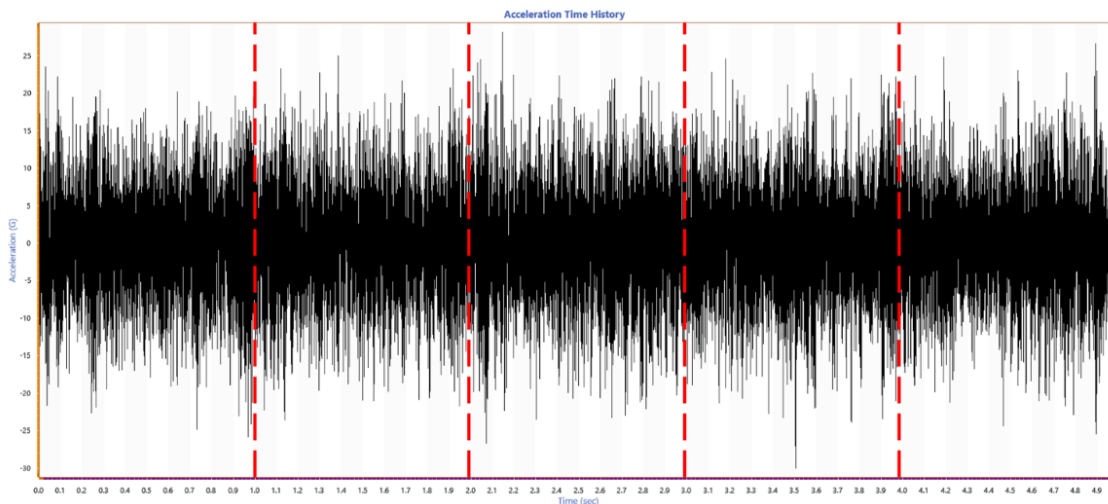
Figure 28. Dividing Time History into Frames [30]

After dividing time history into frames, it is necessary to apply a windowing function because FFT assumes that the data is an infinite series which means that starting and ending points of each frame are interpreted as though they were next to each other. When random data is checked this is usually not the case therefore, a windowing function needs to be applied. Omitting the window function may result in a transient spike between two points which could lead to the difference between starting and ending points. The transient spike between two samples would show up in the FFT as high frequency energy. For the FFT, if there is sharp transition between starting and ending points it will lead to discontinuity. If discontinuity exists, it is reflected in an FFT calculation and is referred to as spectral leakage. But, applying a windowing function reduces the spectral leakage. In case where random response is tested it would be ideal that starting and ending points are the same in every frame of data and because of that all side effects should be minimized by using windowing function. Figure 29 shows a visual presentation of the application of windowing on each frame.
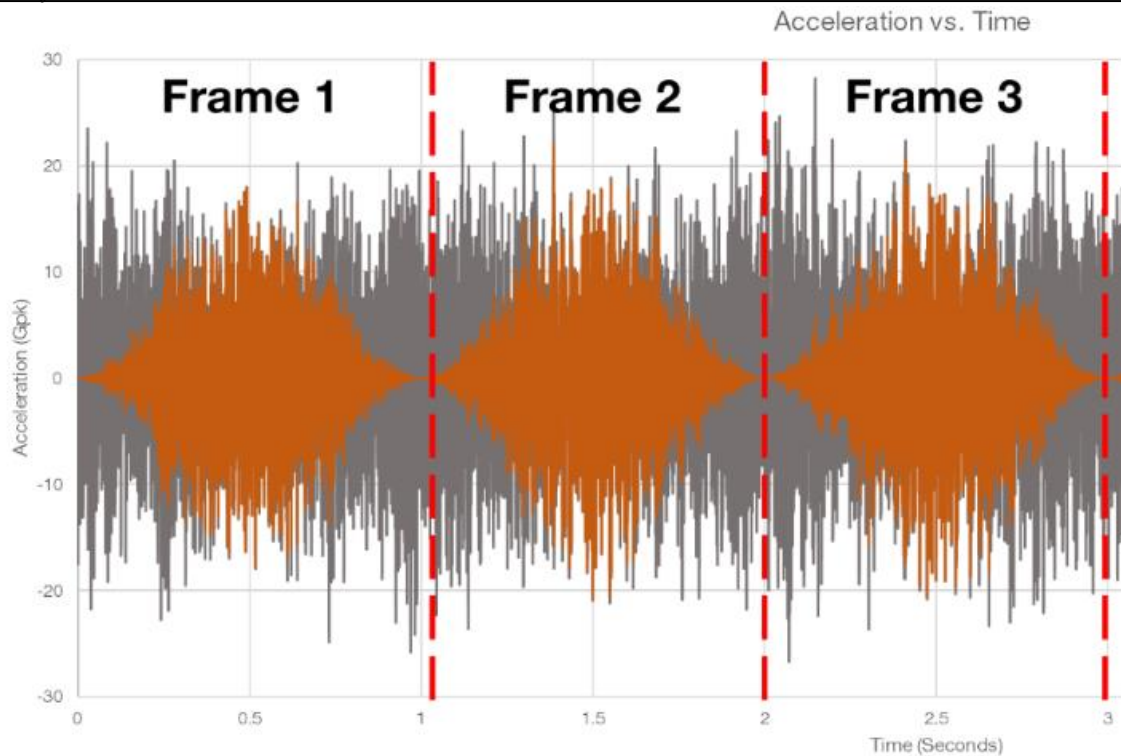
Figure 29. Windowing of Each Frame [30]

For frames that are shown in figure abow the windowed data is used to calculate an FFT. Example how that is supposed to be transffered is shown in figure below.
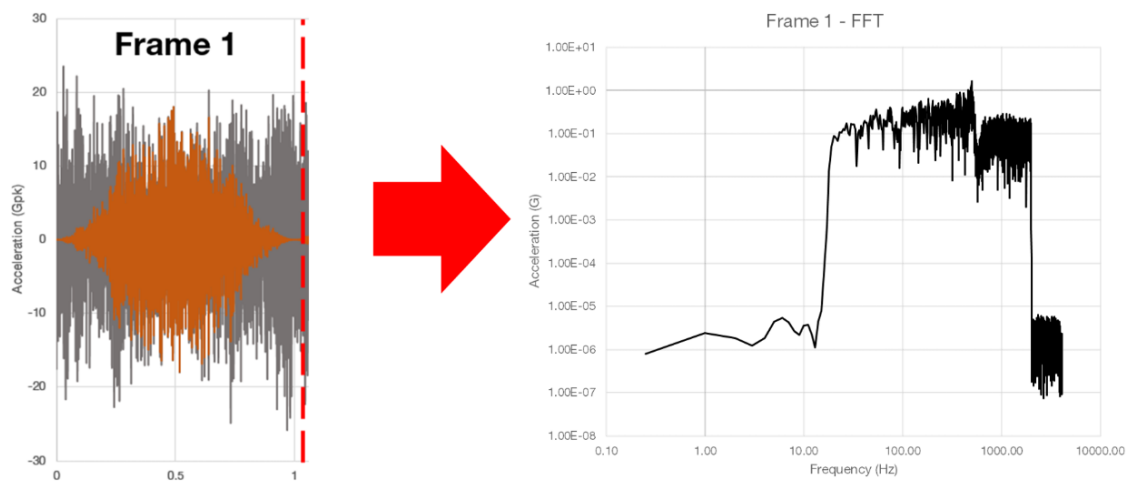
Figure 30. Signal Transformation from Time Domain into Frequency Domain [30]

Advantages of FFT in signal analysis and processing is to show what frequencies are present in a waveform and in what proportion. This is important because this can be used to determine what frequencies are being excited during certain time and the peak acceleration of each frequency.

Next step of this process is to square each frame individually and then it should be averaged together. Since data is divided into frames it would be very useful to include more frames of similar data in the average so that overall variance decreases, and accuracy increase causing the PSD to look much smoother. To simplify things, more FFT's will result in a better PSD. The problem that is happening here is the time that is required to collect and calculate large numbers of FFT's. Final step in the process is to take the squared, averaged FFT and divide by the sample rate. This leads to normalization of everything to a single Hz and creates Power Spectral Density. For acceleration the resulting unit is $(m/s^2)^2/Hz$. PSD is shown in Figure 31.
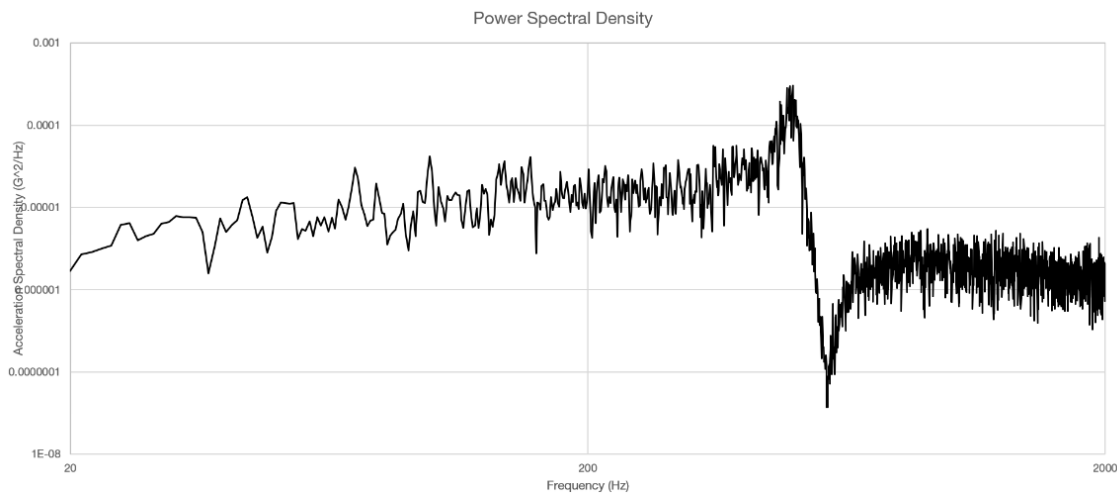
Figure 31. PSD Curve [30]

Adding more frames of data to the PSD, the variance will continue to decrease, and the PSD will become smoother.

If there is a time-history plot, as shown in Figure 32, it is not easy to evaluate the constantly changing acceleration amplitude. Certainly, it is necessary to know if there are any frequencies that cause a large random response at any natural frequencies, but mostly it is necessary to know the overall response of the structure. The square root of the area under PSD curve (grey area) in Figure 32 gives the root mean square (RMS) value of the acceleration, or Grms, which is a qualitative measure of intensity of vibration.
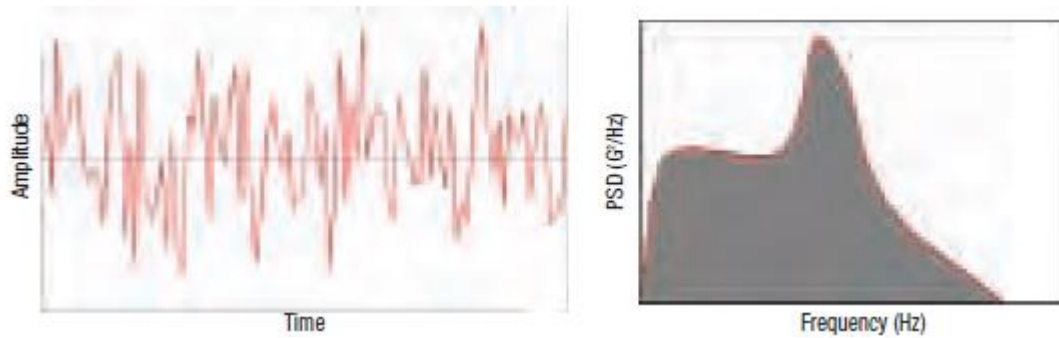
Figure 32. Root Mean Square of the Area Under PSD Curve [28]

3.2.3. *Calculating surface under the PSD curve (root mean square)*

As it is described above there is typical random vibration response curve which is shown in Figure 33. It is necessary to describe the area under Acceleration spectral density (ASD) vs frequency response curve (grey part) by the square root. The ASD values are in G^2/Hz and the frequencies are in Hz.
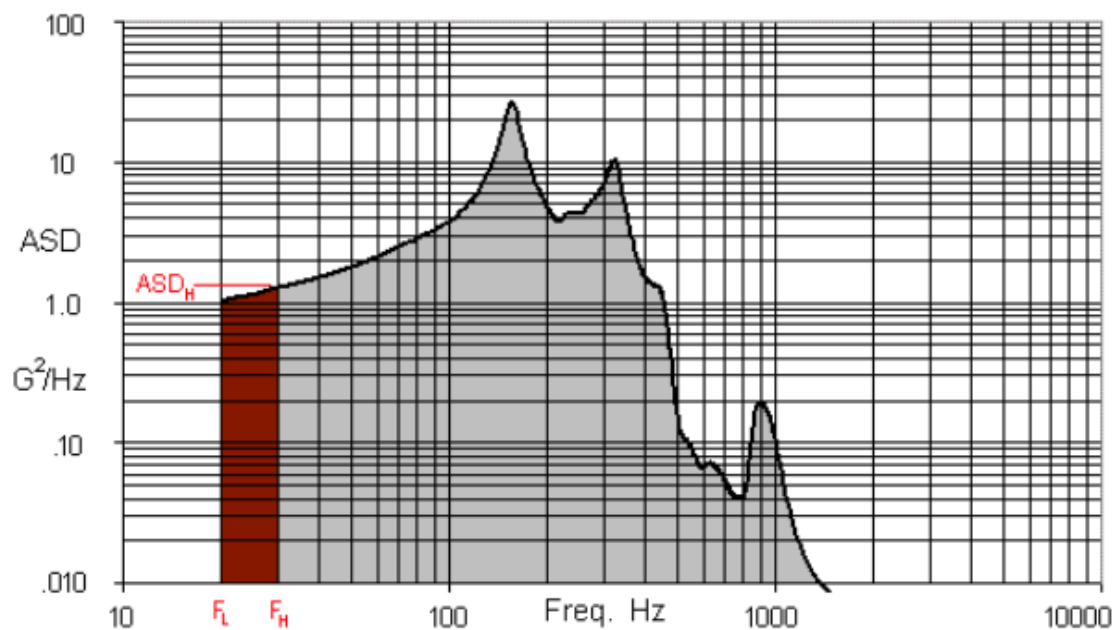
Figure 33. Example of Describing the Area Under the Curve [32]

The process of calculation starts by calculating number of octaves between the two frequencies, where an octave represents unitless doubling of the frequency. The equation to calculate the exact number is [32]:

$$\#octaves = \frac{\log\left(\frac{F_H}{F_L}\right)}{\log(2)} \tag{3.1}$$

Where F_H is the higher frequency and F_L is the lower frequency. Second step includes determination the number of decibel (*dB*), by using logarithmic function of acceleration spectral density. Where decibel is a unitless method of expressing the ratio of two quantities and number of *dB* is described by the following equation:

$$dB = 10\log(ASD_H/ASD_L) \tag{3.2}$$

Where ASD_H and ASD_L are the acceleration spectral densities for the higher and lower frequencies. ASD_L can be greater than ASD_H. Third step is the one where slope, *m*, is calculated of the segment between the frequencies F_L and F_H. The process is done dividing the number of dB by the number of octaves

$$m = dB/\#octaves \tag{3.3}$$

The constants calculated in equations 1.1 through 1.3 cane be used to calculate the area under the curve between the frequencies F_L and F_H.

$$A = 10\log(2)\frac{ASD_H}{10\log(2)+m}\left[F_H - (F_L)\left(\frac{F_L}{F_H}\right)^{m/10\log(2)}\right] \tag{3.4}$$

Finally, last thing that is necessary to do is to take the square root of the area under the curve which is calculated by following equation:

$$g_{rms} = \sqrt{A} \tag{3.5}$$

In order to calculate value for the entire curve it is necessary to sum up all the areas ($A_1 + A_2 + A_3 + \ldots + A_n = A$) and take the square root of the sum.

3.3.   PSD random vibration of connectors

3.3.1.   *Connectors* [33]

The analyst is often faced with modeling problems in which two different parts are connected in some way. Sometimes connections are simple, such as two panels of sheet metal spot welded together, or two plates are bolted together. In other cases, the connection may impose more complicated kinematic constraints, such as constant velocity joints, which transmit constant spinning velocity between misaligned and moving shafts.

Connector elements do not eliminate degrees of freedom (DOF); kinematic constraints are enforced with Lagrange multipliers, which are additional solution variables in Abaqus/Standard. Because of those multipliers force and moment output is provided. Multi-point constraints eliminate degrees of freedom at one of the nodes that is involved in the connection, but connector elements do not eliminate DOF. Because of that, they can be used in many occasions where multi-point constraints cannot be used or do not exist for the function required. An example of when it is good to use connector elements is when it is necessary to connect two rigid bodies at nodes other than the reference node in Abaqus/Standard. The advantage of connectors is the possibility to provide output for those elements, but their disadvantage is that they are not as efficient as for example multi-point constraints and impossibility of applying pretension force. There are two types of connectors that can be used for the analysis: CONN2D2 for two-dimensional and axisymmetric analyses and CONN3D2 for three-dimensional analyses. Both connector elements have at most two nodes, but the position and motion of the second node on the connector element are measured relative to the first node. Since, this analysis is 3D, CONN3D2 elements were used. In Figure 34 it is shown how a shock absorber can be substituted with a simplified connector, which has 2 nodes with the local orientation.
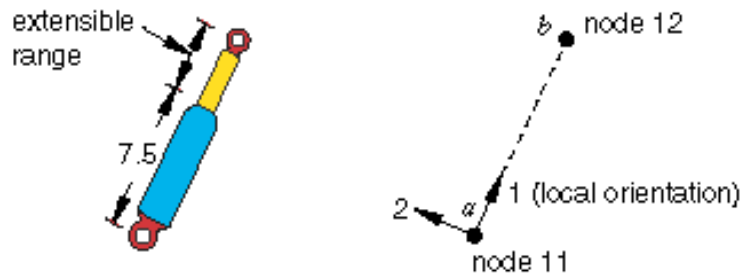
Figure 34. Substitution of Real Part with Connector [33]

From this figure it is possible to see that a local orientation can be used, also it describes how some technical part can be described as equivalent finite element model.

A connector element can be used to connect two point, also can be connected to ground, and the ground node can be the first or second point on the connector element. The initial position of the ground node used for calculating relative position and displacement is the initial position of the other point on the element. All displacements and rotation at the ground node, if they exist, are fixed. Active DOF for the most general connection types are: 1, 2, 3, 4, 5, 6. Figure 35 presents node ordering on elements where ground node can be either the first or second point.
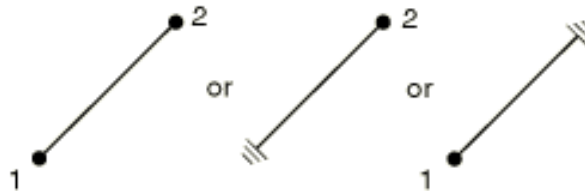
Figure 35. Node Ordering of Connectors [33]

3.3.1.1.   Connectors used in analysis [33]

In the carried-out analysis connector type "Weld" was used. Those types of connectors impose kinematic constraints and use local orientation definitions equivalent to combining connection types join and align. This connector has all degrees of freedom between the two nodes tied in a way that no relative motion or rotation can occur between the two nodes. This connection type Weld is shown in Figure 36.
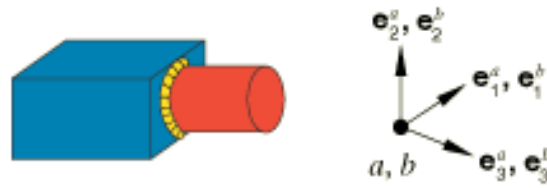
Figure 36. Weld Connectors [33]

It is possible to see that it defines three local directions at node *a* and three local directions at node *b*, which are oriented with e {$e_1^a, e_1^b, \dots, e_3^a, e_3^b$ }.

3.3.2.   *PSD random vibration and RMS output by using Abaqus*

Bolt force assessment was performed by using Abaqus after a random excitation simulation. In the model that is shown in the Figure 37, connectors are representing body of the bolt and the head of the bolt is described as a kinematic coupling. Around the holes where bolts are presented, S4R (shell) or C3D8R (solid) elements were used, depending on the local modelling method. Based on input from PSD, forces that are occurring in connectors were outputted and compared to the existing data from experiment (bolt re-tightening), to check if there is any correlation. The model used in the analysis was modeled with shell and solid elements counting in total 3813437 elements.
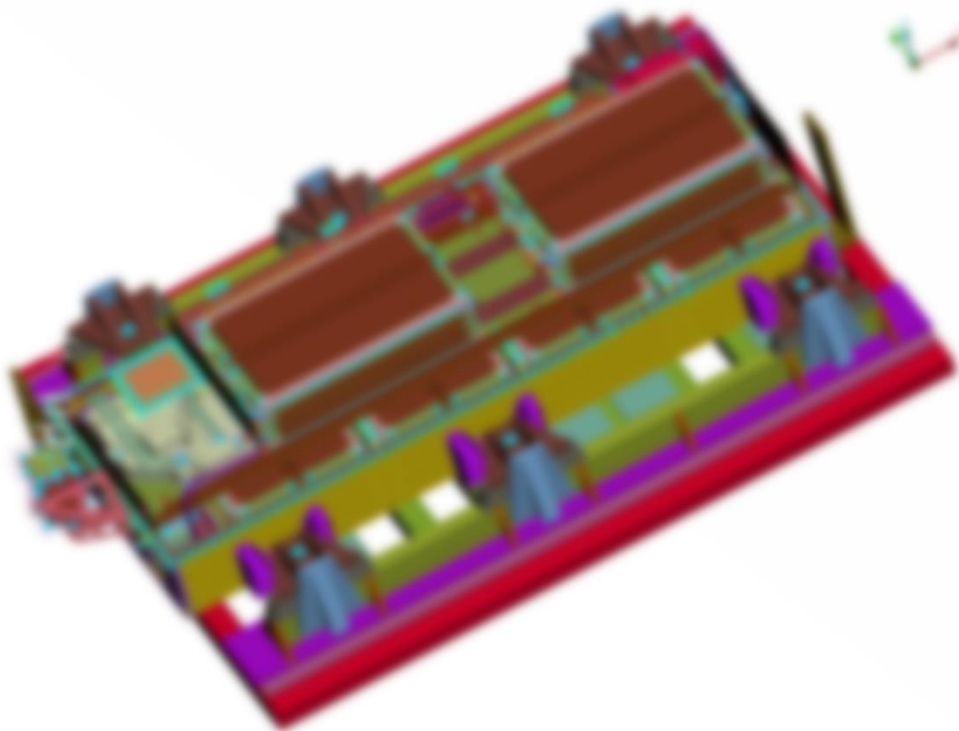
Figure 37. Model Used in Analysis

The input that was used for analysis in sight of acceleration spectral density (ASD) is shown in the figure below. It was performed only in Z direction, based on standard ISO 12405. Also, table 1 below shows the exact values of the ASD curve.
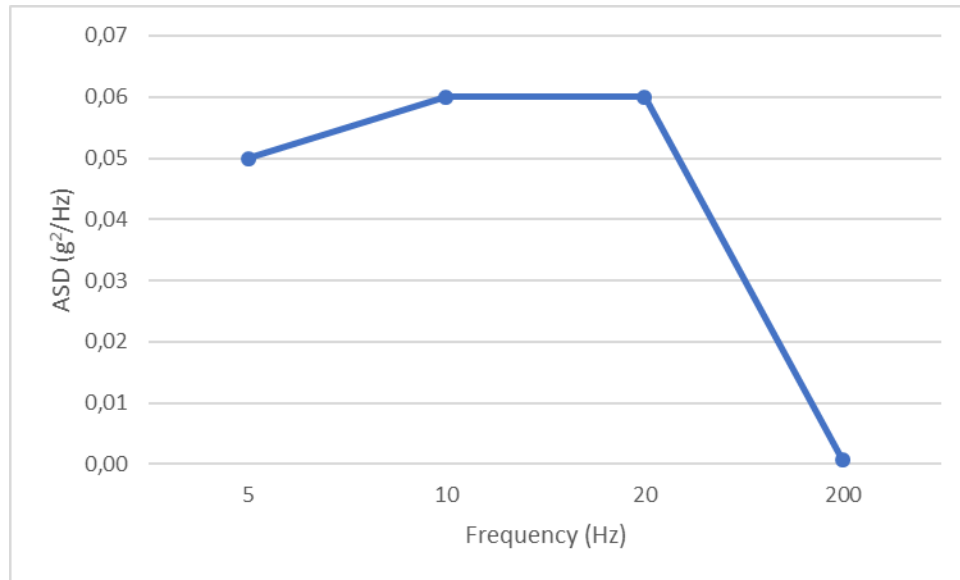
Figure 38. ASD Input

Table 1: Dana Used as an Input

Frequency (Hz)	ASD g²/Hz
5	0,049981244
10	0,059956711
20	0,059956711
200	0,000831289

Furthermore, forces in connectors were outputted and are listed below in the table. Also, those values were compared to the remaining torque, which was estimated with retightening method. That method is described below.

3.3.2.1.   *Retightening method* [34]

A bolt retightening method was used to try and evaluate the post testing bolt pretension. This method requires that additional toque is applied to a bolt which has already been tightened, and then measures the torque value when the bolt begins to move again. Two different method were used, the B-point method and the A-point method. Those two methods are shown in Figure 39.
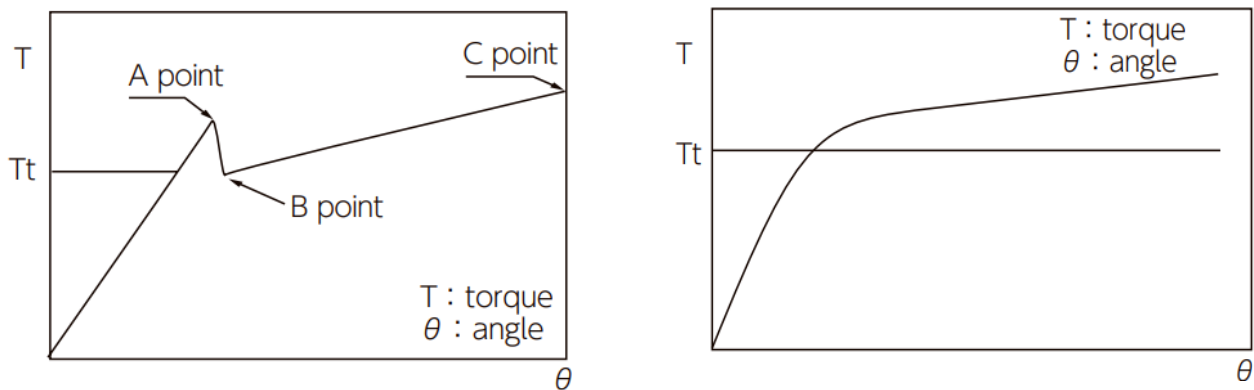
Figure 39. B-Point Method (Left) and A-point Method (Right)[34]

The left side in Figure 39 shows the B-point method where point A represents torque when the static friction of the bolt is exceeded. Point B is the torque after stabilization of slipping which corresponds to the torque after the testing. If there is no pretension loss it should match the initial value, and point C shows maximum torque detected by inspection.

Point B is expected to correspond to the tightening torque of the bolt, if the torque varies from initially applied torque then bolt pretension loss is expected to have occurred. If the response does not match that, which is observed on the left side in Figure 39, then the response on the right is generally observed and the A-point method is used. A disadvantage of the A-point method is that it is less accurate than the B point method, but it is still the next best option when B point is not available.

Still, it is necessary to emphasize that the breakaway method which corresponds to the A-point method is the preferred one for the measurement of residual torque where that is possible. In Figure 40 two graphs are presented for breakaway method where ideal is shown on the left and the real characteristic on the right.
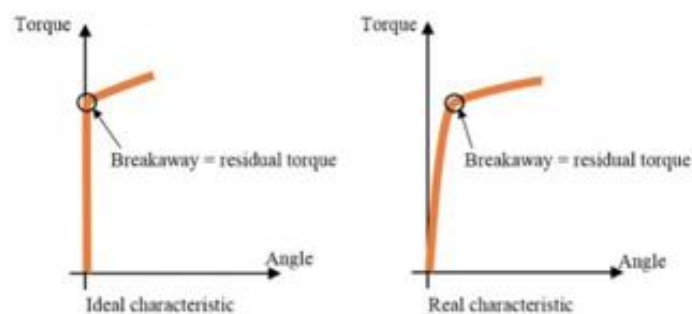
Figure 40. Ideal and Real Characteristic Breakaway Method [34]

But, since the B-point method was mostly used, in Figure 41 shows where the breakaway torque is and where the residual torque is in that method.
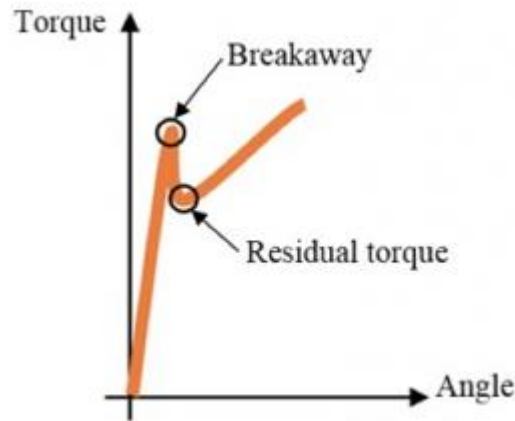
Figure 41. Breakaway and Residual Torque in B-Point Method [34]

3.3.2.2.   Results and comparison with existing data

Below is the table 2 that contains forces data in all three directions. In this table shear forces are representative of summed squares under the root for directions *x* and *y*:

$$F_{\text{shear}} = \sqrt{F_x^2 + F_y^2}$$

(3.6)

Forces in *z* direction are representative for axial forces. In the end, to get magnitude value of all forces it is necessary to sum squared values under the root of shear and axial forces:

$$F_{\text{magnitude}} = \sqrt{F_{\text{shear}}^2 + F_{axial}^2}$$

(3.7)

 The test data shows that some bolts, but not all, are seeing bolt loosening during mechanical testing based on the re-tightening method. Because of that all force's values are compared to

the torque that remained after the experiment, which was validated with retightening method, method that is described above.

Table 2: RMS Forces of Connectors Comparing to Retightening Torque

Bolt	Forces (N)					Initial Torque (Nm)	Retightening Torque (Nm)
	X	Y	Shear Forces	Z (Axial Forces)	Magnitude		
M8x200	3,25	9,61	10,14	56,73	57,63	22	15,83
M8x200	24,34	43,61	49,94	529,43	531,78	22	13,96
M8x200	28,53	44,52	52,88	462, 9	465,92	22	17,37
M8x200	3,34	11,95	12,41	22,38	25,59	22	5,31
M8x200	1,17	7,48	7,57	84,41	84,75	22	17,5
M8x25	192,79	479,04	516,38	536,16	744,39	22	25,35
M8x25	95,02	289,08	304,30	457,22	549,23	22	26,48
M8x25	113,63	333,91	352,71	387,89	524,27	22	26,08
M8x25	212,52	429,03	478,78	526,14	711,37	22	Fractured
M8x25	87,62	319,93	331,71	397,49	517,71	22	Fractured
M6x16	19,92	1,36	19,97	3,37	20,25	8	7,2
M6x16	11,46	3,27	11,92	23,87	26,68	8	7,87
M6x16	6,77	2,39	7,18	11,49	13,55	8	3,31
M6x16	6,18	11,08	12,69	17,22	21,39	8	4,4
M6x14	1,81	12,18	12,31	6,18	13,77	8	7,14
M6x14	3,69	6,33	7,33	3,84	8,28	8	6,7
M6x14	5,58	9,69	11,18	7,53	13,47	8	6,8
M6x14	9,16	4,56	10,23	3,26	10,74	8	6,38
M6x12	50,4	54,09	73,93	56,45	93,02	5	4,51
M6x12	47,53	55,74	73,25	61,18	95,44	5	4,07
M6x12	11,34	12,66	17,00	14,.03	22,04	5	3,42
M6x12	6,83	20,56	21,66	7,81	23,03	5	3,42

In the Table 2 green results of retightening torque present 80% or more of the initial torque (those results are good ones, and are satisficing results), yellow results are presenting from 60% to 80% of the initial torque, and they still satisfy criteria of not loosening bolts. But red results as it can be assumed present not satisfying results and they present below 60% of initial torque, which is not enough to satisfy criteria. Since, it would be logical that those bolts that during the experiment lost most of the initial torque are having the highest forces values in connectors, either shear, or axial, or magnitude forces it can be concluded that those results are not comparable. The outcome indicates that either retightening method is not accurate, or the model is way too simplified. Maybe instead of using connectors, it would be better to use different type of the element for describing the body of the bolt. Also, regarding the method for

measuring what is happening in the bolt, it would be useful to have different method, which would give more accurate results, like strain gauges. Furthermore, parameters like temperature were not considered, and they could also affect the outcome. Because of that, further investigations are necessary and are going to be described in the following chapters.

4. VISCOELASTIC BEHAVIOUR OF COPPER AND NUMERICAL MODELLING OF VISCOELASTIC PROBLEM

Viscoelasticity is the property of the materials that are exposed to viscous and elastic characteristics when certain stress is applied. That type of phenomenon is still not very investigated, but certain models to describe that behavior of material exist. In the following sections theoretical background of viscoelasticity and numerical verification of viscoelasticity are going to be shown.

4.1. Theory of viscoelasticity [35]

Defining dependency between deformation, stress, speed of deformation and time can be described with basic mechanical models of deformable bodies. Basic elements are elastic and viscous element. These elements are shown in Figure 42, where the elastic element is described with linear elastic spring and viscous elements with viscous damper.
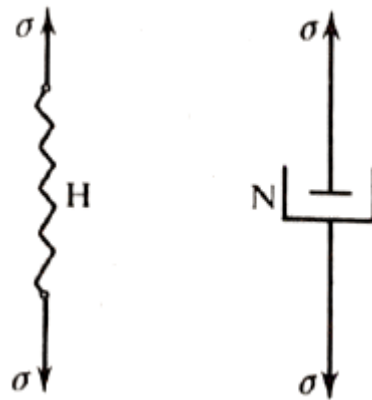
Figure 42. Elastic Spring (Left) and Viscous Damper (Right) [35]

In Figure 42 the stress σ that is occurring in the spring can be described by Hook's law:

$$\sigma = E\varepsilon \tag{4.1}$$

whereas, the stress that is occurring in the damper can be described as:

$$\sigma = \eta\dot{\varepsilon} \tag{4.2}$$

Where η presents coefficient of viscous damping, and $\dot{\varepsilon}$ presents velocity of deformation.

Stresses and deformations that are occurring when a certain load is applied on a deformable body are changing with time even though that load is not changing with the time. That phenomenon is called creep of material. One shape of that phenomenon when deformation is

changing with the time is called creep and the other when stress is changing with the time is called relaxation.

Creep is happening when a constant stress is occurring, while strain is increasing continuously and asymptotically toward some value. It can be at the same time elastic and plastic. In Figure 43 a classical graph of creep with the constant stress is shown.
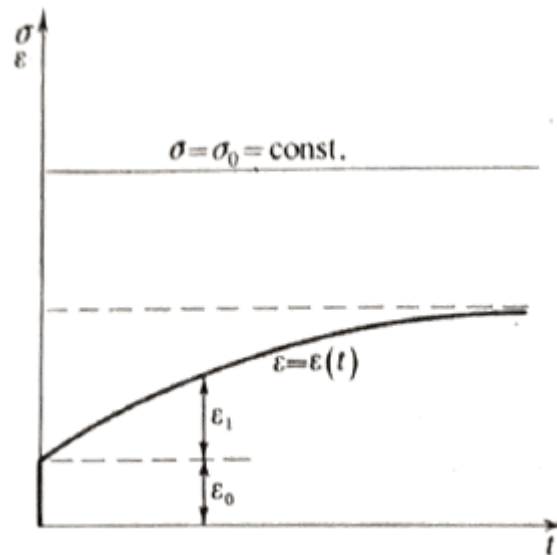
Figure 43. Strain Increase with the Constant Stress [35]

On the other hand, relaxation is observed with the constant strain. Consider that a tensile force is being applied to a stick, and it caused stress, which value is lower than the yield point. When that stress is applied it causes a given deformation, which remains constant. That deformation is equal to the sum of elastic ε_e and viscoelastic ε_v deformations.

$$\varepsilon = \varepsilon_e + \varepsilon_v \tag{4.3}$$

The viscoelastic deformation is increasing with time, which means that elastic deformation has to reduce with time. From that situation it can be concluded that components of total deformations are reallocating during the time. Total deformation is not changing with the time and it is equal to the initial deformation. Since, at the beginning there is elastic deformation, Hook's law can be applied here.

$$\varepsilon = \varepsilon(0) = \frac{\sigma(0)}{E} \tag{4.4}$$

When equations (4.4) and (4.1) are inserted into equation (4.3), the following equation looks like:

$$\frac{\sigma(0)}{E} = \frac{\sigma}{E} + \varepsilon_v \tag{4.5}$$

Where $\sigma(0)$ is stress at the beginning. It is possible to notice that viscoelastic deformation with the time is increasing, so because of that stress σ has to continuously decrease. Also, from equation (4.5) can be concluded that viscoelastic deformation ε_v can't be increased infinitely. In the process of relaxation, viscoelastic deformation ε_v is not exceeding the value of deformation that was happening in the initial condition, ($\varepsilon(0) = \sigma(0)/E$). In the process of relaxation viscoelastic deformation e_v is not exceeding the value that it had at the initial moment.

During relaxation experiment, an initial load is applied and the length of the object has to stay constant. After that, the stress drop is being measured over the time and the curve of relaxation can be generated. The phenomenon of relaxation in some soft metals is already noticeable at room temperature. Also, the main characteristic of relaxation calculation is time, which is not included in standard static calculations. In Figure 44 a typical relaxation curve with constant strain is shown.
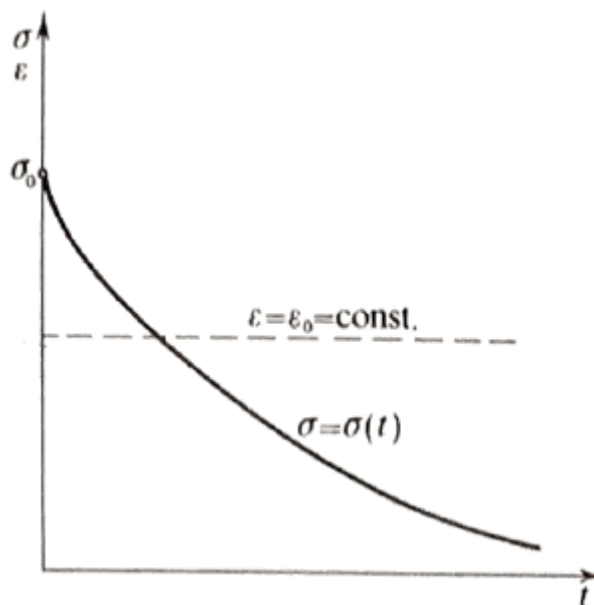
Figure 44. Stress Drop with the Constant Strain [35]

4.1.1. *Linear - elastic behavior of the material* [37]

Constitutive equation, which describes linear elastic deformation of stress strain can be written as the following expression:

$$\sigma_{ij} = D_{ijkl}\varepsilon_{kl}^{e} \tag{4.6}$$

In equation (4.6) D_{ijkl} is the fourth order elasticity tensor, while stress and strain tensors are of second order. In general case (anisotropic material), D_{ijkl} consists of 36 coefficients, and those coefficients can be described with 21 independent material constants. For isotropic materials matrix components of elasticity can be described with two independent constants: Young's modulus of elasticity E, and shear modulus G. The connection between modulus of elasticity and shear modulus is Poisson's ration v, and it follows the following relationship:

$$\frac{E}{G} = 2(1 + v) \tag{4.7}$$

The tensor of elasticity for linear isotropic material is equal to:

$$D_{ijkl} = \lambda\delta_{ij}\delta_{kl} + \mu(\delta_{ik}\delta_{jl} + \delta_{il}\delta_{jk}) \tag{4.8}$$

In equation (4.8) λ and μ are Lame parameters, with the following equation:

$$\lambda = \frac{vE}{(1+v)(1-2v)}, \tag{4.9}$$

$$\mu = G = \frac{E}{2(1+v)}. \tag{4.10}$$

and δ_{ij} is Kronecker symbol, which takes values to the following agreement:

$$\delta_{ij} = \begin{cases} 1, i = j \\ 0, i \neq j \end{cases} \tag{4.11}$$

4.1.2. Viscoelastic behavior of the material

With a combination of an elastic and viscous body, various viscoelastic materials can be described. By that description of the viscoelastic material's behavior, real materials can be approximated.

4.1.2.1. Voight-Kelvin model [35]

That type of material can be shown with a rheological model of elastic spring and viscous damper that are connected in parallel. That rheological model is shown in Figure 45.
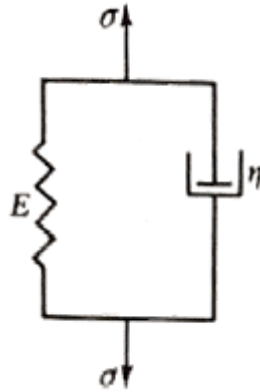
Figure 45. Voight-Kelvin Model [35]

For this model following things apply:

$$\sigma = \sigma_e + \sigma_v \qquad\qquad (4.12)$$

$$\varepsilon = \varepsilon_e = \varepsilon_v \qquad\qquad (4.13)$$

Putting equations (4.1) and (4.2.) into (4.12), the following expression is obtained:

$$\sigma = E\varepsilon + \eta\dot{\varepsilon} = (E + \eta\frac{d}{dt})\varepsilon \qquad\qquad (4.14)$$

For calculation of creep $\sigma = \sigma_0$, and it has to be constant. By using that relation, equation (4.14) becomes an inhomogeneous differential equation which looks like:

$$\sigma_0 = E\varepsilon + \eta\frac{d\varepsilon}{dt} \qquad\qquad (4.15)$$

A general solution of differential equation would be:

$$\varepsilon = \varepsilon_h + \varepsilon_p \tag{4.16}$$

That equation consists of a homogeneous equation and a particular integral. The homogeneous equation would look like:

$$0 = E\varepsilon + \eta\frac{d\varepsilon}{dt} \tag{4.17}$$

$$\varepsilon_h = Ce^{rt} \tag{4.18}$$

$$\dot{\varepsilon}_h = Cre^{rt} \tag{4.19}$$

Substituting equations (4.18) and (4.19) into (4.17), and editing the expression, gives the following:

$$0 = 1 + r\frac{\eta}{E} \tag{4.20}$$

Now it is necessary to use an expression that is called the time of creep or relaxation.

$$\tau = \frac{\eta}{E} \tag{4.21}$$

Now, after substituting expression (4.21) into (4.20), editing the expression, and substituting it into equation (4.18), the following is obtained:

$$\varepsilon_h = Ce^{\frac{-t}{\tau}} \tag{4.22}$$

After solving the homogeneous equation, it is necessary to solve particular integral:

$$\varepsilon_p = at + b \tag{4.23}$$

$$\dot{\varepsilon}_p = a \tag{4.24}$$

Substituting equations (4.23) and (4.24), and using expression (4.21) into (4.15), the following equation is obtained:

$$\varepsilon_p = \frac{\sigma_0}{E} \qquad (4.25)$$

Now, expressions (4.25) and (4.22) has to be substituted into expression (4.16), and it is necessary to use the initial conditions ($t = 0$ and $\varepsilon = 0$) to get an equation that is describing the creep of material:

$$\varepsilon = \frac{\sigma_0}{E}(1 - e^{\frac{-t}{\tau}}) \qquad (4.26)$$

Also, this type of procedure for defining the equation that is describing relaxation is necessary to perform. To calculate relaxation $\varepsilon = \varepsilon_0$ has to be constant. Since that has to be constant, $\dot{\varepsilon}=0$, and putting that in equation (4.15), the following expression is obtained:

$$\sigma_0 = E\varepsilon \qquad (4.27)$$

From this equation it can be concluded that the Voight-Kelvin model can't describe relaxation properly, but this model is still good enough to describe the phenomenon of creep. Also, in the following figure the creep of the material is presented, which is described by Voight-Kelvin model.
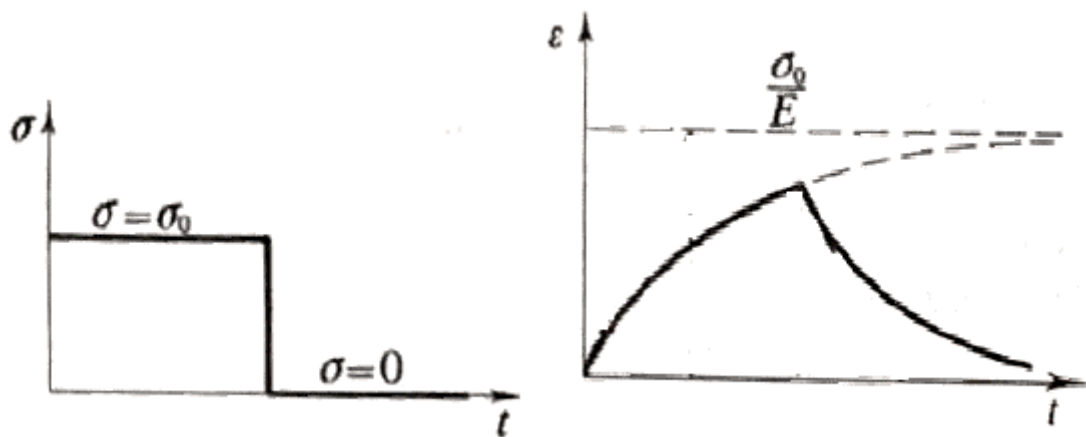
Figure 46. Creep behavior of material based on Voight-Kelvin model [35]

4.1.2.2. *Maxwell model* [35]

Just like the Voight-Kelvin model, this type of model is also going to be described as a rheological model with an elastic spring and a viscous damper, but they will be connected in series. It is shown in Figure 47, how this model looks.

Figure 47. Maxwell Model [35]

Since here is a series connection, the following things apply for this model:

$$\sigma = \sigma_e = \sigma_v \tag{4.28}$$

$$\varepsilon = \varepsilon_e + \varepsilon_v \tag{4.29}$$

Now, it is necessary to derive expression (4.29) to get.

$$\dot{\varepsilon} = \dot{\varepsilon}_e + \dot{\varepsilon}_v \tag{4.30}$$

Using expression (4.2), deriving expression (4.1) and putting everything in equation (4.30), the following expression is obtained:

$$\dot{e} = \frac{\dot{\sigma}}{E} + \frac{\sigma}{\eta} \tag{4.31}$$

This is a differential equation of the Maxwell model. Now, it is necessary to apply the same procedure as it was done for the Voight-Kelvin model.

Just like in the Voight-Kelvin model, in the Maxwell model $\sigma = \sigma_0$, and it has to be constant. Because of that, when σ is derived, it becomes zero. If all these relations are put in equation (4.31), and initial conditions are used ($t = 0$, $\varepsilon = \frac{\sigma_0}{E}$), the equation of creep is obtained for the Maxwell model:

$$\varepsilon = \frac{\sigma_0}{\eta} t + \frac{\sigma_0}{E} \tag{4.32}$$

Now, the same process has to be defined for relaxation. It has to start from the relation that $\varepsilon = \varepsilon_0$, and it has to be constant. Therefore, after ε is derived, it becomes zero. This relation has to be used and put in equation (4.31).

$$0 = \frac{\dot{\sigma}}{E} + \frac{\sigma}{\eta} \qquad (4.33)$$

It is necessary to use a homogeneous equation with the stress:

$$\sigma = Ce^{rt} \qquad (4.34)$$

$$\dot{\sigma} = Cre^{rt} \qquad (4.35)$$

Equations (4.34) and (4.35) with the time of relaxation (4.21) have to be used and substituted into equation (4.33). After these things and initial conditions are used ($t = 0$, $\sigma = \sigma_0$), the following equation describing the relaxation of the material is obtained. If the time of relaxation is higher, stress will drop slower.

$$\sigma = \sigma_0 e^{\frac{-t}{\tau}} \qquad (4.36)$$

It can be concluded that the Maxwell model can describe relaxation very well. It is a useful model for some materials like thermoplastic polymers, soft metals, and fresh concrete, but it has a problem in describing the creep of materials. Because it describes it as a linear behavior but in reality, those materials are not behaving linearly.
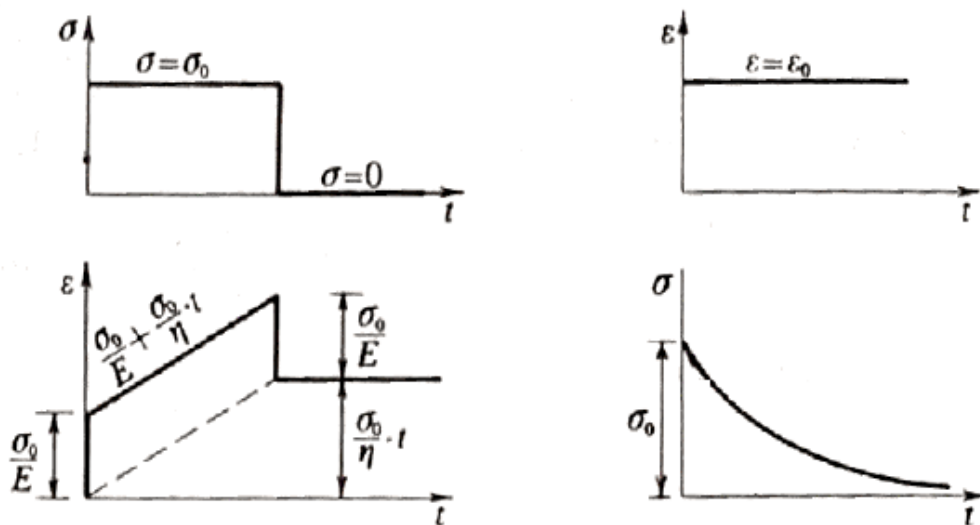
Figure 48. Creep Behaviour of Material (left), and Relaxation Behaviour of Material (right) Based on Maxwell Model [35]

4.2.   Copper stress relaxation experiments

It is necessary to investigate the behavior of copper and stress loss with constant strain. Also, it has to be defined, which model suits the behavior of the copper. Because of that, in this section, some relaxation experiments on copper are going to be shown.

In the first that was done by Riggins [38] , chickens from the day of hatching, were fed with the copper supplemented skim milk for 20 days, so that their bones can adopt as much copper characteristic as possible. After 20 days, chicken bones were taken for the experiment. The stress relaxation experiments were performed by putting the bone in the machine, fixing it and allowing the temperature to stabilize for 15 minutes. After everything was stabilized, the stress relaxation experiment was performed for 30 minutes. In Figure 49 are shown the results of chicken bone.
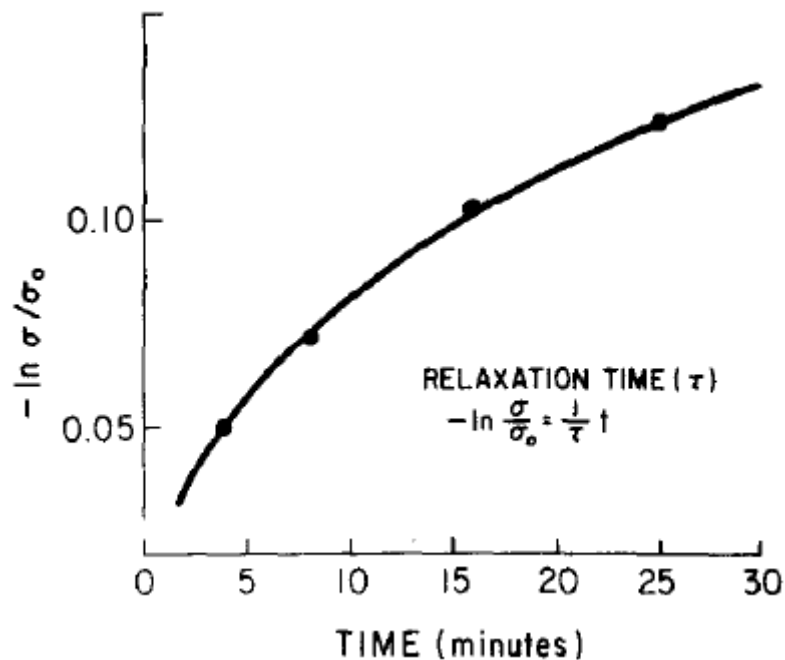
Figure 49. Relaxation of Copper Supplemented Bone [38]

In the second test copper with ng (nanograined), nt (nanotwinned), and cg (coarse-grained) microstructures were used. Pure copper of 3 mm thickness was annealed for four hours at 400 °C to get a cg microstructure. High pure ng and nt were synthesized with $CuSO_4$ electrolyte. The stress-relaxation tests were carried out on a universal testing machine at room temperature. After the dog-bone shaped specimens were placed in the machine, they were stretched, to obtain a certain stress level. That stress level was 115 MPa for the cg, 350 MPa for ng, and 550 MPa for nt microstructure. When the desired stress level for each microstructure was reached, the

process of relaxation, with the constant strain started. Each specimen was monitored as a function of time for 300 seconds [39]. In the following figure, the stress drop versus relaxation time at room temperature is shown.
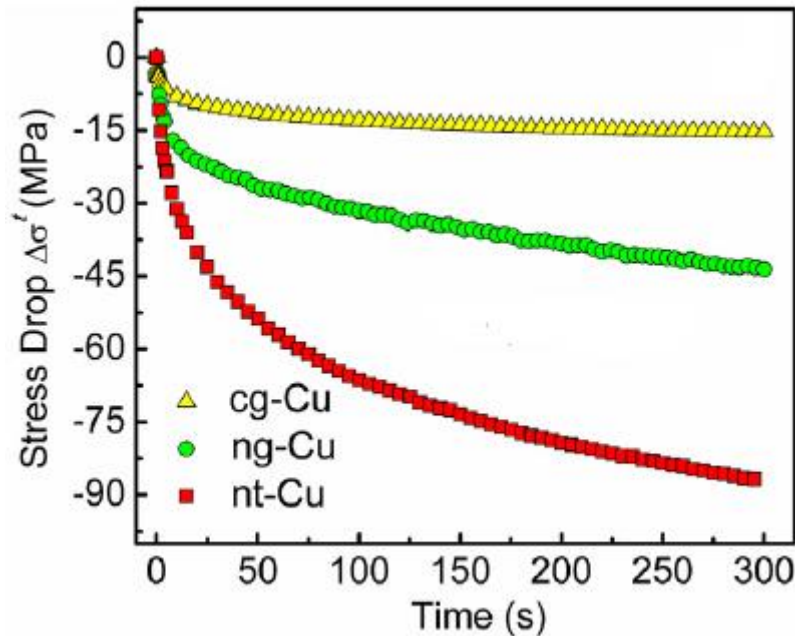
Figure 50. The Stress Drop Versus Time for 3 Different Microstructures [39]

In figure 50, stress drop $\Delta\sigma^{\mathrm{t}}$ presents difference, which can be expressed as $\Delta\sigma^{\mathrm{t}} = \sigma(t) - \sigma_0$, where σ_0 is initial stress. Since for different microstructures, different initial stresses were applied stress drop in 300 seconds of relaxation was different. Also, it is possible to see, in this case, when initial stress is bigger it will result in a bigger stress drop.

Comparing Figure 48 with Figures 49 and 50, it is possible to notice that copper's behavior suits very well to the Maxwell model. In figure 49, the graph is made as a logarithmic function, instead of an exponential function, because $\ln(e) = 1$. Theoretical background says that the Maxwell model is convenient for describing stress relaxation. Because of that, that type of model is going to be used for describing the viscoelastic behavior of the material. Then, that material is going to be used to describe the finite element (FE) model.

4.3.   Numerical viscoelastic analysis [40], [41][42]

When nonlinear analysis is observed, which relaxation of material is, various types of nonlinearity exist:

- Material nonlinearity (viscoelasticity, relaxation, creep, plasticity)
- Nonlinear boundary conditions (contacts)
- Geometric nonlinearity (buckling, large strain, large displacements)

Usually a problem can consist of multiple nonlinear combinations. When the material's behavior is nonlinear displacements are not directly proportional to loading. Because of that, the superposition principle can't be used. The global finite element equation for nonlinear problems is expressed as follows:

$$\mathbf{K(V, R)V = R} \tag{4.37}$$

In that equation $\mathbf{V}$ is global nodal displacement vector, $\mathbf{R}$ is global nodal force vector, and $\mathbf{K}$ is global stiffness matrix. Global matrix depends on current displacement and load. This process is not possible to solve in a single step. To solve the process incremental-iterative methods have to be applied. To apply that method, it is necessary to linearize equation (4.37), whereby from basic equilibrium is seeking a balance of near station, which is defined by an increment of load or displacement. After linearization is applied, equation (4.37) takes the form:

$$\mathbf{K_t(\overline{V})\Delta V = R_{ext} - R_{int}(\overline{V})} \tag{4.38}$$

In that equation, $\mathbf{\overline{V}}$ is initial displacement vector, $\mathbf{\Delta V}$ is incremental displacement vector, $\mathbf{R_{ext}}$ is external force vector, $\mathbf{R_{int}}$ is internal force vector, and $\mathbf{K_t}$ is tangent stiffness matrix.

Equilibrium will be achieved when external and internal forces are equal, which will lead that the right side of equation is equal to 0. Also, in that situation it could mean that $\mathbf{\Delta V}$ is zero. That type of nonlinearity between load and displacement is shown in Figure 51.
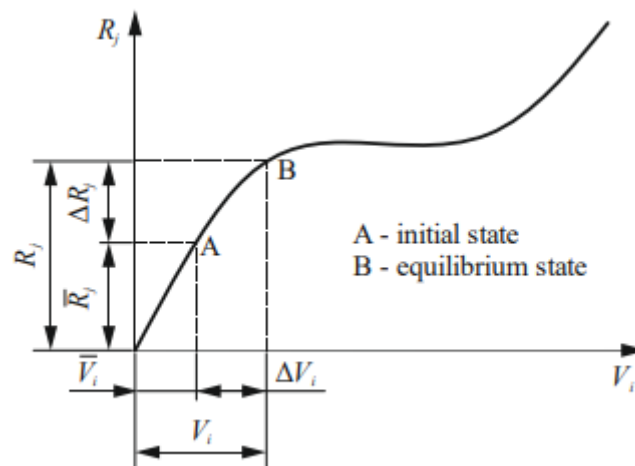
**Figure 51. Typical Nonlinear Relationship Between
Load and Displacement [40]**

The procedure of nonlinear numerical analysis starts by solving equation (4.38). From that equation, global displacement increments can be extracted and those displacements are transformed into local coordinate systems of finite elements, from which strain increments are calculated. In every integration point of each finite element increments of deformation are integrated so that stress increment can be obtained:

$$\Delta\sigma = \int_{\varepsilon}^{\varepsilon+d\varepsilon} D^{ep}\, d\varepsilon \tag{4.39}$$

The backward Euler method that is based on the return mapping algorithm is a method, which is used for integration of the constitutive equation. In each interval, it consists of the elastic predictor and the plastic corrector. Elastic predictor examines if the model in a certain point of integration is in elastic or plastic area. If the elastic predictor falls outside the yield surface, it means that the assumption of elasticity was wrong. In that case it is necessary that the updated stress is obtained by the plastic corrector. But this thesis is dealing with the viscoelastic problem, which means that stress that is applied in the material should be below the yield point. When stress increment can be calculated and it can be used to update elasto-plastic stiffness tensor $\mathbf{D^{ep}}$. Considering material nonlinearity, the tangent stiffness matrix for elasticity can be written:

$$\mathbf{k_t} = \mathbf{k_e} + \mathbf{k_{uL}} + \mathbf{k_{uN}} + \mathbf{k_{\sigma L}} + \mathbf{k_{\sigma N}} \tag{4.40}$$

where:

$$\mathbf{k}_e = \int_V \mathbf{B}_L^T \mathbf{D} \mathbf{B}_L \, dV \text{ is elastic stiffness matrix} \tag{4.41}$$

$$\mathbf{k}_{uL} = \int_V (\mathbf{B}_L^T \mathbf{D} \mathbf{B}_N(\overline{\mathbf{v}}) + \mathbf{B}_N^T(\overline{\mathbf{v}}) \mathbf{D} \mathbf{B}_L) \, dV \text{ is linear initial displacement matrix} \tag{4.42}$$

$$\mathbf{k}_{uN} = \int_V \mathbf{B}_N^T(\overline{\mathbf{v}}) \mathbf{D} \mathbf{B}_N(\overline{\mathbf{v}}) \, dV \text{ is nonlinear initial displacement matrix} \tag{4.43}$$

$\mathbf{k}_{\sigma L}$ is linear initial stress matrix

$\mathbf{k}_{\sigma N}$ is nonlinear initial stress matrix

In equations above $\mathbf{D}$ stands for elasticity matrix, while $\mathbf{B}_L = \mathbf{D}_{KL}\mathbf{N}$, and $\mathbf{B}_N = \mathbf{D}_{KN}\mathbf{N}$ stand for linear and nonlinear strain-displacement matrices, respectively where $\mathbf{D}_{KL}$ is linear kinematic differential operator, and $\mathbf{D}_{KN}$ is a nonlinear kinematic differential operator. Also, $\mathbf{N}$ represents the shape function matrix. The elastic stiffness matrix, linear initial displacement matrix and nonlinear initial displacement matrix together form the elastic stiffness matrix $\mathbf{k}_{eU}$, while linear initial stress matrix and nonlinear initial stress matrix together form initial stress matrix $\mathbf{k}_\sigma$. Those matrices can be expressed as:

$$\mathbf{k}_\sigma \Delta \mathbf{v} = \int_V (\mathbf{B}_N^T(\Delta \mathbf{v}) \mathbf{D}(\mathbf{B}_L + \frac{1}{2}\mathbf{B}_N(\overline{\mathbf{v}})) \, dV \, \overline{\mathbf{v}} \tag{4.44}$$

From equation (4.44) the linear and nonlinear initial stress matrices are expressed as follow:

$$\mathbf{k}_{\sigma L} \Delta \mathbf{v} = \int_V (\mathbf{B}_N^T(\Delta \mathbf{v}) \mathbf{D} \mathbf{B}_L \, dV \, \overline{\mathbf{v}} \tag{4.45}$$

$$\mathbf{k}_{\sigma N} \Delta \mathbf{v} = \frac{1}{2} \int_V \mathbf{B}_N^T(\Delta \mathbf{v}) \mathbf{D} \mathbf{B}_N(\overline{\mathbf{v}}) \, dV \, \overline{\mathbf{v}} \tag{4.46}$$

Now, along with tangent stiffness matrix $\mathbf{k}_t$, both external and internal forces $\mathbf{R}_{ext}, \mathbf{R}_{int}$ can be calculated as follows:

$$\mathbf{R}_{ext} = \int_V \mathbf{N}^T(\overline{\mathbf{q}} + \Delta \mathbf{q}) \, dV + \int_S \mathbf{N}_S^T(\overline{\mathbf{q}}_b + \Delta \mathbf{q}_b) \, dS \tag{4.47}$$

$$\mathbf{R_{int}} = \int_V (\mathbf{B_L} + \mathbf{B_N}(\bar{\mathbf{v}}))^T \mathbf{D}(\mathbf{B_L} + \frac{1}{2}\mathbf{B_N}(\bar{\mathbf{v}}))dV\bar{\mathbf{v}} \tag{4.48}$$

In those equations $\mathbf{q}$ is the volume load vector, $\mathbf{q_b}$ is the surface load vector, and $\mathbf{N_s}$ stands for the edge shape function matrix.

4.4. Elements used for viscoelastic analysis [33][43]

4.4.1. *Quadratic tetrahedral element*

The first element used in the analysis is 3D second order solid tetrahedron (10 nodes) with full integration (10 integration points). In SIMULIA Abaqus this type of element is named C3D10. One element with 10 nodes is shown in Figure 52.

Figure 52. Quadratic Tetrahedral Element [33]

As it was mentioned above and it can be seen from the figure this element has 10 nodes. Since each node has three degrees of freedom, that is in total 30 degrees of freedom per element. Those 3 degrees of freedom are oriented in all 3 directions of the Cartesian coordinate system. Element nodal displacement vector is:

$$\begin{aligned} \mathbf{v}^T &= [\mathbf{v}_1 \quad \mathbf{v}_2 \quad \mathbf{v}_3 \quad \mathbf{v}_4 \quad \mathbf{v}_5 \quad \mathbf{v}_6 \quad \mathbf{v}_7 \quad \mathbf{v}_8 \quad \mathbf{v}_9 \quad \mathbf{v}_{10}] \\ \mathbf{v}_i^T &= [u_i \quad v_i \quad w_i], \ i=1,2,3,\ldots,10 \end{aligned} \tag{4.49}$$

Displacement components in Cartesian coordinate system can be expressed as follow:

$$u = a_1 + a_2x + a_3y + a_4z + a_5x^2 + a_6y^2 + a_7z^2 + a_8xy + a_9yz + a_{10}xz$$

$$v = a_{11} + a_{12}x + a_{13}y + a_{14}z + a_{15}x^2 + a_{16}y^2 + a_{17}z^2 + a_{18}xy + a_{19}yz + a_{20}xz \quad (4.50)$$

$$w = a_{21} + a_{22}x + a_{23}y + a_{24}z + a_{25}x^2 + a_{26}y^2 + a_{27}z^2 + a_{28}xy + a_{29}yz + a_{30}xz$$

In this way, this element, which is a second order element can describe the linear stress field. Therefore, it can describe fields of pure bending exactly.

An advantage of this element is that it can provide geometrical versatility and because of that most meshing algorithms use this type of element.

4.4.2   Linear brick element

The second element used in the analysis of this thesis, is 3D first order solid hexahedron (linear brick with 8 nodes), with full integration (8 integration points). In SIMULIA Abaqus this type of element is named C3D8, and it is shown in Figure 53.

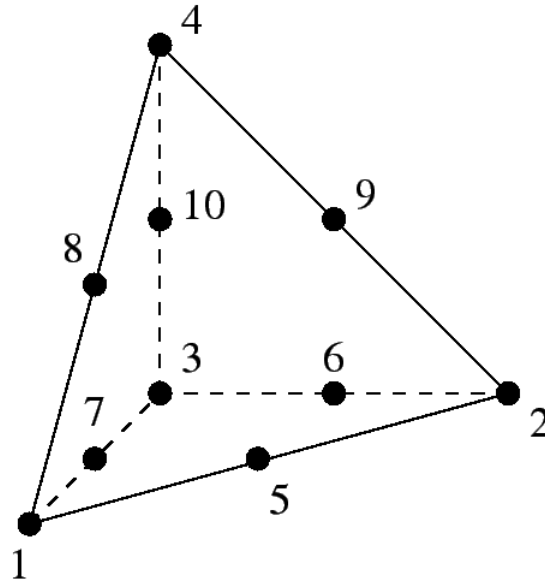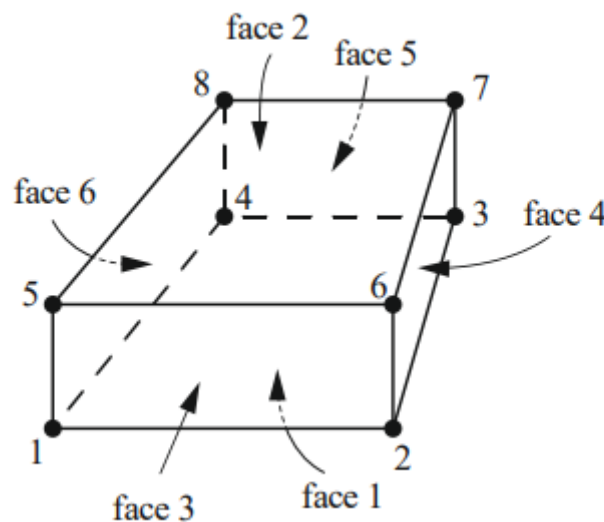**Figure 53. Linear Brick Element [33]**

As it was mentioned above and it can be seen from the figure this element has 8 nodes. Since each node has three degrees of freedom, that is in total 24 degrees of freedom per element.

Those 3 degrees of freedom are oriented in all 3 directions of Cartesian coordinate system. Element nodal displacement vector is:

$$\mathbf{v}^{\mathrm{T}} = \begin{bmatrix} \mathbf{v}_1 & \mathbf{v}_2 & \mathbf{v}_3 & \mathbf{v}_4 & \mathbf{v}_5 & \mathbf{v}_6 & \mathbf{v}_7 & \mathbf{v}_8 \end{bmatrix}$$
$$\mathbf{v}_i^{\mathrm{T}} = \begin{bmatrix} u_{\mathrm{i}} & v_{\mathrm{i}} & w_{\mathrm{i}} \end{bmatrix}, \ i=1,2,3,\dots,8 \tag{4.51}$$

Displacement components in Cartesian coordinate system can be expressed as follow:

$$u = a_1 + a_2 x + a_3 y + a_4 z + a_5 xy + a_6 yz + a_7 zx + a_8 xyz$$

$$v = a_9 + a_{10}x + a_{11}y + a_{12}z + a_{13}xy + a_{14}yz + a_{15}zx + a_{16}xyz \tag{4.52}$$

$$w = a_{17} + a_{18}x + a_{19}y + a_{20}z + a_{21}xy + a_{22}yz + a_{23}zx + a_{24}xyz$$

When uniform stress distribution is used, this type of element is suitable. These hexahedral elements formulated as an isoparametric can be of an arbitrary shape (with some distortion limitations), but still they are not convenient for highly curved or complex geometry.

Shape functions are derived in the natural coordinate system ξ, η and ζ with the origin at the center of the gravity of the element.

$$N_i = \frac{1}{8}(1 + \xi\xi_i)(1 + \eta\eta_i)(1 + \zeta\zeta_i), \quad i = 1 \dots 8 \tag{4.53}$$

Where ξ_i η_i, ζ_i are the node coordinates.

The displacement field is now written as a function of the shape function and nodal displacement and can be expressed as follows:

$$\mathbf{u} = \mathbf{N}\mathbf{v} \tag{4.54}$$

In that equation **u** represents displacement components in directions of the local coordinate system, and shape function matrix **N** is expressed as follow:

$$\mathbf{N} = \begin{bmatrix} N_1 & 0 & 0 & N_2 & 0 & 0 & N_8 & 0 & 0 \\ 0 & N_1 & 0 & 0 & N_2 & 0 \dots 0 & N_8 & 0 \\ 0 & 0 & N_1 & 0 & 0 & N_2 & 0 & 0 & N_8 \end{bmatrix} \tag{4.55}$$

4.5.   Verification of numerical example

Since the Finite Element Method (FEM) is a numerical method that provides approximate results, it is necessary to compare those results with some theoretical or experimental ones. Because of that, one simple problem is going to be solved analytically, which is going to be based on theory. Those results are going to be compared to the numerical ones for different finite element types (brick C3D8, and tetrahedral C3D10). It tends to have as small difference in results as possible. Also, a different number of finite elements is going to be used to discretize geometry to perform a sensitivity analysis.

4.5.1   *Stress relaxation*

In this section, one simple example is going to be solved, which is going to prove whether or not numerical and analytical results are matching. The geometry of this problem looks like a cuboid. That cuboid is going to be pressed for 0,022 mm, and after that by using the Maxwell model, to describe the relaxation and determine the stress loss after a certain number of hours (in section 4.1.2.2. it is already said that type of model can describe relaxation of soft metals very well). Since theoretical background says that pretension in bolted connections is stabilized after 3 to 4 days (section 2.3.2.), three days is going to be used as a parameter of the relaxation time. The material, which is going to be used in this analysis is 99% copper alloy. Since, there will not be any kind of heating, all parameters used in the analysis are at 20 °C Properties of that material are shown in the table below, and geometry of this example is shown in Figure 54.

Table 3: Copper Properties

Copper Alloy				
E (MPa)	v	σ_y (MPa)	σ_{UTS} (MPa)	ρ (t/mm^3)
110000	0,3	140	220	8,93e-09
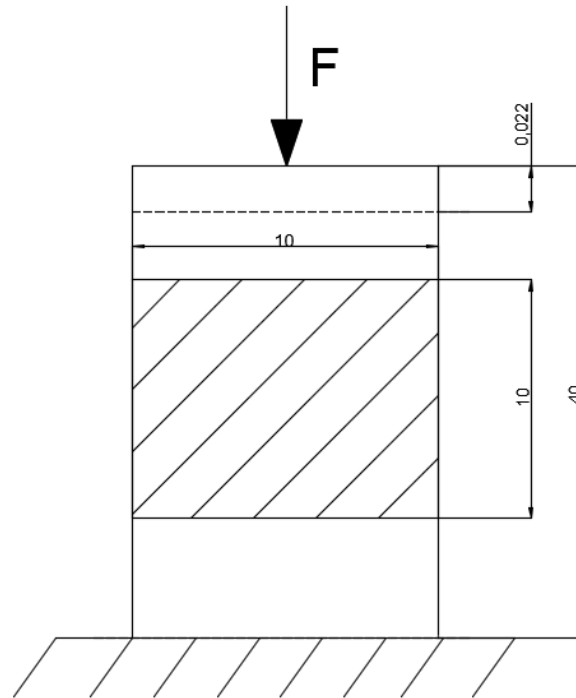
Figure 54. Verification Example

4.5.1.1. *Analytical solution of the stress relaxation*

The essential point of this example is to stay below the yield point, in the elastic regime. Because of that, displacement of 0,022 mm was used. This problem can be solved easily by using Hook's law and all relations that are connected to Hook's law. To start the calculation of the stress relaxation, initial stress that is caused by force F has to be defined. Stress can be calculated by using the following expression:

$$\sigma_0 = \frac{F}{A} \tag{4.56}$$

From that equation, force F is unknown, and the following expressions have to be used to define the force F:

$$\sigma_0 = \varepsilon E \tag{4.57}$$

$$\varepsilon = \frac{\Delta l}{l} \tag{4.58}$$

In equations above, all parameters are familiar ($\Delta l = 0{,}022$ mm, and $l = 40$ mm). Now, by using familiar parameters and equations (4.56), (4.57) and (4.58) force F can be calculated. The value is shown below:

$$F = 6050 \text{ N} \tag{4.59}$$

Force is now known and surface A is known, so equation (4.56) can be used to calculate what is the stress that is caused by the force F:

$$\sigma_0 = 60{,}5 \text{ MPa} \tag{4.60}$$

The first condition to perform viscoelastic behavior is that the value of σ_0 must be below the yield point. Comparing the value (4.60) to that in table 3 it can be seen that the first condition is satisfied and the procedure can continue.

Now, when the main parameter to perform relaxation of the material is familiar, model for the defining relaxation (the Maxwell model), and equation (4.36) can be used. Also, the expression (4.21) has already been said to be 3 days, which is equal to 72 hours.

Since $\sigma_0 = 60{,}5$ MPa, and $\tau = 72$ h, by using equation (4.36), relaxed stress after 72 hours is:

$$\sigma_0 = 22{,}26 \text{ MPa} \tag{4.61}$$

In the figure below is shown how the material is relaxing. Later that analytical graph is going to be compared to the numerical one, to see if it is matching.
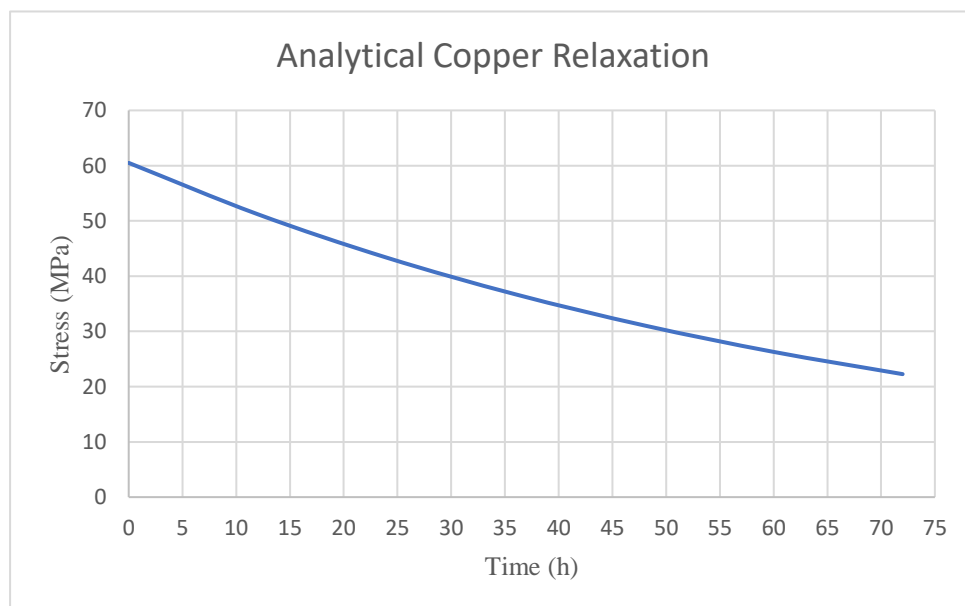

Figure 55. Copper Relaxation

4.5.1.2.   *Numerical solution of the stress relaxation*

In Figure 56 numerical models, which are discretized with quadratic tetrahedron elements C3D10, and linear brick elements C3D8 are shown. Both models are presented with the same number of nodes, which is 13 through the thickness. Also, there are presented enlarged photos with 7, 9, 11 nodes for both types of elements to show the different the different version of the model that were used.
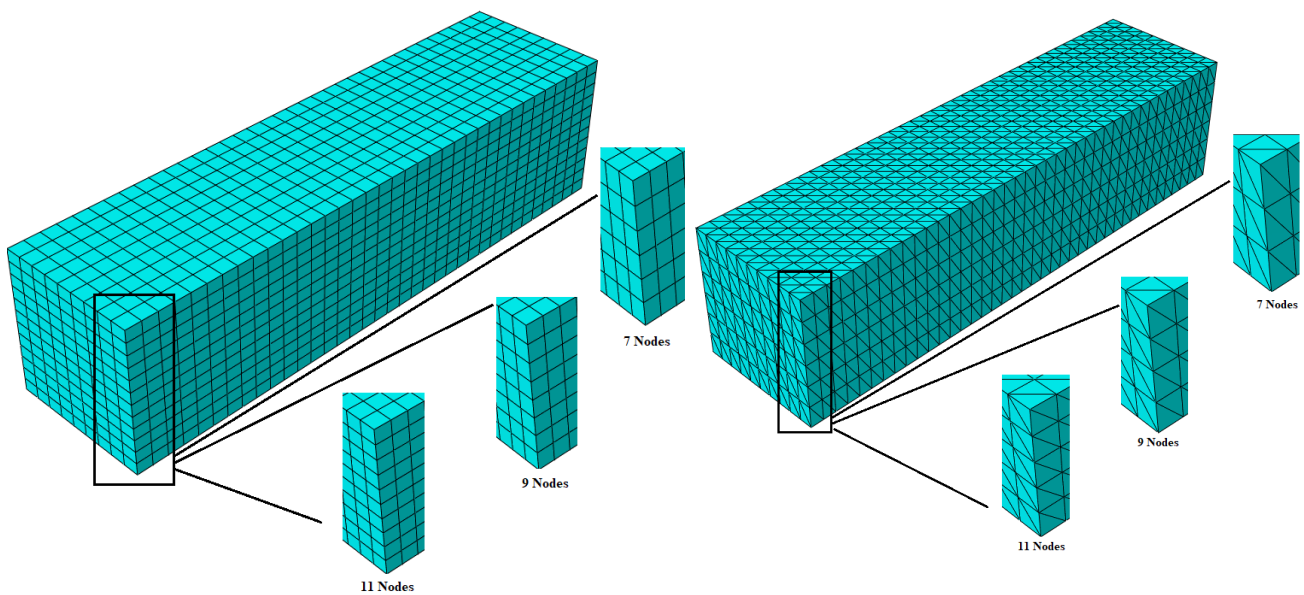
Figure 56. Stress Relaxation Models Discretized with Brick Elements (left) and Tetrahedron Elements (right)

Boundary conditions and load are applied according to Figure 54, and relaxation time for simulation is set to be 72 hours. Results for both numerical models are read on the middle surface. Since load was directly applied to the surface, the results of the stress relaxation were read on the middle surface. As it was mentioned above, two types of elements were used to discretize the geometry, but to obtain a convergency, the number of elements was increasing through the thickness of the model. Analytical, numerical results and relative difference to analytical solution are shown in Table 4.

Table 4: Comparison of Results

Analytical Solution [MPa]		22,26			
Number of Nodes Through the Thickness		7	9	11	13
Tetrahedral Mesh	Stress [MPa]	23,218	22,736	22,519	22,511
Relative Difference to Analytical Solution		4,3%	2,14%	1,16%	1,13%
Hexahedral Mesh	Stress [MPa]	22,574	22,414	22,334	22,331
Relative Difference to Analytical Solution		1,41%	0,69%	0,33%	0,31%

It can be concluded that both elements with a bigger number of nodes through the thickness are giving similar results. When the table is observed it can be seen, that differences in results exist, but they are very close. Also, it is obvious that hexahedral mesh is giving better results than tetrahedral mesh. Even though that hexahedral mesh is giving better results of both meshes, relative difference to analytical solution for a bigger number of nodes is below 2%.

Convergence for both types of elements is shown in Figure 57.
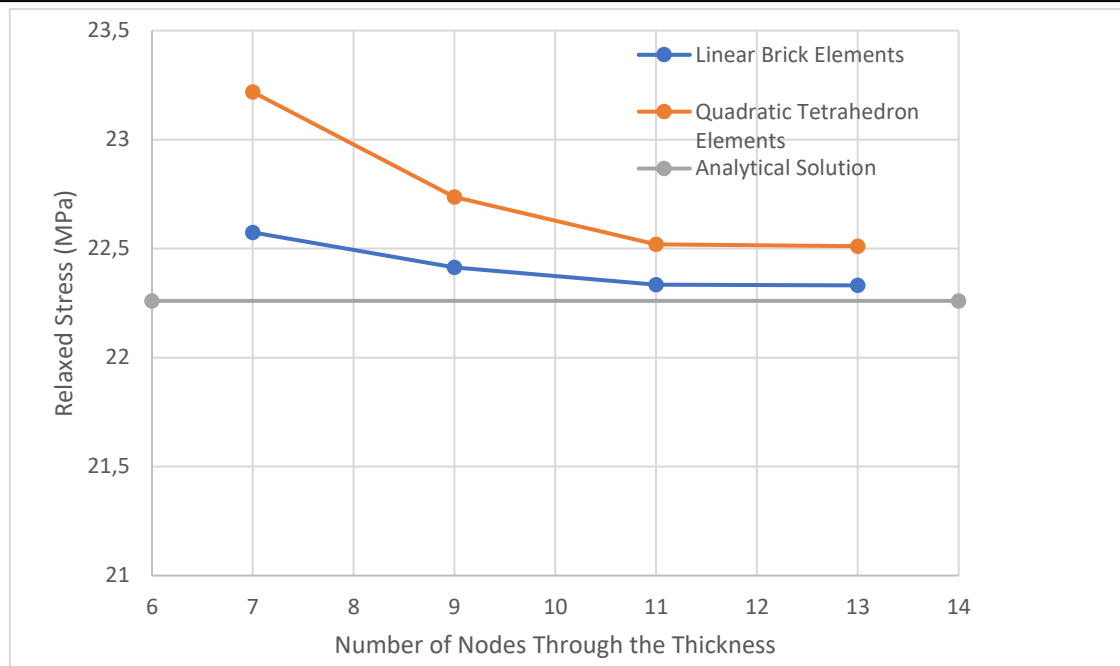
Figure 57. Convergence of the Elements

Although differences in results are negligible, hexahedral mesh is providing better results, and because of that, that type of element is going to be used in further analysis. Results that are obtained from that mesh are shown on the middle surface in the figure below.
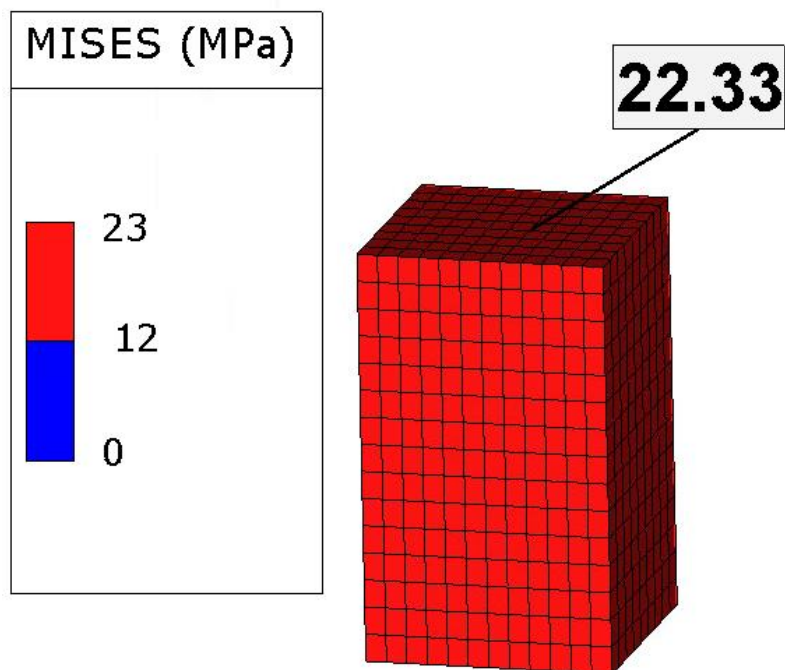
Figure 58. Relaxed Stress on the Middle Surface

The following two graphs are present behavior of the material over the time, and how does it match with the densest meshes used in the analysis. Although for further analyses, hexahedral mesh is going to be used, the behavior of the material for both types of the elements are presented so that it can be seen that they match to the analytical solution very closely.

Figure 59. Stress Relaxation for Tetrahedral Elements (left) and Brick Elements (right) Compared to Analytical Solution

5. RELAXATION OF THE PRELOADED BOLTED CONNECTIONS

In this section, it is going to be shown how the viscoelastic behavior of the material is influencing the relaxation of the bolted connection. As it was already mentioned, when certain pretension load is applied on the bolt, it doesn't stay constant eternally. Due to embedding, which is the comm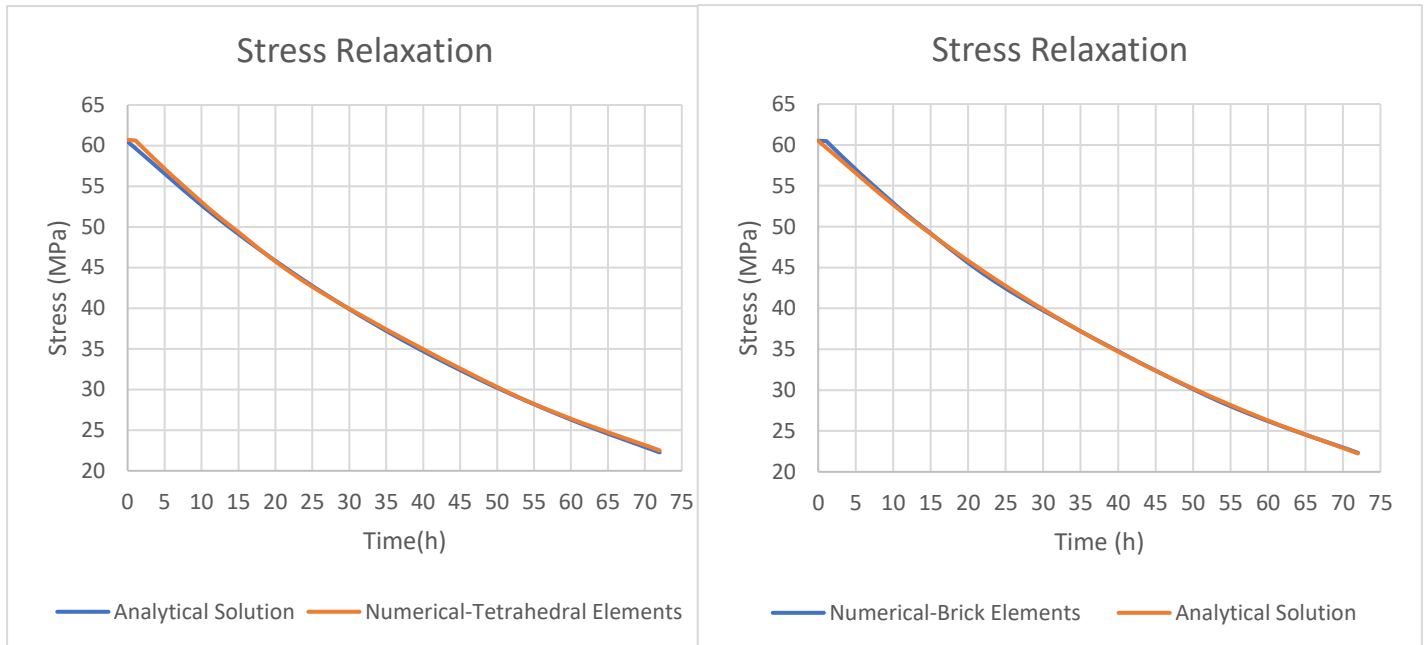on reason for relaxation of the bolted connections, pretension force will start to drop immediately, and it will stop dropping after perfect fit up between contact surfaces are gained. Because of that, the viscoelastic behavior of the copper, which was used in the verification section, will be used to describe the relaxation of the preloaded bolted connections. Also, it will be shown how the viscoelastic behavior of the material is influencing pretension in bolted connections.

5.1. Parts geometry

For performing numerical simulation of the bolted connections, it was essential to have two busbars, a bolt and a nut. Parts used for the analysis are shown in Figure 60.
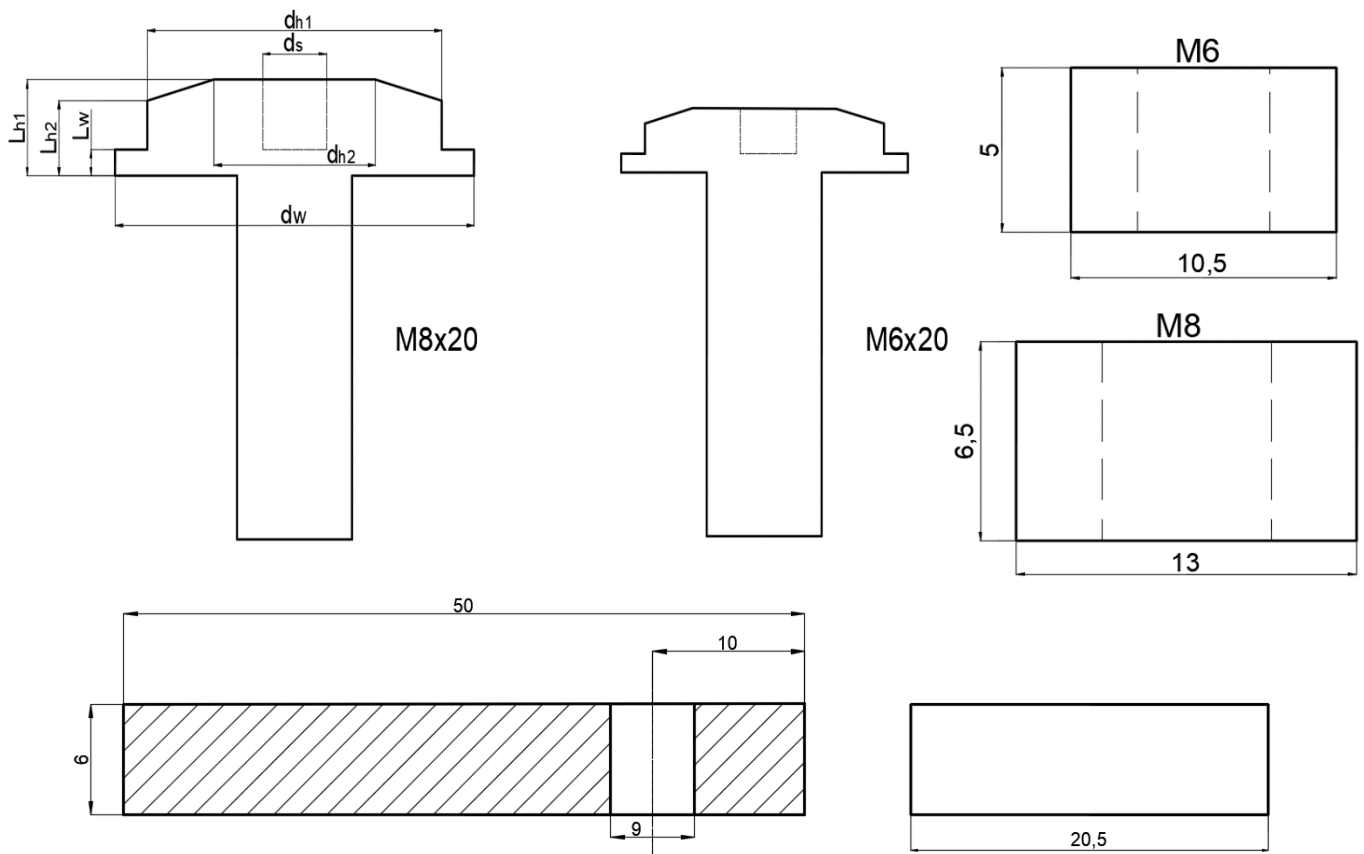

Figure 60. Geometry of Parts Used for Analysis

To create an assembly, an overlapping of 20 mm between busbars was used. Those assemblies will be shown in the upcoming section, which will be related to the mesh. Since it was necessary to retain clarification of the drawings, dimensions of the M6x20 bolt are not presented, but those dimensions are placed on the same spot and have the same meaning as those dimensions of the M8x20 bolt. Also, in Figure 60, it is possible to notice that two types of bolts were used in the analysis, and because of that values of dimensions are presented in the table below.

Table 5: Values of the Bolts M6&M8 Dimensions

Bolt	d_w(mm)	d_{h1}(mm)	d_{h2} (mm)	d_s(mm)	L_w(mm)	L_{h1}(mm)	L_{h2}(mm)
M6x20	13,3	10	7	4	1,1	3,3	2.7
M8x20	17,4	13	9	4,5	1,55	4,4	3,8

In this table, the symbols indicate the following:

$$d_w = \text{diameter of the washer head}$$

$$d_{h1} = \text{outer diameter of the head}$$

$$d_{h2} = \text{inner diameter of the head}$$

$$d_s = \text{diameter of the slot}$$

$$L_w = \text{length of the washer head}$$

$$L_{h1} = \text{sum of the length of the washer head and inner diameter of the head}$$

$$L_{h2} = \text{sum of the length of the washer head and outer diameter of the head}$$

5.2. Materials

In the analysis, two types of materials were used. For busbars, copper was used, the same one as it was used in the verification section, and bolts were made of the steel grade 8.8. Those materials and their characteristics at 20 °C are presented in the Table 6.

Table 6: Material Properties

	E (MPa)	v	σ_y (MPa)	σ_{UTS} (MPa)	ρ (t/mm^3)
Copper	110000	0,3	140	220	8,93e-09
Steel 8.8	210000	0,3	615,1	805,8	7,85e-09

5.3. Mesh models

All parts, whose geometry is described in section 5.1. were used in the analysis, and were built by using ANSA software. It is a pre-processor for finite element analysis, which is widely used in automotive sector. All parts have been made with the brick elements of first order (C3D8), whose characteristics are described in section 4.4.2. The size of each element used in the analysis in length, height, and width was approximately between 1 and 1,5 mm.

To create an assembly for the analysis, two busbars with 20 mm overlap were clamped together with M8 bolt and nut, or M6 bolt and nut. Also, to accomplish convergency and for getting a more effective solution of the problem, total alignment between nodes of the elements, which are in contact was used. Two assemblies, which were used in the analysis are shown in the figure below.
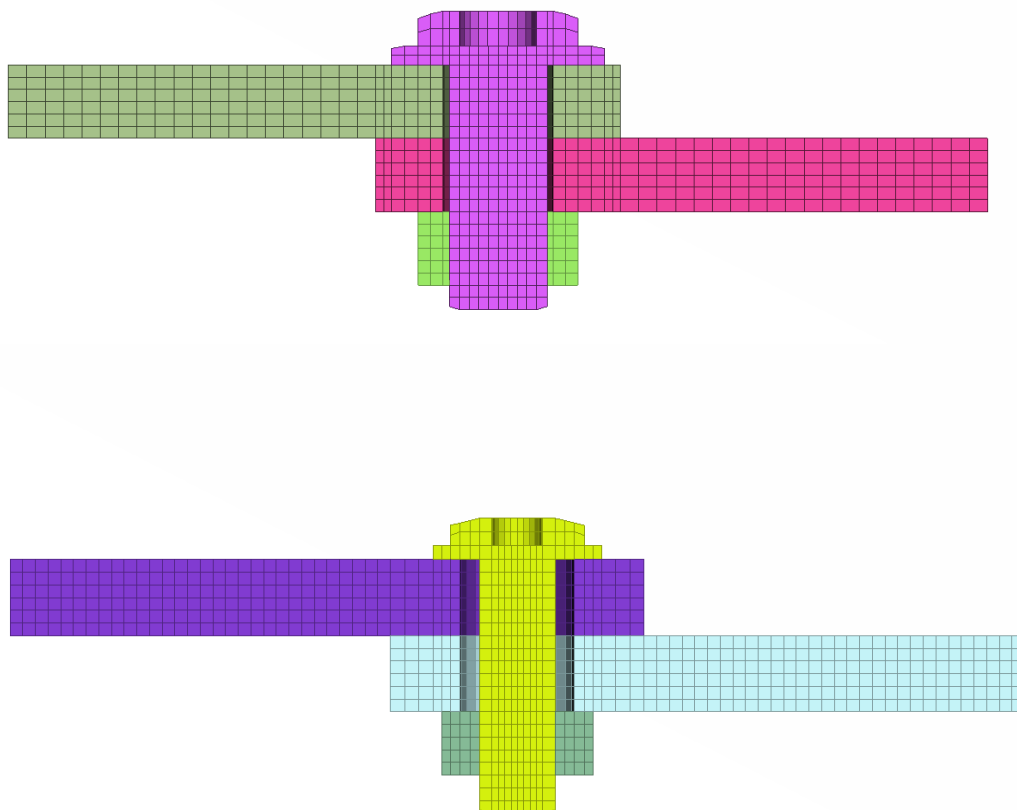

Figure 61. Mesh Models with M8 Bolt & Nut (Upper), and M6 Bolt & Nut (Lower)

Further, each component (busbar, M8 bolt & nut, and M6 bolt & nut) of the meshed models are shown in Figure 62.
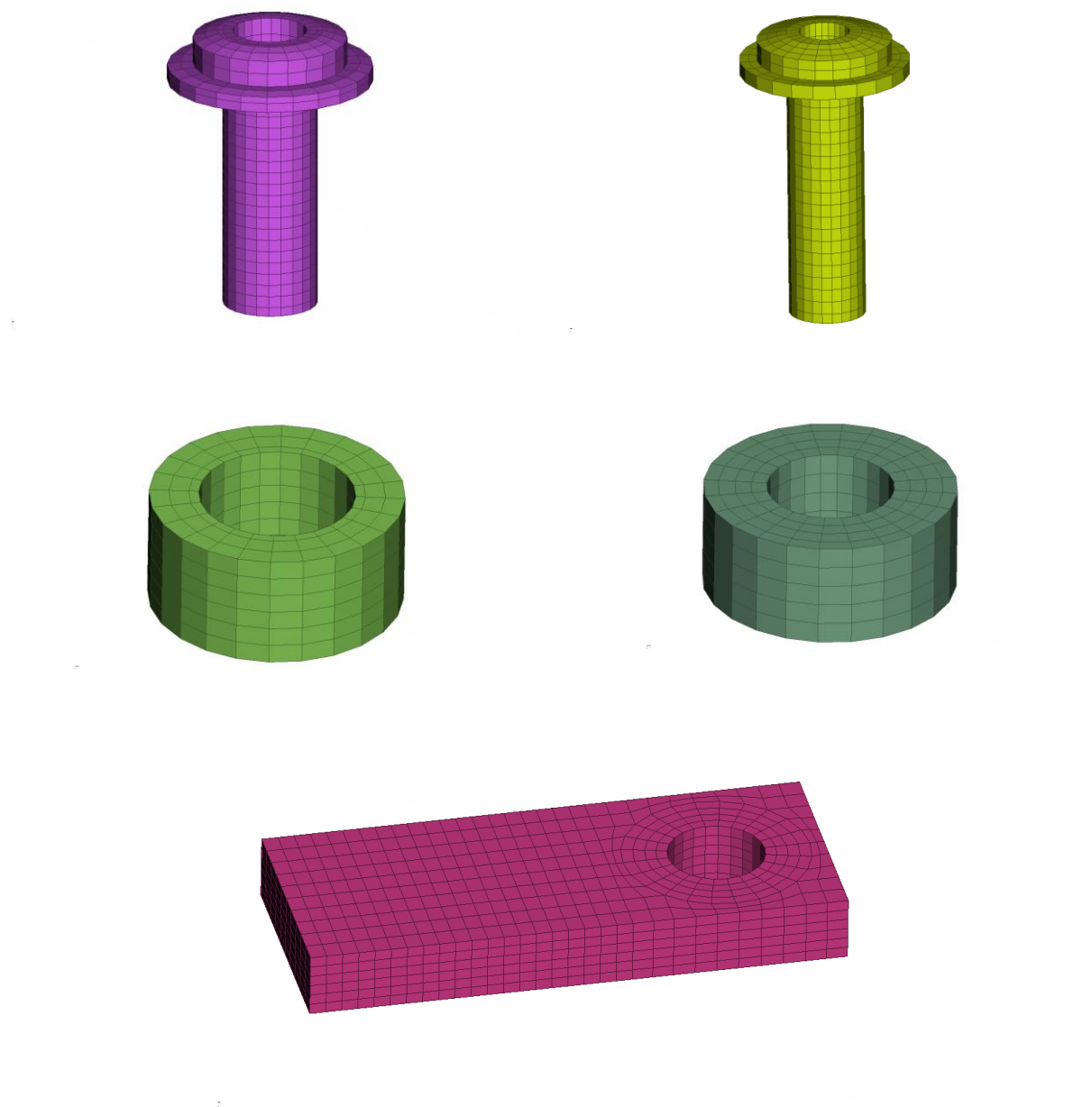

Figure 62. Each Component of the Assemblies

On the left side (purple and green) M8 bolt & nut are shown, and on the right side (yellow and grey) M6 bolt & nut are shown.

5.4.   Boundary conditions and pretension

Boundary conditions were applied to each end of the busbars to fix the model. It was applied in a way that should represent a clamp, so that all six degrees of freedom are constrained, even though solid elements have 3 DOFs. The nodes through which, the model was constrained are highlighted on the M8 model in Figure 63 below.
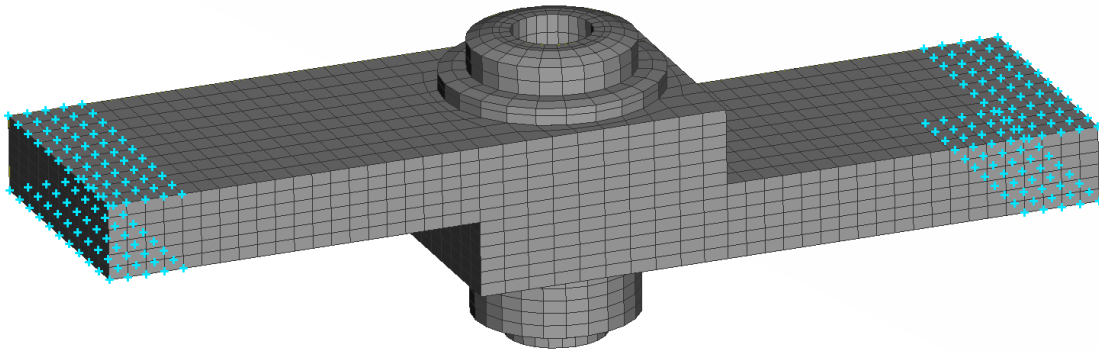
Figure 63. Boundary Conditions of Bolted Connection

Further, to apply pretension force it is necessary to have a pretension surface, and node in which force will be applied. The pretension surface and node are shown in Figure 64, and the node is positioned above the surface, so that it doesn't interact with it, and so that the normal and the pretension force application direction can be defined within the solver.
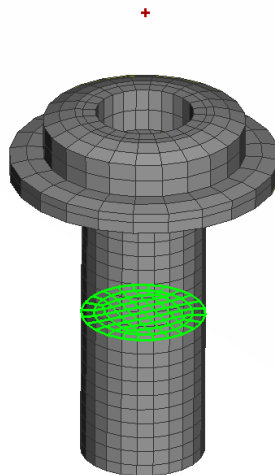
Figure 64. Pretension Surface and Node

5.5.   Contacts

Two types of contacts were used in assemblies. The first one is contact pair, type surface to surface. That type of contact was used between the following elements: bolt head, which was master surface and upper busbar, busbars, and nut, which was master surface and lower busbar. Those contacts are shown in the figure below.
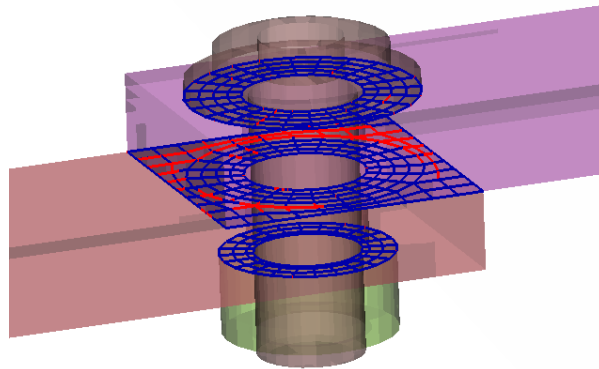
Figure 65. Location of the General Contacts

The second thing, which was used is a tie constraint. This type of constraint makes two elements, which are in the contact to be together during the simulation, so that it can simplify the thread base. This was used between the inner surface of the nut, and the outer surface of the bolt, and also total alignment between nodes was performed. This is shown in Figure 66.
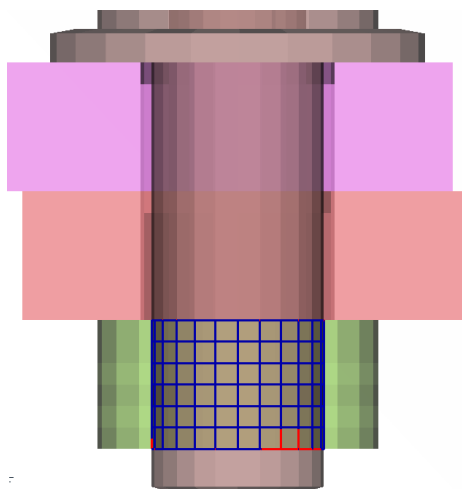
Figure 66. Location of the Tie Constraint

5.6. Results

In this section figures, with results are going to be displayed. Assemblies and stresses that occurred when pretension was applied and after connection relaxed are going to be presented. Also, the effects of applying pretension force on busbars will be shown, along with the stress distribution that pretension caused on the busbars.

For the beginning, it will be shown M6 and M8 bolted connection assembly.
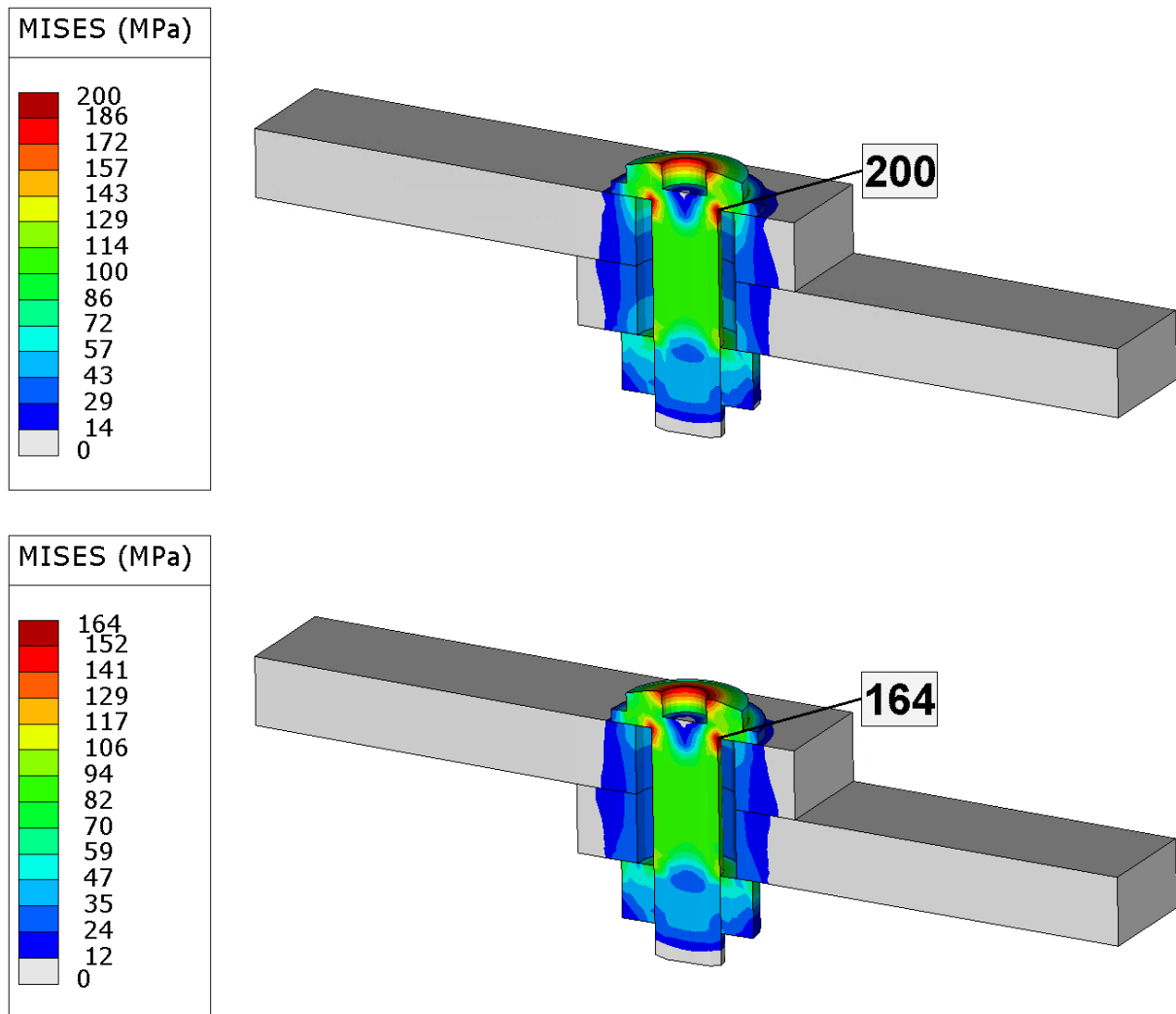
Figure 67. Equivalent Von Mises Stress Distribution When Pretension was Applied (Upper Figure) and When Bolted Connection Relaxed (Lower Figure) for M6
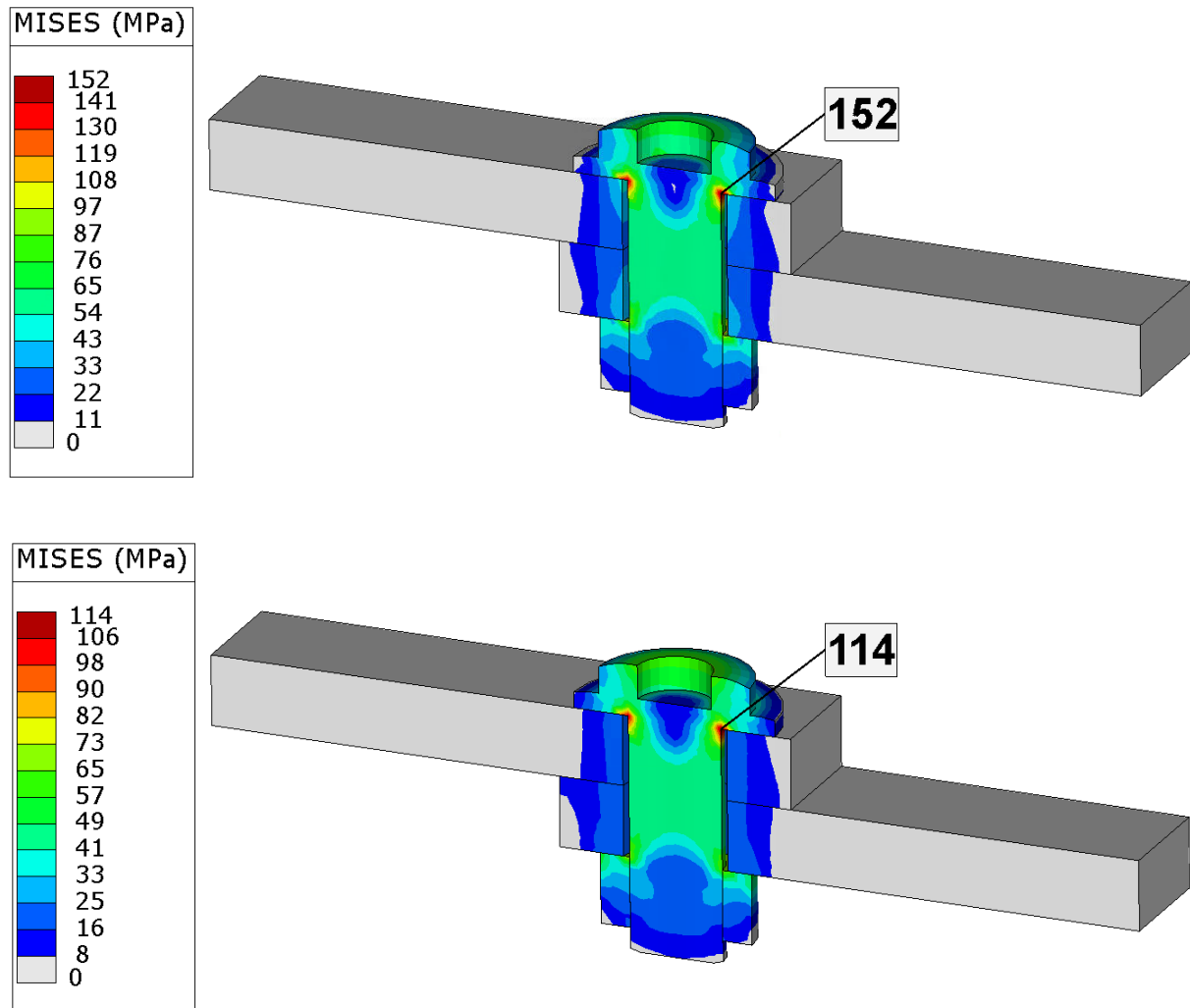
Figure 68. Equivalent Von Mises Stress Distribution When Pretension was Applied (Upper Figure) and When Bolted Connection Relaxed (Lower Figure) for M8

So, from these figures, it is possible to notice that the biggest stress occurs on the bolt at the connection between the head and the body of the bolt.

Since viscoelastic behavior of the material is being studied, it is essential that all stresses, which occur due to pretension, on the busbars are below the yield limit. For copper, which is the material of the busbars, the yield point is 140 MPa.

Firstly, all stresses that occurred on the busbars when pretension force was applied and when bolted connection relaxed will be displayed for the M6 bolt. Those stresses are shown in the following figures.

Figure 69. Equivalent Von Mises Stress Distribution Before (Upper Figure) and After (Lower Figure) Relaxation for M6 Bolt

It is noticeable that all stresses on the busbars are below the yield limit, which satisfies the criteria for performing the viscoelastic behavior of the material.

Now, it is also important to check what is the contact pressure between the surfaces, which are in interaction. So, just like for the stresses contact pressures for M6 bolt are going to be shown in the following figures.

Figure 70. Contact Pressure Before (Upper Figure) and After (Lower Figure) Relaxation for M6 Bolt

From these figures, it is also noticeable that the highest contact pressure is below the yield point. Since the highest contact pressure is observed on the upper busbar, only that busbar and the relaxed contact pressure are shown.

This procedure was repeated for the M8 bolted connection. The first results presented will, again, be the stresses that occurred on the busbars when pretension force was applied and when the bolted connection relaxed. Those stresses are displayed in the following figures.
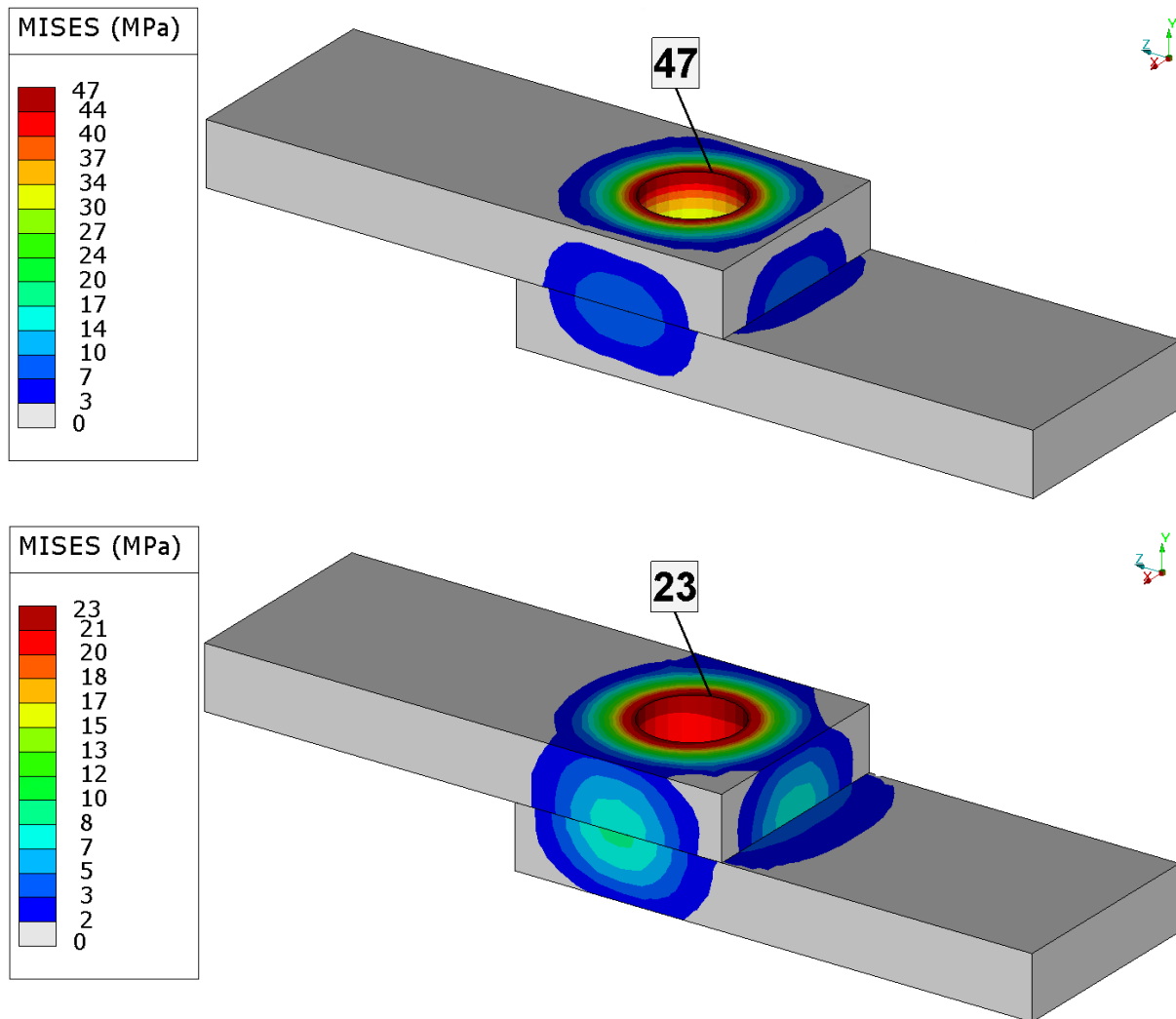
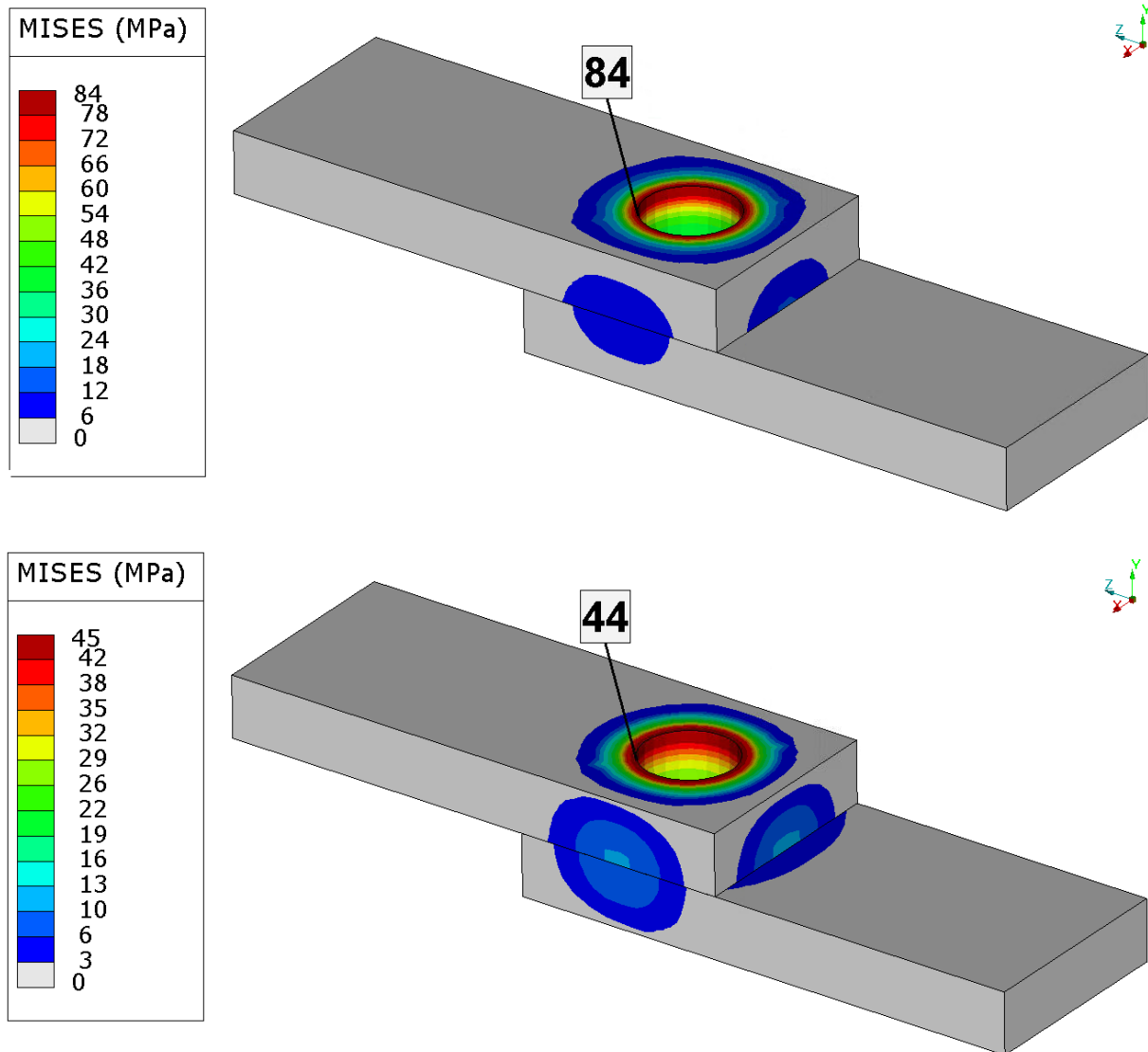**Figure 71. Equivalent Von Mises Stress Distribution Before (Upper Figure) and After (Lower Figure) Relaxation for M8 Bolt**

It is visible that the highest stress on the busbars is below the yield point, which again satisfies the criteria for performing the viscoelastic behavior of the material.

Just like for M6 bolt, contact pressure of bolted connection for the M8 bolt is also going to be shown, and it is displayed in Figure 72.

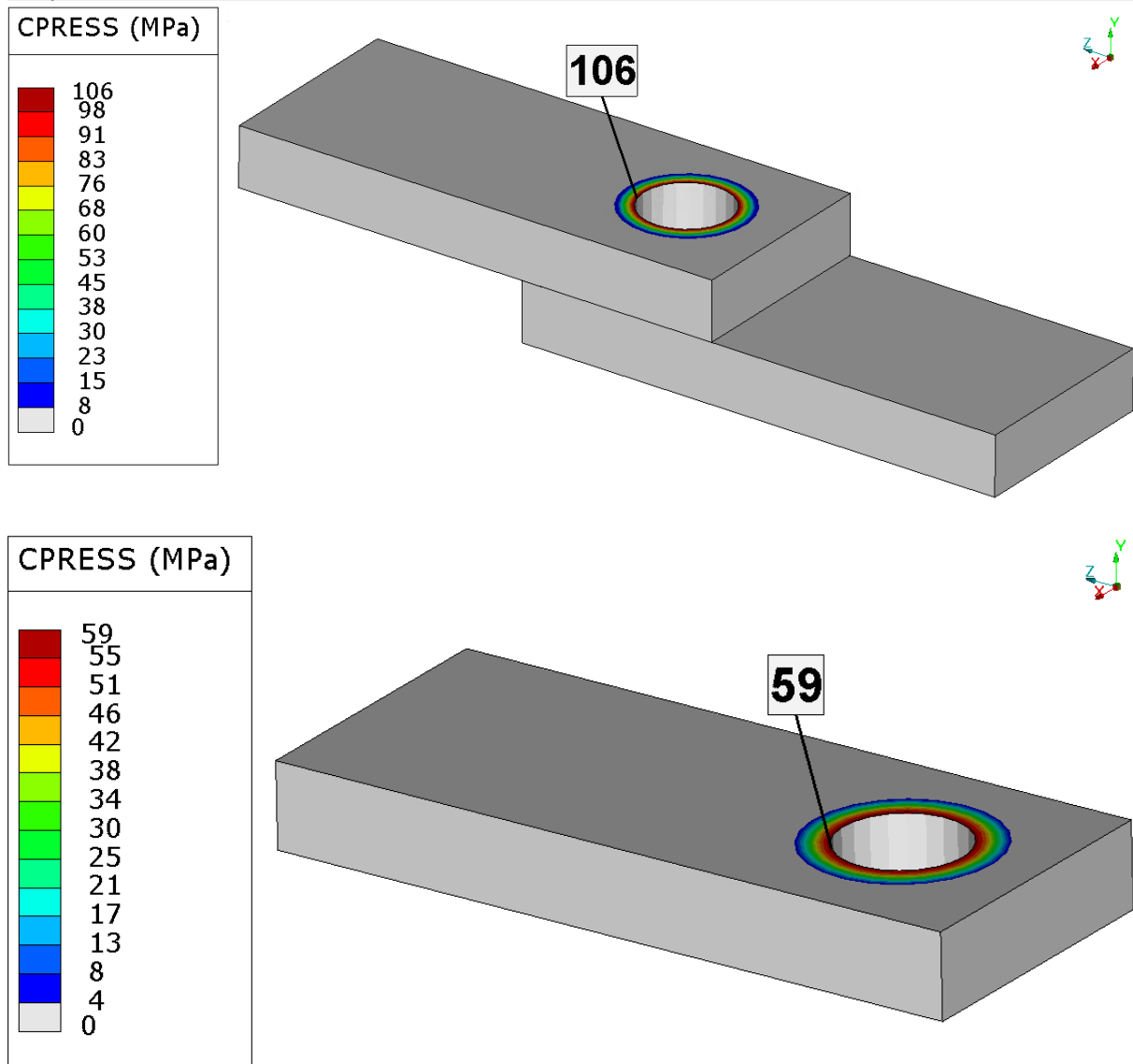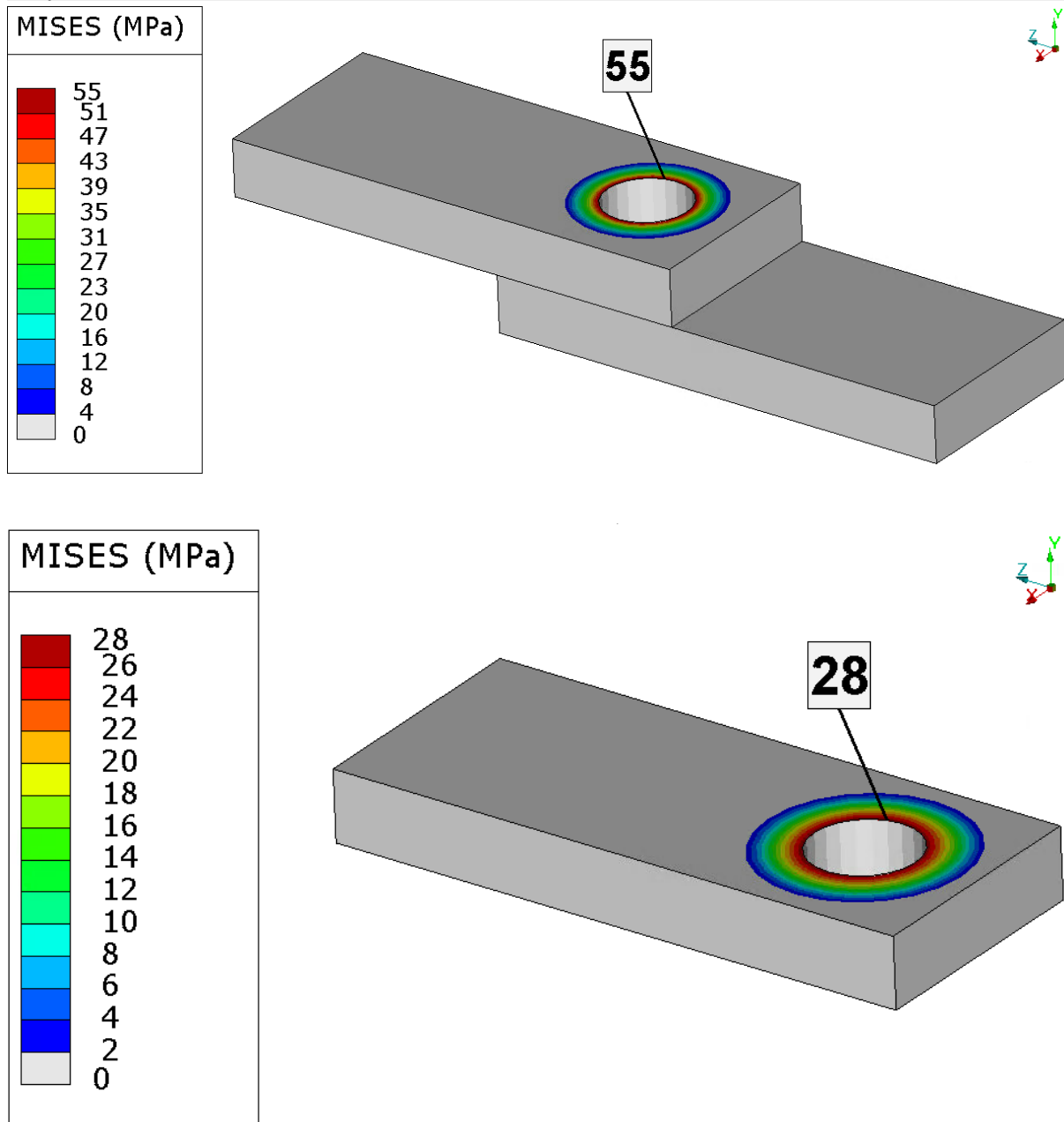**Figure 72. Contact Pressure Before (Upper Figure) and After (Lower Figure) Relaxation for M6 Bolt**

From all figures it is possible to conclude that the material yield limit was never exceeded. Because of that stresses are in the elastic area and the viscoelastic procedure of the material can be performed.

It was necessary to check how the viscoelastic behavior of the material is affecting pretension of the bolts. A pretension force of 3000 N was applied to both bolts. Relaxation time was specified as 72 hours, since from theoretical background it was said that relaxation of the bolted connections last 3 to 4 days. Results obtained from numerical simulation are shown in Table 7.

Table 7: Pretension Loss

Bolt	Initial Pretension (N)	Relaxed Pretension (N)	Pretension loss %
M6	3000	2384,19	20,53%
M8	3000	2272,66	24,25%

Also, it is going to be presented graphically how pretensions is dropping with the time. It is shown in the figure below.

Figure 73. Pretension Loss

From the table and the figure above, it can be concluded the viscoelastic behavior of the material is affecting the pretension force of the bolted connection. Here in this thesis based on the theoretical approach it is visible that bigger pretension loss will occur with the bigger bolt M8.

6. CONCLUSIONS

6.1. Summary

The four main parts of this thesis can be identified:

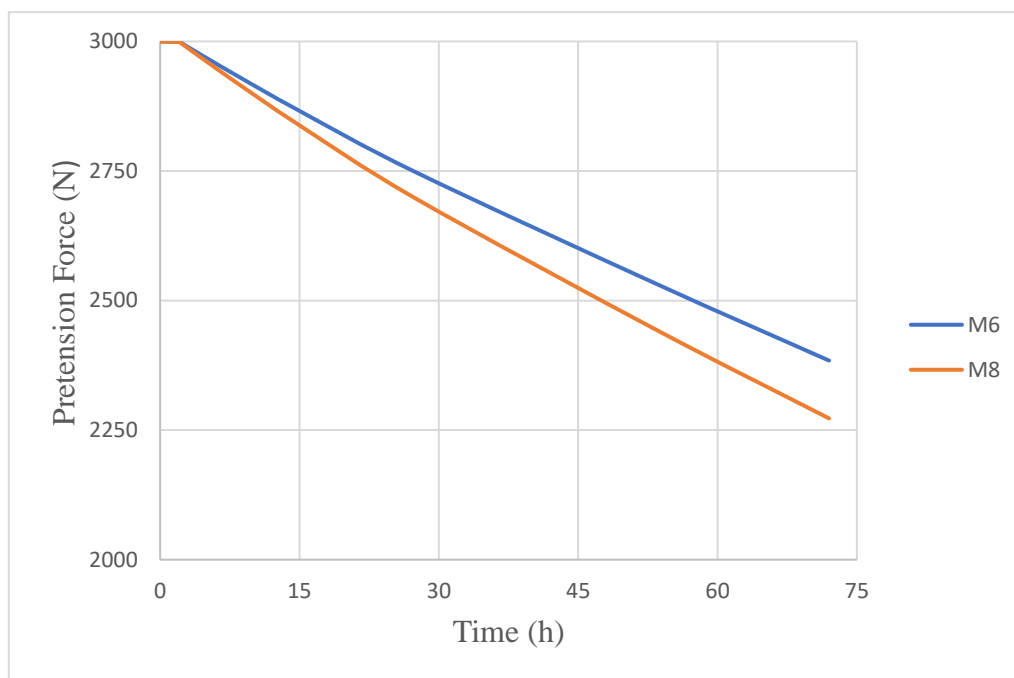- It was necessary to study theoretical background. In that theoretical background it was investigated about the bolts and bolted connections. It was essential to find out what is the pretension and how that pretension is dropping with the time or when a certain load is applied to the bolted connection.

- In the second part, the model was exposed to vibration loading and connectors, which represented the body of the bolt were compared to the results from the shaker table.

- Third part describes what is the viscoelastic behavior of the material, model which can be used to describe a procedure of the viscoelastic behavior of the material, and which model is describing relaxation well because the relaxation of the bolted connections was studied.

- In the fourth part it was checked how the viscoelastic behavior of the material is affecting pretension force in the bolted connection.

6.1.1. Outlines and conclusions related to the first part

As it was mentioned above, in the first section it was performed a thorough study of the bolts, bolted connections and experiments, which were performed on those bolted connections. Those experiments were examining how the certain load will affect the pretension force. Also, relaxation tests were studied. It was studied when the pretension force will get constant. The importance of that theoretical background lays in the base of the numerical performance of the relaxation test. It was concluded that after 3 to 4 days relaxation force will get constant, and because of that it was taken as a parameter for the relaxation time. Also, in the theoretical background can be found other experiments which were performed on the bolts and bolted connections, which can be a good base for future tests.

6.1.2. Outlines and conclusions related to the second part

In this part it can be found the model of the battery pack, which was subjected to the PSD random vibration. In that model, to simplify the geometry, instead of the 3D elements, the connectors were. Those connectors represent the body of the bolt. It was necessary to output the force which occurred in those connectors when that vibration load was applied. When those forces were obtained, they were compared to the already existing data. Before the whole process was subjected to the numerical simulation, the battery pack was set up on the shaker table, and it was checked what is the remaining torque in the bolts after experiments. The method for defining the remaining torque was the retightening method, which is described in section 3.3.2.1. When all results were gathered, they were compared to see if they make sense. After comparison of the results, it was concluded that they are not showing reliably results. Because of that as a conclusion it can be said that connectors are not type of the element, which can tell what is happening with the bolt.

6.1.3. Outlines and conclusions related to the third part

This part describes what is the viscoelastic behavior of the material, what are the models, which can describe the viscoelastic behavior (creep and relaxation), and which of these models can be used for describing the relaxation. Firstly, it was studied theoretical background, for the elastic and the viscoelastic behavior of the material. After that, it was given an example with experimental results. From these results, it can be seen that model, which will be used for describing the viscoelastic behavior of the copper suits it well. Also, finite elements that are going to be used in the analysis are described in this part. After the theoretical part was written, it was necessary to perform verification of one simple problem. In that problem, it was used material, which was going to be used for performing relaxation of the bolted connections. The model was pressed and to describe relaxation it was used the Maxwell model. Obtain results were compared to the analytical ones. Since, results for both types of elements used in the analysis gave very close results to the analytical ones, it can be concluded that verification of the problem was successful. Because of that, that type of the material, and that stress relaxation constitutive model can be used for describing the relaxation of the bolted connections.

6.1.4.   Outlines and conclusions related to the fourth part

In the last part of this thesis, 2 copper plates which were clamped together with M6 or M8 bolt were used. It was necessary to perform relaxation of the bolted connection, to check how the viscoelastic behavior of the material is affecting pretension. It was necessary to satisfy the condition, when pretension was applied, that it doesn't cause the stress, which is above the yield point. When that was satisfied, it was possible to perform the viscoelastic procedure. When the whole procedure was done it was checked how much it affected pretensions in the bolt. It is possible to notice from figures and results that is affecting pretension of the bolt, and for the bigger bolt, it is possible to see that bigger loss occurred. Because of that, it is possible to conclude that phenomenon is affecting the pretension of the bolt, and, since this is based on the theoretical approach, it is necessary to perform a certain type of the experiment to check what is the real loss of the pretension.

6.2.   Recommendations for further works

Since the whole thesis is based on the theoretical background and the theoretical approach, it is necessary to mention what would be recommendations for further works, so that more realistic results could be gained.

Firstly, it is necessary to perform experiments, which will tell us, what is the real pretension loss in the bolted connections. This part is important because it would tell what is really happening when certain busbars are clamped together, and in what time the pretension force will get stabilized.

Also, the parameter, which has a big influence on the outcome and is variable is friction. It is necessary to find out, what is the real value of the friction between steel and copper (head of the bolt and the busbar). That data could be calculated from the already existing formulas, since from the experiments pretension force and the torque will be familiar.

The last thing, which is important as a recommendation is to find a way how to prevent the loss of pretension. One simple way, like retightening of the bolt and the nut after an hour or two might give a result in stopping the pretension to drop.

Bibliography

[1] Gaffney, B. *Vehicle Battery Pack Design and Consideration of Repurposing*, Toronto, 2015.

[2] *https://www.nissan-global.com/EN/TECHNOLOGY/OVERVIEW/li_ion_hev.html*

[3] Pan, L., Zhang, C., *A High Power Density Integrated Charger for Electrical Vehicles with Active Ripple Compensation,* University of Bristol, 2015.

[4] Weiwei, L., Teruhiko, Y., *Bridge Engineering*, Classifications, Design Loading, and Analysis Methods, pages 111-136, 2017.

[5] Son, P. M., *Bolts Pulling Test. Reverser for Bolts testing*, International Journal for Computational Civil and Structural Engineering, 2018.

[6] Ramey, E., Jenkins, R., *Experimental Analysis of Thread movement in Bolted Connections Due to Vibrations*, Auburn University, 1995.

[7] Križan, S., *Flange Joint Sealing Testing Device,* Master's thesis, Zagreb 2012.

[8] Grimismo, E. L., Aalberg, A., Langseth, M., Clausen, A.H., *Failure Modes of Bolt and Nut Assemblies under Tensile Loading*, Journal of Constructional Steel Research, 2016.

[9] Solomon, N., Solomon, I. Severin, T., Dulucheanu, C., Sanduleac E., *Compression Press Bolts Failure Analysis*, New technologies and Products in Machine Manufacturing Technologies, 2011.

[10]   Toribio, J., Gonzalez, B., Matos, J., C., Ayaso F., *Analysis of Failure in Steel Bolted Connections*, Department of Material Engineering, 2011.

[11]   Li, Y., Liu, Z., Wang, Y., Cai, l., Zheng, M., *Experimental study on behavior of time-related preload relaxation for bolted joints subjected to vibration in different direction,* Beijing university of Technology, 2019.

[12]   Nakalswamy, K., *Experimental and Numerical Analysis of Structures with Bolted Joints Subjected to Impact Load*, University of Nevada, Las Vegas, 2010.

[13]   Hemmati Vand, E., Oskouei, R., Chakherlou, T., *An Experimental Method for Measuring Clamping Force in Bolted Connections and Effect of Bolt Threads Lubrication on its Value,* University of Kashan, Iran, 2008.

[14]   Heistermann, C., *Behavior of Pretensioned Bolts in Friction Connections,* Lulea University of Technology, 2011.

[15]   Kranjčević, N., *Vijci i navojna vretena,* University of Zagreb, 2014.

[16]   Pedrosa, B., Rebelo, C., Gervasio H., da Silva L., Correia J., *Fatigue of Preloaded Bolted Connection with Injection Bolts*, Structural Engineering international, 2019.

[17]   Yang X., Nassar, S., *Analytical and Experimental Investigation of Self-Loosening of Preloaded Cap Screw Fasteners*, Department of Mechanical Engineering, Fastening and Joining Research Institute, 2011.

[18]   Chen, Y., Gao, Q., Guan, Z*., Self-Loosening Failure of Bolt Joint under Vibration considering the Tightening Process,* State key Laboratory of Structural Analysis for Industrial Equipment, 2017.

[19]   Junker, H., G., *New Criteria for Self-Loosening of Fasteners Under Vibration*, European Research and Engineering, Standard Pressed Steel, 1969.

[20]   Zadoks, R., I., *An Investigation of the Self-Loosening Behavior of Bolts under Transverse Vibration*, Mechanical and Industrial Engineering Department, 1997.

[21]   Eccles, B., *Self-Loosening of Threaded Fasteners,* Bolt Science, 2011.

[22]   Bickford, J., H., *An Introduction to the Design and Behavior of Bolted Joints,* New York, 1995

[23]   Friede, R., Lange, J., *Loss of preload in bolted connections due to embedding and self loosening,* Rio de Janeiro, 2010.

[24]   *Threaded fasteners handbook,* Noordwijk, 2010.

[25]   Yang, J., Dewolf, T., *Relaxation in high-strength bolted connections using galvanized steel,* Journal of bridge engineering, 2000.

[26]   Van Baren, J., *What is Random Vibration Testing*, Vibration Research Corporation, Jenison, Michigan, 2012.

[27]   Shiina, T., *Derivation of PSD Profiles for Random Vibration Test Based on the Field Data Obtained in Japan,* 2014.

[28]   Kumar, M., S., *Analyzing Random Vibration Fatigue, 2008.*

[29]   Saito, K., *A Method for Generating Random Vibration Using Acceleration Kurtosis and Velocity Kurtosis,* Kobe University

[30]   https://vru.vibrationresearch.com/lesson/new-lesson-15/

[31]   Teixeira, G., *Random Vibration Fatigue: Frequency Domain Critical Plane Approaches, 2013.*

[32]   https://femci.gsfc.nasa.gov/random/randomgrms.html

[33]   Abaqus Analysis User's Guide, Dassault Systemes, 2016.

[34]   Inspecting Tightening Torque, Tohnichi Torque Handbook, vol9.

[35]   Pustajić, D., Cukor, I., *Teorija plastičnosti i viskoelastičnosti*, Zagreb, 2009.

[36]   Tehnicčka enciklopedija, *X. Svezak,* Zagreb 1986.

[37]   Alfirević, I., *Uvod u tenzore I mehaniku kontinuuma*, Zagreb, 2003.

[38]   Riggins, R., Cartwright, A., Ruckers, R., *Viscoelastic properties of copper deficient chick bone*, California, 1979.

[39]   Yang, X., Wang, Y., Wang, G., Zhai, H, Dai, L., H., Zhang, T., *Time, stress, and temperature-dependent deformation in nanostructured copper: Stress relaxation test,* Shanghai, 2015.

[40]   Sorić, J., *Nelinearna numerička analiza konstrukcija,* Zagreb, 2016.

[41]   Šušak, I, *Numerical Assessment of the influence of preheating and boundary conditions on welding residual stresses and deformations,* Master's thesis, Zagreb, 2019.

[42]   Šubat, A., *Thermomechanical numerical analysis of engine exhaust manifold,* Master's thesis, Zagreb, 2017.

[43]   Sorić, J., *Metoda konačnih elemenata,* Zagreb, 2004.

APPENDIX

I.   CD-R disc